Springer Theses
Recognizing Outstanding Ph.D. Research

Kohei Miyata

Highly Luminescent Lanthanide Complexes with Specific Coordination Structures

Springer

Springer Theses

Recognizing Outstanding Ph.D. Research

For further volumes:
http://www.springer.com/series/8790

Aims and Scope

The series "Springer Theses" brings together a selection of the very best Ph.D. theses from around the world and across the physical sciences. Nominated and endorsed by two recognized specialists, each published volume has been selected for its scientific excellence and the high impact of its contents for the pertinent field of research. For greater accessibility to non-specialists, the published versions include an extended introduction, as well as a foreword by the student's supervisor explaining the special relevance of the work for the field. As a whole, the series will provide a valuable resource both for newcomers to the research fields described, and for other scientists seeking detailed background information on special questions. Finally, it provides an accredited documentation of the valuable contributions made by today's younger generation of scientists.

Theses are accepted into the series by invited nomination only and must fulfill all of the following criteria

- They must be written in good English.
- The topic should fall within the confines of Chemistry, Physics, Earth Sciences, Engineering and related interdisciplinary fields such as Materials, Nanoscience, Chemical Engineering, Complex Systems and Biophysics.
- The work reported in the thesis must represent a significant scientific advance.
- If the thesis includes previously published material, permission to reproduce this must be gained from the respective copyright holder.
- They must have been examined and passed during the 12 months prior to nomination.
- Each thesis should include a foreword by the supervisor outlining the significance of its content.
- The theses should have a clearly defined structure including an introduction accessible to scientists not expert in that particular field.

Kohei Miyata

Highly Luminescent Lanthanide Complexes with Specific Coordination Structures

Doctoral Thesis accepted by
Hokkaido University, Sapporo, Japan

Springer

Author
Dr. Kohei Miyata
Hokkaido University
Sapporo
Japan

Supervisor
Prof. Yasuchika Hasegawa
Hokkaido University
Sapporo
Japan

ISSN 2190-5053 ISSN 2190-5061 (electronic)
ISBN 978-4-431-54943-7 ISBN 978-4-431-54944-4 (eBook)
DOI 10.1007/978-4-431-54944-4
Springer Tokyo Heidelberg New York Dordrecht London

Library of Congress Control Number: 2014935969

Parts of this thesis have been published in the following journal articles:

K. Miyata, Y. Hasegawa, Y. Kuramochi, T. Nakagawa, T. Yokoo, T. Kawai, "Characteristic Structures and Photophysical Properties of Nine-Coordinated Europium(III) Complexes with Tandem-connected Phosphane Oxide Ligands", *Eur. J. Inorg. Chem.* **2009**, *32*, 4777.

K. Miyata, T. Nakagawa, R. Kawakami, Y. Kita, K. Sugimoto, T. Nakashima, T. Harada, T. Kawai, Y. Hasegawa, "Remarkable Luminescence Properties of Lanthanide Complexes with Asymmetric Dodecahedron Structures", *Chem. Eur. J.* **2011**, *17*, 521.

K. Miyata, T. Ohba, A. Kobayashi, M. Kato, T. Nakanishi, K. Fushimi, Y. Hasegawa, "Thermostable Organo-phosphor: Low-vibrational Coordination Polymers That Exhibit Different Intermolecular Interactions", *ChemPlusChem* **2012**, *77*, 277.

K. Miyata, T. Nakanishi, K. Fushimi, Y. Hasegawa, "Solvent-dependent Luminescence of Eu(III) Complexes with Bidentate Phosphine Oxide", *J. Photochem. Photobiol. A: Chem.* **2012**, *235*, 35.

K. Miyata, Y. Konno, T. Nakanishi, A. Kobayashi, M. Kato, K. Fushimi, Y. Hasegawa, "Chameleon Luminophore for Sensing Temperatures: Control of Metal-to-Metal and Back Energy Transfer in Lanthanide Coordination Polymers", *Angew. Chem. Int. Ed.* **2013**, *52*, 6413.

Supervisor's Foreword

There has been significant recent interest in the development of luminescent metal complexes for applications such as optical materials, organic light-emitting diodes (OLEDs), and fluorescent sensors. These luminescence properties are strongly dominated by the type of organic ligand and the coordination structure, which together control the ligand field. In particular, the ligand fields of transition-metal complexes are affected by the particular geometrical structure, and a large number of studies have reported the link between the structure and the luminescence properties of luminescent metal complexes.

In this thesis, luminescent lanthanide complexes with specific coordination structures are introduced by Dr. Kohei Miyata. Specific coordination structures result in lanthanide complexes with remarkable photophysical properties. This thesis provides academic studies of specific coordination structures (mono-capped square-antiprism, dodecahedron, and coordination-polymer structures) of luminescent lanthanide complexes. Dr. Miyata has also successfully prepared thermostable and thermosensing luminophores composed of lanthanide ions and characteristic organic ligands. I believe that his studies contribute to successful exploration of new science and technology in our future.

Lanthanide complexes with characteristic photophysical properties, narrow emission bands, and long emission lifetimes, have been regarded as attractive luminescent materials for use in electroluminescent (EL) devices, lasers, and luminescent biosensing applications. Luminescent lanthanide complexes with specific coordination structures may lead to the development of new fields in photophysical, coordination, and materials chemistry.

Hokkaido, January 2014 Prof. Yasuchika Hasegawa

Acknowledgments

I am sincerely grateful to Prof. Yasuchika Hasegawa, Laboratory of Advanced Materials Chemistry, Division of Materials Chemistry, Graduate School of Engineering, Hokkaido University, for his kind guidance, valuable suggestions, and hearty encouragement throughout this work.

I would also like to express my gratitude to Assoc. Prof. Koji Fushimi and Asst. Prof. Takayuki Nakanishi, Graduate School of Engineering, Hokkaido University, for their kind help and useful advice.

I thank Prof. Tsuyoshi Kawai, Assoc. Prof. Takuya Nakashima, and Asst. Prof. Junpei Yuasa Graduate School of Materials Science, Nara Institute of Science and Technology (NAIST), for their helpful discussions and guidance in my master's thesis.

I acknowledge Prof. Masako Kato and Asst. Prof. Atsushi Kobayashi, Graduate School of Science, Hokkaido University, for their kind help in X-ray single-crystal analyses and valuable suggestions.

I also express my appreciation to Prof. Emer. Hideo Hirohara, Prof. Tsutomu Kumagai, Assoc. Prof. Yoshinori Inoue, and Asst. Prof. Munenori Takehara of the Department of Materials Science, University of Shiga Prefecture, for their kind support in my bachelor's thesis.

I gratefully acknowledge the financial support of the Japan Society for the Promotion of Science (Grant-in-Aid for JSPS fellows) and the Global COE Program "Catalysis as the Basis for Innovation in Materials Science" from the Ministry of Education, Culture, Sports, Science and Technology, Japan.

Finally, I am particularly grateful to my family, Kiichi Tanaka, Matsue Tanaka, Toshio Miyata, Atsuko Miyata, and Kazuna Miyata, for their constant understanding and support.

Contents

Chapter 1
General Introduction

1.1 Luminescence of Trivalent Lanthanide Ion

The luminescence properties of lanthanide (rare-earth) compounds have been fascinating many researchers for decades [1–9]. An attractive feature of luminescent lanthanide compounds is their line-like emission, which results in a high color purity of the emitted light. The trivalent ions of the lanthanide series are characterized by a gradual filling of the 4f orbitals, from $4f^0$ (for La(III)) to $4f^{14}$ (Lu(III)) as summarized in Table 1.1. One of the most interesting features of these ions is their photoluminescence. Several lanthanide ions show luminescence in the visible or near-infrared spectral regions upon irradiation with ultraviolet (UV) radiation. The color of the emitted light depends on the lanthanide ion. For instance, Eu(III) emits red light, Tb(III) green light, Sm(III) orange light, and Tm(III) blue light. Yb(III), Nd(III), and Er(III) are well-known for their near-infrared luminescence, and Gd(III) emits in the UV region. Therefore, lanthanide(III) compounds are the popular luminescent materials for application in electroluminescent (EL) devices, optical amplifiers, lasers, bio-sensing, and so on.

The lanthanides in the stable (III) oxidation state are simply characterized by an incompletely filled 4f shell. The 4f orbital is shielded from the surroundings by the filled $5s^2$ and $5p^2$ orbitals. Therefore, the influence of the host media on the optical transition within the $4f^n$ configuration is small. The energy levels of the trivalent Eu ion are given in Fig. 1.1. The energy levels are actually split by the geometric field (crystal or ligand fields). As a matter of fact, the splitting is very small due to the shielding by $5s^2$ and $5p^2$ electrons, whereas the geometric field strength in the case of the transition metal ions (d^n) is characteristically several tens of thousands of cm^{-1}; for the lanthanide(III) ions (f^n), it amounts to several hundreds of cm^{-1}.

In a configurational coordinate diagram, these level appear as parallel parabolas (small off-set, Fig. 1.2), because the 4f electrons are well shielded from their surroundings. Emission transitions yield, therefore, sharp lines in the spectra. The emission of light radiation for lanthanide(III) ions comes mainly from the electric dipole transition. Transitions that occur in the 4f inner shell of free ions are forbidden because they do not correspond to a change of parity. However, the

K. Miyata, *Highly Luminescent Lanthanide Complexes with Specific Coordination Structures*, Springer Theses,
DOI: 10.1007/978-4-431-54944-4_1, © Springer Japan 2014

Table 1.1 Electronic structure of the trivalent lanthanide ions

Element	Symbol	Atomic number (Z)	Configuration Ln(III)	Ground state Ln(III)
Lanthanum	La	57	[Xe]	$^1S_0$
Cerium	Ce	58	[Xe]$4f^1$	$^2F_{5/2}$
Praseodymium	Pr	59	[Xe]$4f^2$	$^3H_4$
Neodymium	Nd	60	[Xe]$4f^3$	$^4I_{9/2}$
Promethium	Pm	61	[Xe]$4f^4$	$^5I_4$
Samarium	Sm	62	[Xe]$4f^5$	$^6H_{5/2}$
Europium	Eu	63	[Xe]$4f^6$	$^7F_0$
Gadolinium	Gd	64	[Xe]$4f^7$	$^8S_{7/2}$
Terbium	Tb	65	[Xe]$4f^8$	$^7F_6$
Dysprosium	Dy	66	[Xe]$4f^9$	$^6H_{15/2}$
Holmium	Ho	67	[Xe]$4f^{10}$	$^5I_8$
Erbium	Er	68	[Xe]$4f^{11}$	$^4I_{15/2}$
Thulium	Tm	69	[Xe]$4f^{12}$	$^3H_6$
Ytterbium	Yb	70	[Xe]$4f^{13}$	$^2F_{7/2}$
Lutetium	Lu	71	[Xe]$4f^{14}$	$^1S_0$

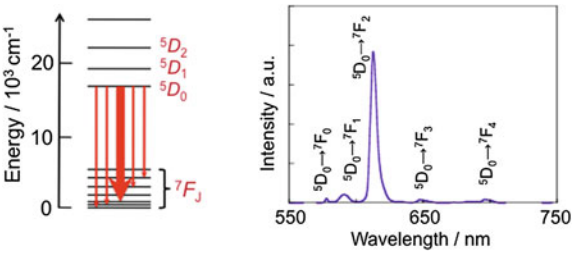

Fig. 1.1 The energy levels and emission spectra of Eu(III) ions

transitions that are forbidden by odd parity become partially allowed by mixing 4f and 5d states through the ligand field. Since the parity does not change dramatically in such a transition, the lifetime of the excited state is long (>1 μs).

1.2 Luminescent Lanthanide Complex

The 1930s and early 1940s witnessed the first spectroscopic studies of lanthanide ions in solution. Freed et al. found that the relative intensities of the absorption lines of Eu(III) were different in various solvents [10], and Weissman discovered that complexes of Eu(III) with certain ultraviolet absorbing ligands were highly luminescent when excited with ultraviolet light [11]. Since Eu(III) itself has only a few very weak absorption bands, the solution of this ion does not exhibit very bright luminescence. Obviously, certain organic ligands can serve to photosensitize the luminescence of lanthanide ions. It was also found that lanthanide ions

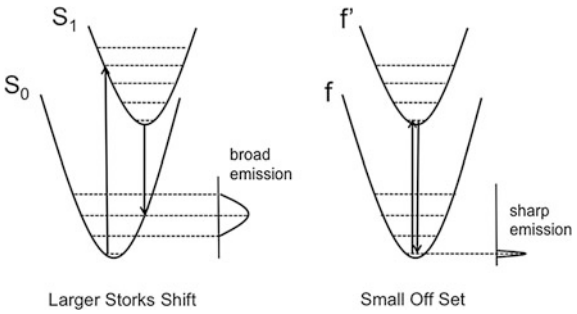

Fig. 1.2 Comparison of the emission process of lanthanide(III) ions with that of general organic compounds or metal complexes

quench the fluorescence of organic ligands [12]. Those studies can be considered as the starting points for the research and development of luminescent lanthanide complexes. It took, however, about 20 years before photochemists took a serious interest in these materials. At the 1990s, the field received a new impulse when it became clear that lanthanide complexes could find widespread use in medical diagnostics [13]. In the second half of that decade, lanthanide ions also started to receive the attention of the growing group of supramolecular chemists.

Luminescent lanthanide complexes consist of a lanthanide ion encapsulated in a ligand. Generally speaking, the ligand can be tailored to contain built-in functionalities that give the overall complex desired properties. Parameters such as solubility, electrochemical activity, binding affinity for other molecular building blocks, responsively to external stimuli (such as the presence of certain ions) etc. are all influenced by the overall structure of the ligand. In most cases, the ligand contains a light-absorbing group in the form of an organic chromophore as illustrated in Fig. 1.3a [14–21]. Such a group is generally referred to as the antenna chromophore, in analogy to the light-harvesting center in photo-synthetic reaction center. The photonic energy absorbed by this antenna can be transferred to the encapsulated lanthanide ion, thus circumventing the photo-excitation bottleneck posed by the small absorption of lanthanide ions.

Indirect excitation, in other words, sensitization has to be used and proceeds in three steps. First, light is absorbed by the immediate environment of the Ln(III) ion through the attached organic ligands. Energy is then transferred onto one or several excited states of the metal ion, and finally, the metal ion emits light. A multitude of organic ligands bearing aromatic chromophores has been proposed for this purpose, derived, for instance, from bipyridine, terpyridine, terphenylene, quinoline, or substituted phenyl and naphthyl groups. Although often discussed and modeled in terms of a simple ligand (S_1) → ligand (T_1) → Ln* energy flow which can be optimized by adjusting the energy gap between the lowest ligand triplet state and the Ln(III) emitting level [22–24], sensitization of trivalent lanthanide ions is an exceedingly complex process involving numerous rate constants (Fig. 1.3b) [25, 26]. The characteristic luminescent properties of lanthanide complexes have been extensively studied [27–69].

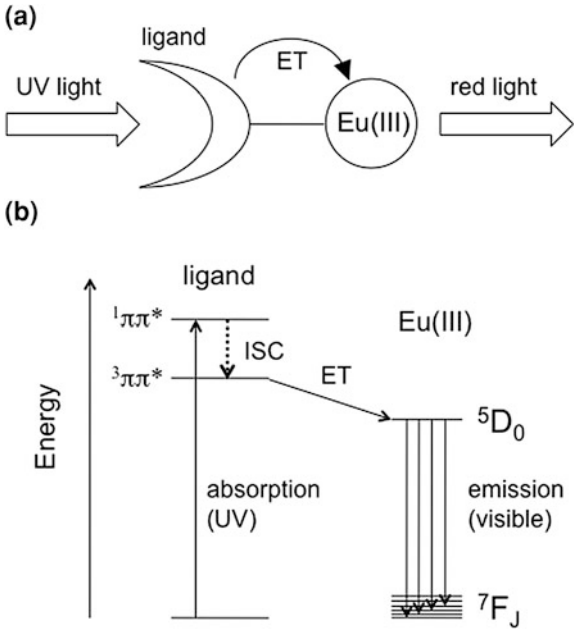

Fig. 1.3 **a** A schematic representation of the antenna effect occurring in monometallic Eu(III) complexes possessing aromatic light-harvesting chromophores and **b** associated energy level diagram (ISC = intersystem crossing, ET = energy transfer)

The author describes the strategies for design of strong-luminescent lanthanide complexes from the next section.

1.3 Molecular Design for Enhancement of Luminescence of Lanthanide Complex

1.3.1 Suppression of Vibrational Relaxation

The energy transfer process via vibrational excitation has been considered as a dominant process that quenches the excited states of lanthanide ion. For instance, in the case of Nd(III), the difficulty in the enhancement of luminescence of Nd(III) in liquid systems is explained as being due to the radiationless relaxation of the emitting level ($^4F_{3/2}$) via vibrational excitation of the liquid matrix, which is made up of ligand and solvent molecules (Fig. 1.4a). The vibrational transition probability is proportional to the Frank–Condon factor, i.e., the overlap integrals between the energy gap and the vibrational energy. In terms of the energy gap theory, the rate constant for the radiationless transition W_{RT} is given by the following expression:

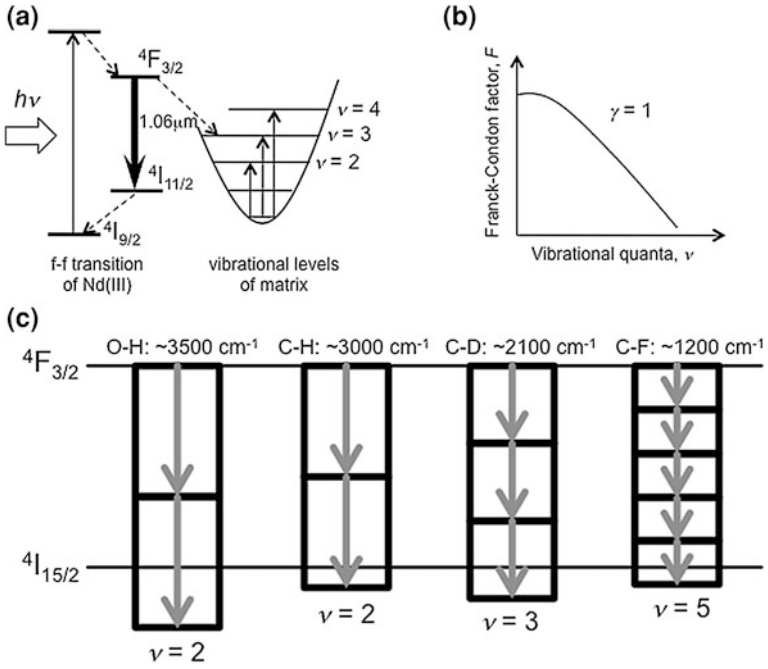

Fig. 1.4 **a** The radiationless transition via vibrational relaxation, **b** Franck–Condon function, **c** the vibrational energy levels and matching the electronic energy gap of Nd(III) ion

$$W_{RT} = \frac{2\pi\rho}{\hbar} J^2 F \tag{1.1}$$

where ρ is the density of states, J is the coupling constant between the electronic wave functions due to nuclear motion, and F the Frank–Condon factor. The factor F should be estimated quantitatively when the approximation using the undistorted oscillator model is adopted. In the model, F is given by

$$F = \frac{\exp(-\gamma)\gamma^{v}}{v!} \tag{1.2}$$

If γ is assumed to be 1, the Frank–Condon factor decreases with increasing vibrational quantum number v, as shown in Fig. 1.4b. The energy gap of the crucial radiative transition in Nd(III) ($^4F_{3/2}$–$^4I_{15/2}$: 5400 cm^{-1}) matches well the vibrations of the C–H and O–H bonds (5900 and 6900 cm^{-1}, respectively) with vibrational quantum number $v = 2$, and vibrational excitation leads to effective quenching of the excited state of Nd(III). In contrast, C–D, C–O, C–C, and C–F bonds give larger vibrational quanta ($v = 3$, 5 Fig. 1.4c). In theoretical calculations, the Frank–Condon factors of C–H and C–F are determined to be 0.18 and 0.0031, respectively. These facts suggest that if organic ligands surrounding

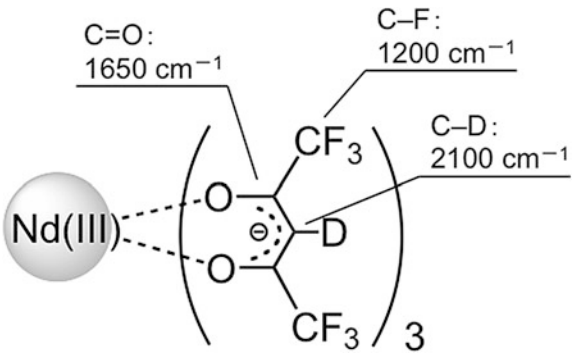

Fig. 1.5 Chemical structure of $Nd(hfa\text{-}D)_3$

Nd(III) ion can be constructed with C–D and C–F bonds instead of C–H bonds, the radiationless transition through vibrational excitation should be suppressed (Fig. 1.5). This theoretical understanding led to the first successful utilization of deuterated hexafluoroacetylacetone (hfa-D) as an effective ligand, which enables the resulting Nd(III) complex to exhibit near-infrared luminescence. The absence of C–H and O–H vibrations should make it possible to observe luminescence from Nd(III) in an organic solvent [70].

1.3.2 Control of Coordination Structure

The luminescence properties of lanthanide complexes are mainly derived from the electric transitions in 4f orbitals. Generally, 4f orbitals of lanthanide are shielded from direct perturbations by outer filled 5s and 5p shells [71]. The electric dipole transitions from the 4f inner shell of lanthanide ions are intrinsically forbidden because of their odd parity. However, they can be partially allowed upon mixing 4f and 5d states through the ligand field effects. The partially allowed transitions and electrically shielded nature of the excited states promote long emission lifetimes and characteristic sharp emission bands. Radiative rates of lanthanide complexes are linked to their geometric structures. If there is no inversion symmetry at the lanthanide ion sites, uneven ligand field components can mix with opposite-parity states in $4f^n$-configuration levels. Electric dipole transitions of lanthanide complexes are then no longer strictly forbidden in the ligand fields, resulting in faster radiative rates and higher emission quantum yields. Richardson and Reid have estimated the transition intensity parameters of lanthanide complexes from the ligand field [72, 73]. Binnemans has proposed to evaluate the transition intensity by using Judd-Ofelt analysis [14]. Since these studies, it has been widely accepted that the radiative transition probability between 4f orbitals is enhanced by reducing the coordination structure's geometrical symmetry [74–82].

In order to prepare intensely luminescent lanthanide complexes, a large radiative rate constant is necessary based on reducing the geometrical symmetry.

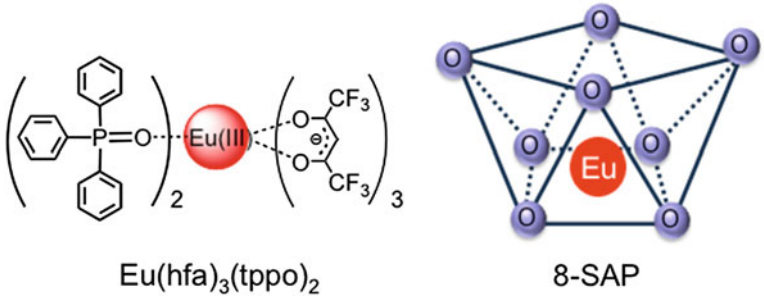

Fig. 1.6 Chemical and coordination structure of $Eu(hfa)_3(tppo)_2$

Lanthanide complexes with odd parity can be created using certain geometric and coordination structures. Hasegawa has reported on Eu(III) complexes with low-vibrational frequency (LVF) hfa (hexafluoroacetylacetone) and tppo (triphenylphosphine oxide) ligands, $Eu(hfa)_3(tppo)_2$, for which the chemical structure is shown in Fig. 1.6 [83]. The coordination structure composed of LVF phosphine oxides (P = O: 1125 cm^{-1}) and hfa ligands are expected to provide the Eu(III) complex with a high emission quantum yield and a relatively small nonradiative rate constant. The coordination geometry of $Eu(hfa)_3(tppo)_2$ is categorized as a square antiprism (8-SAP) which has no inversion center. The characteristic 8-SAP structure is composed of three hfa and two tppo ligands, which leads to a reduction of the geometrical symmetry of the Eu(III) complex and consequently $Eu(hfa)_3(tppo)_2$ shows a high emission quantum yield ($\Phi = 65$ %) and a fast radiative rate constant.

1.4 Lanthanide Complex with Thermostability

Lanthanide complexes have been also recognized as attractive compounds for fabricating lanthanide-doped polymers which are applicable to luminescent displays, plastic optical devices, and thin-film lasers [84–86]. In order to achieve the effective luminescence of lanthanide ion in polymer matrices, lanthanide complexes are required to possess high thermal stability. Luminescent plastics including lanthanide complexes are manufactured by mixing plasticizers and polymers at extremely high temperature. For example, polycarbonate, which is one of the major plastics for industrial products, is processed at 290 °C [87]. The thermostability of lanthanide complexes should be stable above 300 °C for optic applications such as lightings, displays, and optoelectronic devices. With this criterion in mind, Manseki has developed thermostable tetranuclear Eu(III) complexes, $[Eu_4(\mu\text{-}O)(L)_{10}]$ (L = 2-hydroxy-4-octyloxybenzophenone), having effective photosensitized luminescence as illustrated in Fig. 1.7 [88]. Differential scanning calorimetry (DSC) measurements indicated that the decomposition points

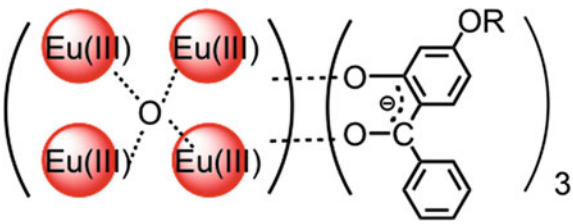

Fig. 1.7 Chemical structure of $[Eu_4(\mu\text{-}O)(L)_{10}]$ (L = 2-hydroxy-4-octyloxy benzophenone)

of tetranuclear Eu(III) complexes were 309 °C. Although many types of luminescent organic dyes are generally decomposed at temperatures under 200 °C, this disadvantage can be overcome by using polynuclear complex and coordination polymer (Sect. 1.5).

1.5 Lanthanide Coordination Polymer

Lanthanide coordination polymers and metal-organic frameworks composed of lanthanide ions and organic linker ligands have attracted considerable attention. The one-dimensional alternating sequence of metal ions and organic ligands exhibits remarkable characteristics as novel organic materials with (1) ease of preparation, (2) various structures, and (3) unique physical properties by the combination of metal ions and organic ligands [89–94]. Although lanthanide coordination polymers have been an active research field for about a decade [95–98], most of the attention has been paid to the structural characterization of these compounds. More recently, luminescence studies of the coordination polymers have been reported [99–106].

One of the significant characteristics of coordination polymers is their high thermal stability as well as polynuclear complexes. For instance, Carlos has reported novel three-dimensional lanthanide-organic frameworks with 2, 5-pyridinedicarboxylic acid [107]. Reddy has developed thermostable Eu(III) coordination polymers with 4-(dipyridin-2-yl)aminobenzoate ligands [63]. However, their emission quantum yields have been relatively low, because previous lanthanide coordination polymers contain numerous C–H and O–H bonds close to the metal center, which lead to the radiationless transition via vibrational relaxations as introduced in Sect. 1.3 [108–110]. To enhance emission quantum yields of lanthanide coordination polymers, the coordination sites of the organic linker ligands should be composed of low-vibrational frequency (LVF) modes for the suppression of vibrational relaxation. Luminescent coordination polymer with both high thermostability and strong-luminescent property is required as a novel luminophore in the field of future opto-electronic devices.

1.6 Objectives

As mentioned above, design of coordination structures of lanthanide complexes enable precise manipulations of the electron transitions in f orbitals. The geometrical, vibrational, and steric structures of lanthanide complexes are directly linked to luminescence properties such as emission quantum yield, radiative, and nonradiative rate constants. The control of the coordination structures of lanthanide complexes is expected to provide desirable emission properties. Lanthanide polynuclear complexes and coordination polymers have been also studied from the viewpoint of thermostability of complexes. However, the correlation between coordination structures and photophysical properties of lanthanide complexes has been scarcely investigated, and the optimum coordination environment for strong-luminescent properties has been still unclear. Additionally, lanthanide coordination polymer with both high thermostability and strong-luminescent properties has not been previously reported.

In this thesis, the control of coordination structures and functionalization of luminescent lanthanide(III) complexes with LVF hfa and phosphine oxide ligands were investigated. In particular, the author constructed (1) lanthanide coordination polymer with thermostability and thermosensing ability and (2) lanthanide complexes with novel asymmetric coordination structures to improve their emission quantum yields.

1.7 Contents of this Thesis

This thesis consists of a total of seven chapters. In this chapter, the previous studies are overviewed and the significance and objectives in this study are described. In Chap. 2, lanthanide coordination polymers composed of Eu(III) ions and phosphine oxide linkers are proposed to improve thermostability of lanthanide compounds. The characteristic structures, thermogravimetric analyses and remarkable photophysical properties of coordination polymers are also demonstrated. Chapter 3 presents a novel temperature-sensing material, chameleon luminophore, that has a high thermostability and thermosensing ability based on the results of Chap. 2. It is composed of color-changing luminescent coordination polymers containing Eu(III) and Tb(III) ions. The dual emission bands of Eu(III) and Tb(III) ions are expected to enable more accurate temperature measurements than previous lanthanide complexes. Temperature-sensing dyes with thermostable structures and dual sensing units are demonstrated for the first time. In Chap. 4, novel nona-coordinated Eu(III) complexes with three kinds of low-vibrational frequency triphosphine oxides are reported. The characteristic luminescence properties of nona-coodinated Eu(III) complexes are elucidated in terms of geometrical, vibrational, and chemical structures. In Chap. 5, Eu(III) and Sm(III) complexes with novel asymmetric structures composed of oxo-linked bidentate phosphine

oxides are reported. From the results of the structural and photophysical measurements, remarkably strong luminescence properties of lanthanide complexes with characteristic trigonal dodecahedron structures (8-TDH) are demonstrated for the first time. Based on the findings of Chap. 5, solvent-dependent luminescence of octa-coordinated Eu(III) complexes are described in Chap. 6. The relationships between photophysical properties and coordination structures in various organic media are discussed. Finally, all the results and achievements in this study are summarized in Chap. 7.

References

1. J.-C.G. Bünzli, *Luminescent Probes. In Lanthanide Probes in Life, Chemical and Earth Sciences: Theory and Practice* (Elsevier, Amsterdam, 1989)
2. A.J. Kenyon, Prog. Quantum Electron. **26**, 225 (2002)
3. G. Blasse, B.C. Grabmaier, *Luminescent Materials* (Spinger-Verlag, Berlin, 1994)
4. G. Blasse, Prog. Solid State Chem. **18**, 79 (1988)
5. M. Elbanowski, B. Makowsaka, J. Photochem. Photobiol. A **99**, 85 (1996)
6. J.-C.G. Bünzli, C. Piguet, Chem. Soc. Rev. **2005**, 34 (1048)
7. Y. Hasegawa, Y. Wada, S. Yanagida, J. Photochem. Photobiol. C **5**, 183 (2004)
8. B.M. Tissue, Chem. Mater. **10**, 2837 (1998)
9. K. Binnemans, Chem. Rev. **109**, 4283 (2009)
10. S. Freed, S.I. Weissman, F.E. Fortress, H.F. Jacobson, J. Chem. Phys. **7**, 824 (1939)
11. S.I. Weissman, J. Chem. Phys. **10**, 214 (1942)
12. P. Yuster, S.I. Weissman, J. Chem. Phys. **17**, 1182 (1949)
13. I. Hemmila, J. Alloy Compd. **225**, 480 (1995)
14. K. Binneman, R. Van Deun, C. Gorller-Walrand, S.R. Collinson, F. Martin, D.W. Bruce, C. Wickleder, Phys. Chem. Chem. Phys. **2**, 3753 (2000)
15. F.R. Goncalves e Silva, R. Longo, O.L. Malta, C. Piguet, J.-C.G. Bünzli, Phys. Chem. Chem. Phys.**2**, 5400 (2000)
16. D.M. Epstein, L.L. Chappell, H. Khalili, R.M. Supkowski, W.D. Horrocks Jr, J.R. Morrow, Inorg. Chem. **39**, 2130 (2000)
17. N. Fatin-Rouge, E. Toth, D. Perret, R.H. Backer, A.E. Merbach, J.-C.G. Bünzli, J. Am. Chem. Soc. **122**, 10810 (2000)
18. J.J. Lessmann, W.D. Horrocks Jr, Inorg. Chem. **39**, 3114 (2000)
19. M.D. McGehee, M.A. Diaz-Garcia, F. Hide, R. Gupta, E.K. Miller, D. Moses, A.J. Heeger, Appl. Phys. Lett. **72**, 1536 (1998)
20. P.J. Skinner, A. Beeby, R.S. Dickins, D. Parker, S. Aime, M. Botta, J. Chem. Soc. Perkin 2 **7**, 1329 (2000)
21. H. Tsukube, M. Hosokubo, M. Wada, S. Shinoda, H. Tamiaki, Inorg. Chem. **40**, 740 (2001)
22. M. Latva, H. Takalob, V.M. Mukkala, C. Matachescu, J.C. Rodriguez-Ubis, J. Kankare, J. Lumin. **75**, 149 (1997)
23. F. Gutierrrez, C. Tedeschi, L. Maron, J.P. Daudey, R. Poteau, J. Azema, P. Tisnes, C. Picard, Dalton Trans. 1334 (2004)
24. R.D. Archer, H. Chen, L.C. Thompson, Inorg. Chem. **37**, 2809 (1998)
25. F.R. Goncalves e Silva, O.L. Malta, C. Reinhard, H.U. Gudel, C. Piguet, J.E. Moser, J.-C.G. Bünzli, J. Phys. Chem. A **106**, 1670 (2002)
26. G.F. De Sa, O.L. Malta, C. De Mello Donega, A.M. Simas, R.L. Longo, P.A. Santa-Cruz, E.F. Da Silva Jr, Coord. Chem. Rev. **196**, 165 (2000)
27. R. Pal, D. Parker, Chem. Commun. 474 (2007)

28. G.S. Kottas, M. Mehlstäubl, R. Fröhlich, L. De Cola, Eur. J. Inrog. Chem. **22**, 3465 (2007)
29. S. Petoud, G. Muller, E.G. Moore, J. Xu, J. Sokolnicki, J.P. Riehl, U.N. Le, S.M. Cohen, K.N. Raymond, J. Am. Chem. Soc. **129**, 77 (2007)
30. J.P. Leonard, P. Jensen, T. McCabe, J.E. O'Brien, R.D. Peacock, P.E. Kruger, T. Gunnlaugsson, J. Am. Chem. Soc. **129**, 10986 (2007)
31. A. De Bettencourt-Dias, S. Viswanathan, A. Rollett, J. Am. Chem. Soc. **129**, 15436 (2007)
32. X.Y. Chen, X. Yang, B.J. Holliday, J. Am. Chem. Soc. **130**, 1546 (2008)
33. E.G. Moore, J. Xu, C.J. Jocher, I. Castro-Rodriguez, K.N. Raymond, Inorg. Chem. **47**, 3105 (2008)
34. O. Moudam, B.C. Rowan, M. Alamiry, P. Richardson, B.S. Richards, A.C. Jones, N. Robertson, Chem. Commun. 6649 (2009)
35. M. Osawa, M. Hoshino, T. Wada, F. Hayashi, S. Osanai, J. Phys. Chem. A **113**, 10895 (2009)
36. D.P. Li, C.H. Li, J. Wang, L.C. Kang, T. Wu, Y.Z. Li, X.Z. You, Eur. J. Inorg. Chem. **2009**, 4844 (2009)
37. N.M. Shavaleev, S.V. Eliseeva, R. Scopelliti, J.-C.G. Bünzli, Chem. Eur. J. **15**, 10790 (2009)
38. G.E. Kiefer, M. Woods, Inorg. Chem. **48**, 11767 (2009)
39. K.A. White, D.A. Chengelis, K.A. Gogick, J. Stehman, N.L. Rosi, S. Petoud, J. Am. Chem. Soc. **131**, 18069 (2009)
40. D.B. A. Raj, S. Biju, M.L.P. Reddy, Dalton Trans. 7519 (2009)
41. B. McMahon, P. Mauer, C.P. McCoy, T.C. Lee, T. Gunnlaugsson, J. Am. Chem. Soc. **131**, 17542 (2009)
42. M.-H. Ha-Thi, J.A. Delaire, V. Michelet, I. Leray, J. Phys. Chem. A **114**, 3264 (2010)
43. J.-C.G. Bünzli, Chem. Rev. **110**, 2729 (2010)
44. M. Tropiano, N.L. Kilah, M. Morten, H.R.J.J. Davis, P.D. Beer, S. Faulkner, J. Am. Chem. Soc. **133**, 11847 (2011)
45. D. Sykes, M.D. Ward, Chem. Commun. **47**, 2279 (2011)
46. M. Sturzbecher-Hoehne, C.N.P. Leung, A. D'Aléo, B. Kullgren, A.-L. Prigent, D.K. Shuh, K.N. Raymond, R.J. Abergel, Dalton Trans. **40**, 8340 (2011)
47. C.M. Andolina, J.R. Morrow, Eur. J. Inorg. Chem. **2011**, 154 (2011)
48. J. Andres, A.-S. Chauvin, Inorg. Chem. **50**, 10082 (2011)
49. Q.-B. Bo, H.-Y. Wang, D.-Q. Wang, Z.-W. Zhang, J.-L. Miao, G.-X. Sun, Inorg. Chem. **50**, 10163 (2011)
50. S.V. Eliseeva, D.N. Pleshkov, K.A. Lyssenko, L.S. Lepnev, J.-C.G. Bünzli, N.P. Kuzmina, Inorg. Chem. **50**, 5137 (2011)
51. J. An, C.M. Shade, D.A. Chengelis-Czegan, S. Petoud, N.L. Rosi, J. Am. Chem. Soc. **133**, 1220 (2011)
52. D.J. Lewis, P.B. Glover, M.C. Solomons, Z. Pikramenou, J. Am. Chem. Soc. **2011**, 133 (1033)
53. M. Varlan, B.A. Blight, S. Wang, Chem. Commun. **48**, 12059 (2012)
54. D.G. Smith, B.K. McMahon, R. Pal, D. Parker, Chem. Commun. **48**, 8520 (2012)
55. R.M. Edkins, D. Sykes, A. Beeby, M.D. Ward, Chem. Commun. **48**, 9977 (2012)
56. A. Nonat, M. Regueiro-Figueroa, D. Esteban-Gomez, A. de Blas, T. Rodríguez-Blas, C. Platas-Iglesias, L.J. Charbonnière, Chem. Eur. J. **18**, 8163 (2012)
57. S. Nadella, P.M. Selvakumar, E. Suresh, P.S. Subramanian, M. Albrecht, M. Giese, R. Frohlich, Chem. Eur. J. **18**, 16784 (2012)
58. D.G. Smith, R. Pal, D. Parker, Chem. Eur. J. **18**, 11604 (2012)
59. E.S. Andreiadis, D. Imbert, J. Pécaut, R. Demadrille, M. Mazzanti, Dalton Trans. **41**, 1268 (2012)
60. D.J. Lewis, F. Moretta, A.T. Holloway, Z. Pikramenou, Dalton Trans. **41**, 13138 (2012)
61. Y.-A. Li, S.-K. Ren, Q.-K. Liu, J.-P. Ma, X. Chen, H. Zhu, Y.-B. Dong, Inorg. Chem. **51**, 9629 (2012)
62. S. Mohapatra, S. Adhikari, H. Riju, T.K. Maji, Inorg. Chem. **51**, 4891 (2012)

63. A.R. Ramya, D. Sharma, S. Natarajan, M.L.P. Reddy, Inorg. Chem. **51**, 8818 (2012)
64. A. de Bettencourt-Dias, P.S. Barber, S. Bauer, J. Am. Chem. Soc. **134**, 6987 (2012)
65. M.O. Rodrigues, J.D.L. Dutra, L.A.O. Nunes, G.F. de Sá, W.M. de Azevedo, P. Silva, F.A.A. Paz, R.O. Freire, S.A. Júnior, J. Phys. Chem. C **116**, 19951 (2012)
66. K.-N.T. Hua, J. Xu, E.E. Quiroz, S. Lopez, A.J. Ingram, V.A. Johnson, A.R. Tisch, A. de Bettencourt-Dias, D.A. Straus, G. Muller, Inorg. Chem. **51**, 647 (2012)
67. A. Ablet, S.-M. Li, W. Cao, X.-J. Zheng, W.-T. Wong, L.-P. Jin, Chem. Asian J. **8**, 95 (2013)
68. J. Xu, L. Jia, N. Jin, Y. Ma, X. Liu, W. Wu, W. Liu, Y. Tang, F. Zhou, Chem. Eur. J. **19**, 4556 (2013)
69. N. Wartenberg, O. Raccurt, E. Bourgeat-Lami, D. Imbert, M. Mazzanti, Chem. Eur. J. **19**, 3477 (2013)
70. Y. Hasegawa, K. Murakoshi, Y. Wada, S. Yanagida, J. Kim, N. Nakashima, T. Yamanaka, Chem. Phys. Lett. **248**, 8 (1996)
71. V.S. Sastri, J.-C.G. Bünzli, V.R. Rao, G.V.S. Rayudu, J.R. Perumareddi, *In Modern Aspects of Rare Earth and Their Complexes* (Elsevier, New York, 2003)
72. E.M. Stephens, M.F. Reid, F.S. Richardson, Inorg. Chem. **23**, 4611 (1984)
73. M.T. Devlin, E.M. Stephens, M.F. Reid, F.S. Richardson, Inorg. Chem. **26**, 1208 (1987)
74. S.F. Mason, R.D. Peacock, B. Stewart, Chem. Phys. Lett. **29**, 149 (1974)
75. S.F. Mason, J. Indian Chem. Soc. **63**, 73 (1986)
76. A.F. Kirby, F.S. Richardson, J. Phys. Chem. **87**, 2544 (1983)
77. M. Montalti, L. Prodi, N. Zaccheroni, L. Charbonnière, L. Douce, R. Ziessel, J. Am. Chem. Soc. **123**, 12694 (2001)
78. K. Driesen, P. Lenaerts, K. Binnemans, C. Görller-Walrand, Phys. Chem. Chem. Phys. **4**, 552 (2002)
79. W. Liu, T. Jiao, Y. Li, Q. Liu, M. Tan, H. Wang, L. Wang, J. Am. Chem. Soc. **126**, 2280 (2004)
80. J.P. Cross, M. Lauz, P.D. Badger, S. Petoud, J. Am. Chem. Soc. **126**, 16278 (2004)
81. P. Nockemann, B. Thijs, N. Postelmans, K.V. Hecke, L.V. Meervelt, K. Binnemans, J. Am. Chem. Soc. **128**, 13658 (2006)
82. A. Wada, M. Watanabe, Y. Yamanoi, T. Nankawa, K. Namiki, M. Yamasaki, M. Murata, H. Nishihara, Bull. Chem. Soc. Jpn **80**, 335 (2007)
83. Y. Hasegawa, M. Yamamuro, Y. Wada, N. Kanehisa, Y. Kai, S. Yanagida, J. Phys. Chem. A **107**, 1697 (2003)
84. T. Jüstel, H. Nikol, C. Ronda, Angew. Chem. Int. Ed. **37**, 3084 (1998)
85. J. Kido, Y. Okamoto, Chem. Rev. **102**, 2357 (2002)
86. J. Yu, L. Zhou, H. Zhang, Y. Zheng, H. Li, R. Deng, Z. Peng, Z. Li, Inorg. Chem. **44**, 1611 (2005)
87. E.S. Wilks, *Industrial Polymer Handbook* (Wiley-VCH, Weinheim, 2000), p. 291
88. K. Manseki, Y. Hasegawa, Y. Wada, S. Yanagida, J. Lumin. **111**, 183 (2005)
89. H. Li, M. Eddaoudi, M. O'Keeffe, O.M. Yaghi, Nature **402**, 276 (1999)
90. B. Moulton, M.J. Zaworotko, Chem. Rev. **101**, 1629 (2001)
91. S.L. James, Chem. Soc. Rev. **32**, 276 (2003)
92. S. Kitagawa, R. Kitaura, S. Noro, Angew. Chem. Int. Ed. **43**, 2334 (2004)
93. I.G. Georgiev, L.R. MacGillivray, Chem. Soc. Rev. **36**, 1239 (2007)
94. R. Cao, D.F. Sun, Y.C. Liang, M.C. Hong, K. Tatsumi, Q. Shi, Inorg. Chem. **41**, 2087 (2002)
95. L. Pan, X.Y. Huang, J. Li, Y.G. Wu, N.W. Zheng, Angew. Chem. Int. Ed. **39**, 527 (2000)
96. L. Pan, K.M. Adams, H.E. Hernandez, X.T. Wang, C. Zheng, Y. Hattori, K. Kaneko, J. Am. Chem. Soc. **125**, 3062 (2003)
97. D. L. Long, A. J. Blake, N. R. Champness, M. Schroder, Chem. Commun. 1369 (2000)
98. O. Guillou, C. Daiguebonne, Lanthanide-containing coordination polymers. In *Handbook on the Physics and Chemistry of Rare Earths*, Vol. 34, Chapter 221, 359, ed by K.A. Gschneidner Jr., J.-C.G. Bünzli, V. Pescharsky (Elsevier, Amsterdam, 2004), p. 359

99. J. Rocha, L.D. Carlos, Curr. Opin. Solid State Mater. Sci. **7**, 199 (2003)
100. M.D. Allendorf, C.A. Bauer, R.K. Bhakta, R.J.T. Houk, Chem. Soc. Rev. **38**, 1330 (2009)
101. M. Eddaoudi, D.B. Moler, H.L. Li, B.L. Chen, T.M. Reineke, M. O'Keeffe, O.M. Yaghi, Acc. Chem. Res. **34**, 319 (2001)
102. A.K. Cheetham, C.N.R. Rao, R.K. Feller, Chem. Commun. 4780 (2006)
103. C. Daiguebonne, N. Kerbellec, K. Bernot, Y. Gerault, A. Deluzet, O. Guillou, Inorg. Chem. **45**, 5399 (2006)
104. X. Guo, G. Zhu, F. Sun, Z. Li, X. Zhao, X. Li, H. Wang, S. Qiu, Inorg. Chem. **45**, 2581 (2006)
105. L. Pan, N. Zheng, Y. Wu, S. Han, R. Yang, X. Huang, J. Li, Inorg. Chem. **40**, 828 (2001)
106. X.P. Yang, R.A. Jones, J.H. Rivers, R.P.J. Lai, Dalton Trans. 3936 (2007)
107. L.D. Carlos, R.A.S. Ferreira, V. de Zea, Bermudez, B. Julian-Lopez, P. Escribano. Chem. Soc. Rev. **40**, 536 (2011)
108. Y. Hasegawa, Y. Kimura, K. Murakoshi, Y. Wada, J. Kim, N. Nakashima, T. Yamanaka, S. Yanagida, J. Phys. Chem. **100**, 10201 (1996)
109. Y. Hasegawa, K. Murakoshi, Y. Wada, J. Kim, N. Nakashima, T. Yamanaka, S. Yanagida, Chem. Phys. Lett. **260**, 173 (1996)
110. G. Stain, E. Würzberg, J. Chem. Phys. **62**, 208 (1975)

Chapter 2
Luminescence Properties of Thermostable Lanthanide Coordination Polymers with Intermolecular Interactions

2.1 Introduction

Luminophores with high thermal stability are promising candidates as active materials for electroluminescent (EL) devices, lasers and luminescent biosensing applications. As described in Chap. 1, lanthanide polynuclear complexes, coordination polymers, and metal-organic frameworks have been widely studied from the viewpoint of thermostable structure [1–7]. For example, Marchetti has reported a thermostable coordination polymer with Eu(III) ions and 4-acyl-pyrazolone ligands [8]. Wang has also reported that the decomposition point of a lanthanide coordination polymer with glutaric acid is over 300 °C [9]. However, their emission quantum yields have been extremely low, because their coordination polymers are attributed to the nonradiative transition via vibrational relaxation of high-vibrational frequency O–H bonds in polymer structure [10, 11]. Luminescent coordination polymer with both high thermostability and emission quantum efficiency is required as a novel luminophore in the field of future opto-electronic devices.

Here, the author considers that the introduction of low-vibrational frequency (LVF) ligands as a linker part in the polymer chains would result in the preparation of a lanthanide coordination polymer with strong luminescence properties. Strongly luminescent lanthanide complexes composed of LVF hfa and bidentate phosphine oxide ligands have been described in former chapters. The author also proposes that the introduction of aromatic aryl groups in the linker part of lanthanide coordination polymer is effective for the construction of thermostable luminophores with intermolecular interactions, such as CH/F, π–π, and CH/π interactions.

In this chapter, the author reports on novel coordination polymers composed of Eu(III) ion and 4 types of aryl units; $[Eu(hfa)_3(dpb)]_n$, $[Eu(hfa)_3(dpbp)]_n$, $[Eu(hfa)_3(dpbt)]_n$, and $[Eu(hfa)_3(dppcz)]_n$ (dpb: 1,4-bis(diphenylphosphoryl) benzene, dpbp: 4,4′-bis(diphenylphosphoryl)biphenyl, dpbt: 4,4′-bis(diphenylphos phoryl)bithiophene, dppcz: 3,6-bis(diphenylphosphoryl)-9-phenylcarbazole) as shown in Fig. 2.1. Their thermal stabilities and luminescence properties are characterized by

K. Miyata, *Highly Luminescent Lanthanide Complexes with Specific Coordination Structures*, Springer Theses,
DOI: 10.1007/978-4-431-54944-4_2, © Springer Japan 2014

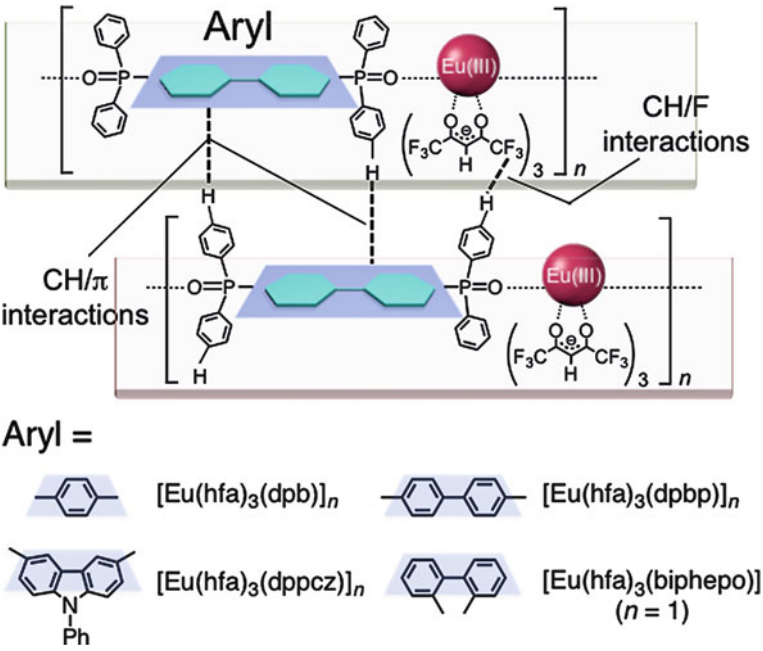

Fig. 2.1 Chemical structures of Eu(III) coordination polymers developed in this study

the thermogravimetric analyses (TGA and DSC), emission quantum yields, emission lifetimes, photosensitized energy transfer efficiency, and the nonradiative rate constants. In particular, $[Eu(hfa)_3(dppcz)]_n$ has both thermal stability (decomposition point =300 °C) and a high emission quantum yield ($\Phi_{Ln} = 83$ % in the solid state). Novel luminophores with heat durability are expected to open up new fields of material chemistry.

2.2 Experimental Section

2.2.1 General

The starting materials, 1,4-difluorobenzene (TCI, >95 %), 4,4′-dibromobiphenyl (TCI, >98 %), 2,2′-bithiophene (TCI, >98 %), 3,6-dibromo-9-phenylcarbazole (TCI, >98 %) were used as received. All other chemicals were reagent grade and were used without further purification. All reactions involving air- and moisture-sensitive reagents were carried out under an argon atmosphere using dried solvents. Synthetic routes of organic ligands are shown in Scheme 2.1. The preparation method of $[Eu(hfa)_3(H_2O)_2]$ was described in Chap 5. Infrared spectra were recorded on a JASCO FT/IR–350 spectrometer. ^{1}H NMR spectra were recorded on a

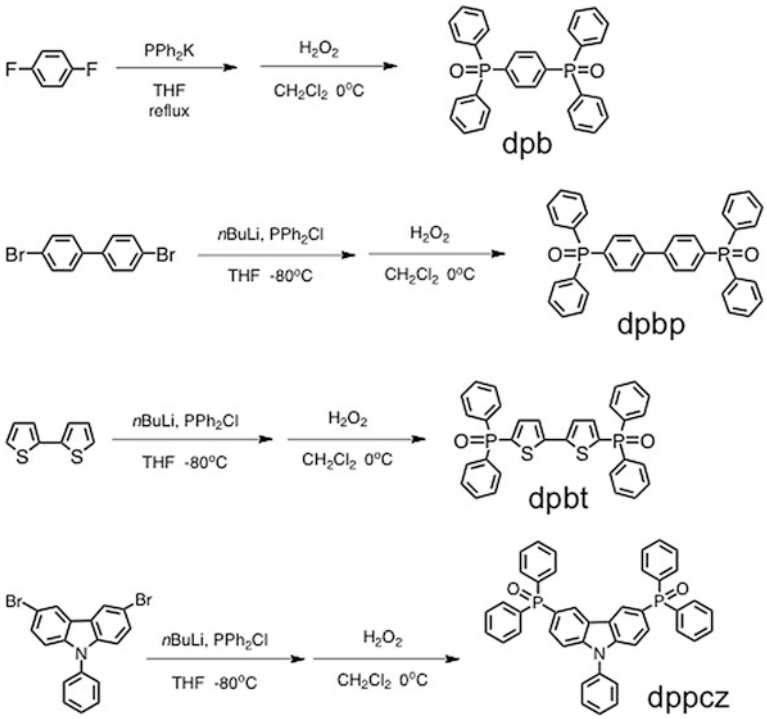

Scheme 2.1 Synthetic routes of organic ligands of Eu(III) coordination polymers

JEOL JNM-EX270 (270 MHz). ^{1}H NMR chemical shifts were determined by tetramethylsilane (TMS) as an internal standard. Elemental analysis and mass spectrometry were performed at the Instrumental Analysis Division in Hokkaido University. Thermogravimetric analysis was performed on a Rigaku TermoEvo TG8120 analyzer in an argon atmosphere at a heating rate of 1 °C min^{-1}. DSC measurement was performed on a MAC DSC3220 at a heating rate of 1 °C min^{-1}.

2.2.2 Syntheses

2.2.2.1 Preparation of 1,4-bis(diphenylphosphoryl)benzene (dpb)

1,4-bis(diphenylphosphoryl)benzene was synthesized according to the published procedure [12]. A solution of 1,4-difluorobenzene (0.80 mL, 8.0 mmol) was added dropwise to a solution of potassium diphenylphosphide (40 mL, 0.5 M THF, 20 mmol). The mixture was allowed to stir for 1 h and then was brought to reflux for 12 h. THF was removed under reduced pressure, and methanol (*ca.* 40 mL) was added. The mixture was then heated to reflux for 30 min. A gray precipitate

was formed, after which the methanol was decanted off. The obtained gray solid and dichloromethane (20 mL) were placed in a flask. The solution was cooled to 0 °C and then 30 % H_2O_2 aqueous solution (5 mL) was added to it. The reaction mixture was stirred for 2 h. The product was extracted with dichloromethane, the extracts washed with brine for three times and dried over anhydrous $MgSO_4$. The solvent was evaporated to afford a white powder. Recrystallization from dichloromethane for gave white crystals of the titled compound.

Yield: 2.5 g (66 %). ^{1}H NMR (270 MHz, $CDCl_3$, 25 °C) δ 7.48–7.78 (m, 24H; P-C_6H_5, C_6H_4) ppm. ESI–Mass (m/z) = 479.1 $[M+H]^+$. Anal. Calcd for $C_{30}H_{24}O_2P_2$: C, 75.31; H, 5.06. Found: C, 74.86; H, 5.11.

2.2.2.2 Preparation of 4,4′-bis(diphenylphosphoryl)biphenyl (dpbp)

4,4′-bis(diphenylphosphoryl)biphenyl was synthesized according to the published procedure [13–15]. A solution of *n*-BuLi (9.3 mL, 1.6 M hexane, 15 mmol), was added dropwise to a solution of 4,4′-dibromobiphenyl (1.9 g, 6.0 mmol) in dry THF (30 mL) at –80 °C. The addition was completed in *ca.* 15 min during which time a yellow precipitate was formed. The mixture was allowed to stir for 3 h at –10 °C, after which a PPh_2Cl (2.7 mL, 15 mmol) was added dropwise at –80 °C. The mixture was gradually brought to room temperature, and stirred for 14 h. The product was extracted with ethyl acetate, the extracts washed with brine for three times and dried over anhydrous $MgSO_4$. The solvent was evaporated, and resulting residue was washed with acetone and ethanol for several times. The obtained white solid and dichloromethane (40 mL) were placed in a flask. The solution was cooled to 0 °C and then 30 % H_2O_2 aqueous solution (5 mL) was added to it. The reaction mixture was stirred for 2 h. The product was extracted with dichloromethane, the extracts washed with brine for three times and dried over anhydrous $MgSO_4$. The solvent was evaporated to afford a white powder. Recrystallization from dichloromethane gave white crystals of the titled compound.

Yield: 1.7 g (54 %). IR (KBr): 1120 (st, P=O) cm^{-1}. ^{1}H NMR (270 MHz, $CDCl_3$, 25 °C) δ 7.67–7.80 (m, 16H; P-C_6H_5, C_6H_4), 7.45–7.60 (m, 12H; P-C_6H_5, C_6H_4) ppm. ESI–Mass (m/z) = 555.2 $[M+H]^+$. Anal. Calcd for $C_{36}H_{28}O_2P_2$: C, 77.97; H, 5.09. Found: C, 77.49; H, 5.20.

2.2.2.3 Preparation of 4,4′-bis(diphenylphosphoryl)bithiophene (dpbt)

A solution of *n*-BuLi (13 mL, 1.6 M hexane, 20 mmol), was added dropwise to a solution of 2,2′-bithiophene (1.2 g, 7.2 mmol) in dry THF (20 mL) at –80 °C. The addition was completed in *ca.* 15 min during which time a yellow precipitate was formed. The mixture was allowed to stir for 3 h at –10 °C, after which a PPh_2Cl (3.7 mL, 20 mmol) was added dropwise at –80 °C. The mixture was gradually brought to room temperature, and stirred for 18 h. The product was extracted with ethyl acetate, the extracts washed with brine for three times and dried over

anhydrous $MgSO_4$. The solvent was evaporated, and resulting residue was washed with methanol for several times. The obtained yellow solid and dichloromethane (40 mL) were placed in a flask. The solution was cooled to 0 °C and then 30 % H_2O_2 aqueous solution (10 mL) was added to it. The reaction mixture was stirred for 2 h. The product was extracted with dichloromethane, the extracts washed with brine for three times and dried over anhydrous $MgSO_4$. The solvent was evaporated to afford a yellow powder. Recrystallization from dichloromethane gave yellow crystals of the titled compound.

Yield: 1.4 g (31 %). IR (KBr): 1122 (st, P=O) cm^{-1}. ^1H NMR (270 MHz, $CDCl_3$, 25 °C) δ 7.45–7.79 (m, 20H; P-C_6H_5), 7.33–7.37 (m, 2H; C_4H_2S), 7.24–7.27 (m, 2H; C_4H_2S) ppm. ESI–Mass (*m/z*) = 567.1 $[M+H]^+$. Anal. Calcd for $C_{32}H_{24}O_2P_2S_2$: C, 67.83; H, 4.27. Found: C, 67.13; H, 4.40.

2.2.2.4 Preparation of 3,6-bis(diphenylphosphoryl)-9-phenylcarbazole (dppcz)

A solution of *n*-BuLi (8.8 mL, 1.6 M hexane, 14 mmol), was added dropwise to a solution of 3,6-dibromo-9-phenylcarbazole (2.4 g, 6.0 mmol) in dry THF (30 mL) at –80 °C. The addition was completed in *ca.* 10 min during which time a white yellow precipitate was formed. The mixture was allowed to stir for 2 h at –10 °C, after which a PPh_2Cl (2.6 mL, 14 mmol) was added dropwise at –80 °C. The mixture was gradually brought to room temperature, and stirred for 18 h to give a white precipitate. The precipitate was filtered, washed with methanol for several times, and dried in vacuo. The obtained white powder and dichloromethane (40 mL) were placed in a flask. The solution was cooled to 0 °C and then 30 % H_2O_2 aqueous solution (8 mL) was added to it. The reaction mixture was stirred for 2 h. The product was extracted with dichloromethane, the extracts washed with brine for three times and dried over anhydrous $MgSO_4$. The solvent was evaporated to afford a white powder. Recrystallization from dichloromethane/hexane gave colorless crystals of the titled compound. Yield: 2.0 g (53 %). IR (KBr): 1122 (st, P=O) cm^{-1}. ^1H NMR (270 MHz, $CDCl_3$, 25 °C) δ 8.43–8.47 (d, J = 10.8 Hz, 2H; P-C_6H_5), 7.63–7.76 (m, 11H; C_4H_2S), 7.43–7.60 (m, 18H; C_4H_2S) ppm. ESI–Mass (*m/z*) = 644.2 $[M+H]^+$. Anal. Calcd for $C_{43}H_{31}NO_2P_2$: C, 78.37; H, 4.85; N, 2.18. Found: C, 78.42; H, 5.00; N, 2.18.

2.2.2.5 General Procedure for the Preparation of Eu(III) Coordination Polymers

Phosphine oxide ligand (1 equiv.) and $[Eu(hfa)_3(H_2O)_2]$ (1 equiv.) were dissolved in chloroform–methanol. The solution was refluxed while stirring for 8 h, and the reaction mixture was concentrated to dryness. A single crystal suitable for X-ray structural determination of Eu(III) coordination polymer was obtained by the diffusion method of methanol–chloroform solution at room temperature.

[Eu(hfa)$_3$(dpb)]$_n$. Yield: 65 mg (42 %; for monomer). IR (KBr): 1652 (st, C=O), 1256–1145 (st, C–F), 1128 (st, P=O) cm^{-1}. ESI–Mass (*m/z*) = 1045.05 [Eu(hfa)$_2$(dpb)]$^+$, 2297.18 [Eu$_2$(hfa)$_5$(dpb)$_2$]$^+$. Anal. Calcd for [$C_{45}H_{27}EuF_{18}O_8P_2]_n$: C, 43.18; H, 2.17. Found: C, 43.12; H 2.28.

[Eu(hfa)$_3$(dpbp)]$_n$. Yield: 98 mg (67 %; for monomer). IR (KBr): 1653 (st, C=O), 1255–1145 (st, C–F), 1127 (st, P=O) cm^{-1}. ESI–Mass (*m/z*) = 1120.08 [Eu(hfa)$_2$(dpbp)]$^+$, 2447.15 [Eu$_2$(hfa)$_5$(dpbp)$_2$]$^+$. Anal. Calcd for [$C_{51}H_{31}EuF_{18}O_8P_2]_n$: C, 46.14; H, 2.35. Found: C, 45.59; H 2.49.

[Eu(hfa)$_3$(dpbt)]$_n$. Yield: 160 mg (68 %; for monomer). IR (KBr): 1651 (st, C=O), 1254–1145 (st, C–F), 1128 (st, P=O) cm^{-1}. ESI–Mass (*m/z*) = 1133.00 [Eu(hfa)$_2$(dpbt)]$^+$, 2473.02 [Eu$_2$(hfa)$_5$(dpbt)$_2$]$^+$. Anal. Calcd for [$C_{47}H_{27}EuF_{18}O_8P_2S_2]_n$: C, 42.14; H, 2.03. Found: C, 42.67; H 2.12.

[Eu(hfa)$_3$(dppcz)]$_n$. Yield: 110 mg (50 %; for monomer). IR (KBr): 1652 (st, C=O), 1256–1145 (st, C–F), 1128 (st, P=O) cm^{-1}. ESI–Mass (*m/z*) = 1210.13, [Eu(hfa)$_2$(dppcz)]$^+$, 1853.34, [Eu(hfa)$_2$(dppcz)$_2$]$^+$. Anal. Calcd for [$C_{57}H_{34}EuF_{18}NO_8P_2]_n$: C, 48.32; H, 2.42; N, 0.99. Found: C, 47.95; H, 2.77; N, 1.06.

2.2.3 Crystallography

Colorless single crystals of Eu(III) coordination polymers were mounted on a glass fiber using paraffin oil. All measurements were made on a Rigaku Mercury CCD area detector with graphite monochromated Mo-Kα radiation. All structures were solved by direct methods (SIR 2004) [16] and expanded using Fourier techniques. The non-hydrogen atoms were refined anisotropically. Hydrogen atoms were refined using the riding model. All calculations were performed using the Crystal Structure crystallographic software package except for refinement, which was performed using SHELXL-97 [17]. The author confirmed the CIF data using the check CIF/PLATON service.

2.2.4 Optical Measurements

Emission spectra of Eu(III) coordination polymers were measured on a JASCO F-6300-H spectrometer and corrected for the response of the detector system. Emission lifetimes (τ_{obs}) were measured using the third harmonics (355 nm) of a Q-switched Nd:YAG laser (Spectra Physics, INDI-50, fwhm = 5 ns, λ = 1064 nm) and a photomultiplier (Hamamatsu photonics, R5108, response time $\leq$1.1 ns). The Nd:YAG laser response was monitored with a digital oscilloscope (Sony Tektronix, TDS3052, 500 MHz) synchronized to the single-pulse excitation. Emission lifetimes were determined from the slope of logarithmic plots of the decay profiles. The emission quantum yields excited at 380 nm (Φ_{tot}) were estimated using JASCO F-6300-H spectrometer attached with JASCO ILF-533 integrating sphere unit

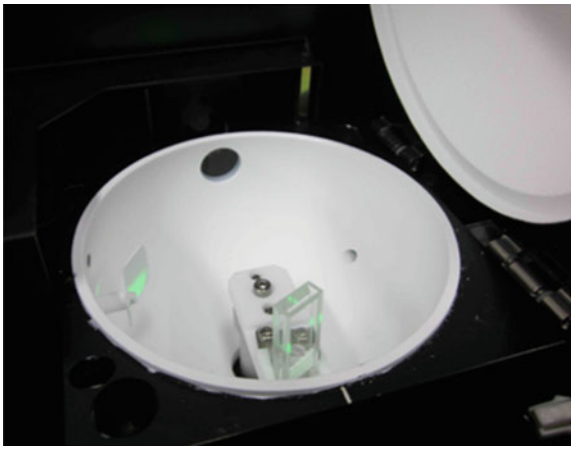

Fig. 2.2 JASCO ILF-533 integrating sphere unit

($\phi = 100$ mm, Fig. 2.2). The wavelength dependences of the detector response and the beam intensity of Xe light source for each spectrum were calibrated using a standard light source.

The photophysical properties of the Eu(III) coordination polymers in the solid state were investigated from estimation of the 4f–4f emission quantum yields (Φ_{Ln}), and the radiative (k_{r}) and nonradiative (k_{nr}) rate constants from the radiative (τ_{rad}) and observed lifetimes (τ_{obs}). The radiative lifetime is defined as an ideal emission lifetime without nonradiative processes. The radiative and observed lifetimes are expressed by

$$\tau_{rad} = \frac{1}{k_r} \tag{2.1}$$

$$\tau_{obs} = \frac{1}{k_r + k_{nr}} \tag{2.2}$$

Φ_{Ln}, k_{r}, and k_{nr} of the Eu(III) compounds are given by

$$\Phi_{Ln} = \frac{k_r}{k_r + k_{nr}} = \frac{\tau_{obs}}{\tau_{rad}} \tag{2.3}$$

$$\frac{1}{\tau_{rad}} = A_{MD,0} n^3 \left(\frac{I_{tot}}{I_{MD}} \right) \tag{2.4}$$

$$k_r = \frac{1}{\tau_{rad}} \tag{2.5}$$

$$k_{nr} = \frac{1}{\tau_{obs}} - \frac{1}{\tau_{rad}} \tag{2.6}$$

where $A_{MD,0}$ is the spontaneous emission probability for the $^5D_0$–$^7F_1$ transition in vacuo (14.65 s^{-1}), n is the refractive index of the medium (an average index of refraction equal to 1.5 was employed [18]), and (I_{tot}/I_{MD}) is the ratio of the total area of the corrected Eu(III) emission spectrum to the area of the $^5D_0$–$^7F_1$ band.

2.3 Results and Discussion

2.3.1 Coordination and Network Structures

Single crystals of Eu(III) coordination polymers with phosphine oxides, $[Eu(hfa)_3(dpb)]_n$, $[Eu(hfa)_3(dpbp)]_n$, $[Eu(hfa)_3(dpbt)]_n$, and $[Eu(hfa)_3(dppcz)]_n$ were successfully prepared for X-ray single crystal analyses by the diffusion method using methanol–chloroform solutions. The resulting crystal data are summarized in Fig. 2.3 and Table 2.1. The ORTEP views show that the phosphine oxide ligand acts as a bidentate bridge between lanthanide ions in one-dimensional polymeric chains. The coordination sites of $[Eu(hfa)_3(dpb)]_n$, $[Eu(hfa)_3(dpbp)]_n$, $[Eu(hfa)_3(dpbt)]_n$, and $[Eu(hfa)_3(dppcz)]_n$ comprise three hfa ligands and two phosphine oxide units. Their structures are categorized as an octa-coordinated square antiprism with no inverted center in the crystal field, so that enhancement of their luminescence properties is expected with allowed electronic transition probabilities [19, 20].

Selected bond lengths between Eu(III) ions and oxygen atoms in coordination sites (Eu–O and Eu–Eu distances) are summarized in Table 2.2. The Eu–Eu distances of $[Eu(hfa)_3(dpb)]_n$, $[Eu(hfa)_3(dpbp)]_n$, $[Eu(hfa)_3(dpbt)]_n$, and $[Eu(hfa)_3(dppcz)]_n$ were determined 9.91, 10.36, 10.60, and 11.76 Å, respectively. These distances may be longer than the critical distance for nonradiative dipole-dipole energy transfer between Eu(III) ions. Average Eu–O distances between Eu(III) ions and oxygen atoms of phosphine oxide ligands in $[Eu(hfa)_3(dpb)]_n$, $[Eu(hfa)_3(dpbp)]_n$, $[Eu(hfa)_3(dpbt)]_n$ and $[Eu(hfa)_3(dppcz)]_n$ were estimated to be 2.31, 2.32, 2.31, and 2.30 Å, respectively, which are shorter than the Eu–O distances of hfa ligands in $[Eu(hfa)_3(dpb)]_n$ (2.41 Å), $[Eu(hfa)_3(dpbp)]_n$ (2.42 Å), $[Eu(hfa)_3(dpbt)]_n$ (2.41 Å), and $[Eu(hfa)_3(dppcz)]_n$ (2.42 Å). These results indicate that the coordination ability of phosphine oxide is stronger than that of the hfa ligands. The strong coordination ability of phosphine oxide in Eu(III) complexes has been reported. The tight-coordination of phosphine oxide molecules with low vibrational frequency (P=O: 1120 cm^{-1}) prevents coordination of high-vibrational molecules such as water, which results in enhancement of their luminescence properties.

X-ray analyses also reveal intermolecular interactions between one-dimensional polymeric chains (Fig. 2.4). Two CH/F interactions in one unit were identified for $[Eu(hfa)_3(dpb)]_n$, $[Eu(hfa)_3(dpbp)]_n$, $[Eu(hfa)_3(dpbt)]_n$, and $[Eu(hfa)_3(dppcz)]_n$. Remarkable CH/π interactions in the polymer chains of $[Eu(hfa)_3(dpbp)]_n$,

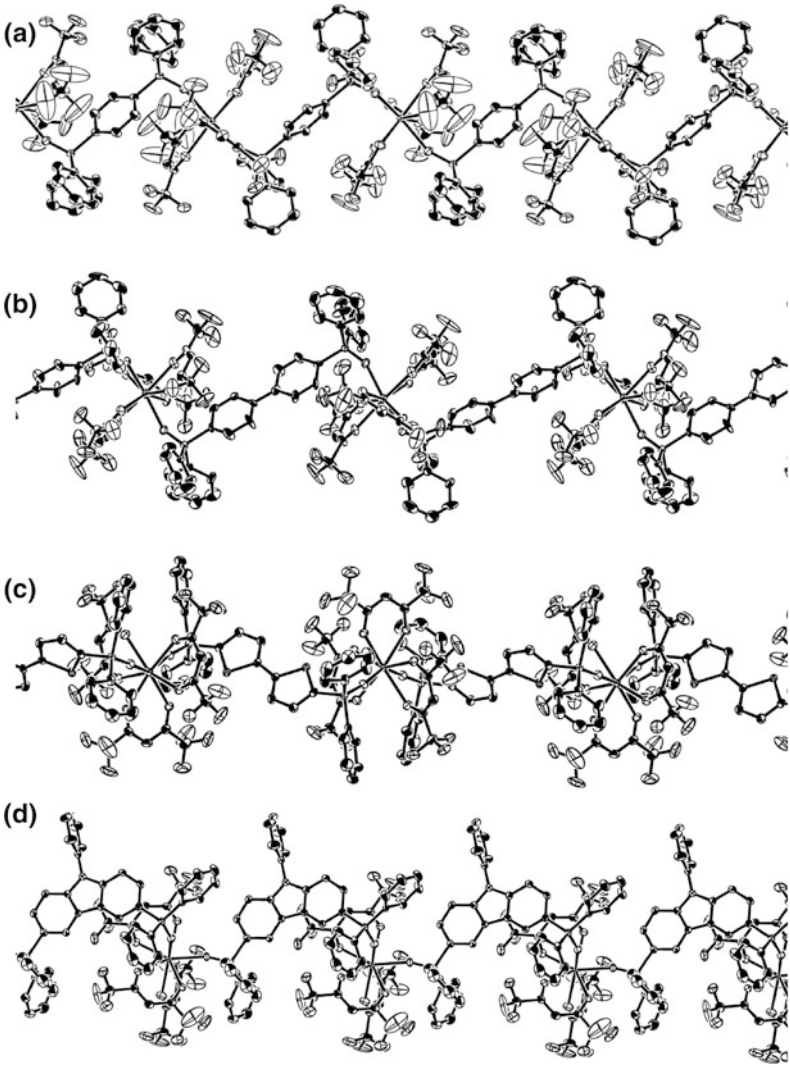

Fig. 2.3 ORTEP drawings (showing 50 % probability displacement ellipsoids) of **a** $[Eu(hfa)_3(dpb)]_n$, **b** $[Eu(hfa)_3(dpbp)]_n$, **c** $[Eu(hfa)_3(dpbt)]_n$, and **d** $[Eu(hfa)_3(dppcz)]_n$

$[Eu(hfa)_3(dpbt)]_n$, and $[Eu(hfa)_3(dppcz)]_n$ were observed. The author considers that tight-binding structures composed of Eu(III) ions and phosphine oxide result in the excellent thermogravimetric and emission properties.

Table 2.1 Crystal data of Eu(III) coordination polymers

	$[Eu(hfa)_3(dpb)]_n$	$[Eu(hfa)_3(dpbp)]_n$	$[Eu(hfa)_3(dpbt)]_n$	$[Eu(hfa)_3(dppcz)]_n$
Chemical formula	$C_{45}H_{27}F_{18}O_8P_2Eu$	$C_{52}H_{31}F_{18}O_8P_2Eu$	$C_{47}H_{27}F_{18}O_8P_2S_2Eu$	$C_{57}H_{34}F_{18}NO_8P_2Eu$
Formula weight	1251.58	1339.69	1339.72	1416.78
Crystal color, habit	Colorless, prism	Colorless, prism	Colorless, prism	Colorless, prism
Crystal system	Triclinic	Monoclinic	Monoclinic	Monoclinic
Space group	*P*-1 (#2)	*C*2/*c* (#15)	*C*2/*c* (#15)	$P2_1/n$ (#14)
a/Å	12.610(3)	23.477(4)	22.786(2)	12.3580(14)
b/Å	13.622(3)	13.367(2)	13.6381(8)	21.170(2)
c/Å	15.282(3)	17.168(3)	17.0846(11)	22.482(3)
α/deg	71.928(8)			
β/deg	79.279(9)	97.5749(8)	103.0178(15)	99.6974(5)
γ/deg	81.346(9)			
V/Å^3	2439.9(9)	5340.5(16)	5172.8(7)	5797.6(11)
Z	2	4	4	4
d_{calc}/g cm^{-3}	1.703	1.666	1.720	1.623
T/°C	−123 ± 1	−123 ± 1	−123 ± 1	−123 ± 1
μ (Mo Kα)/cm^{-1}	14.676	13.472	14.685	12.465
Max 2θ/deg	55.0	55.0	55.0	55.0
No. of measured reflections	19890	21091	20459	45925
No. of unique reflections	10984	6099	5928	13215
R ($I > 2\sigma(I)$)[a]	0.0335	0.0266	0.0258	0.0319
R_w ($I > 2\sigma(I)$)[b]	0.0949	0.0668	0.0689	0.0796

[a] $R = \Sigma \, ||F_o| - |F_c|| / \Sigma \, |F_o|$

[b] $R_w = [(\Sigma \, w \, (|F_o| - |F_c|)^2 / \Sigma \, w \, F_o^2)]^{1/2}$

Table 2.2 Selected bond lengths (Å) of Eu(III) coordination polymers

Bond	$[Eu(hfa)_3(dpb)]_n$	$[Eu(hfa)_3(dpbp)]_n$	$[Eu(hfa)_3(dpbt)]_n$	$[Eu(hfa)_3(dppcz)]_n$
Eu−O1 (P=O)	2.307	2.319	2.314	2.321
Eu−O2 (P=O)	2.312	2.319	2.314	2.284
Average bond length	2.310	2.319	2.314	2.303
Eu−O3 (C=O)	2.457	2.416	2.407	2.420
Eu−O4 (C=O)	2.362	2.423	2.413	2.404
Eu−O5 (C=O)	2.407	2.411	2.407	2.408
Eu−O6 (C=O)	2.409	2.411	2.413	2.446
Eu−O7 (C=O)	2.424	2.416	2.398	2.392
Eu−O8 (C=O)	2.399	2.423	2.398	2.445
Average bond length	2.410	2.417	2.406	2.419
Eu−Eu	9.910	10.367	10.602	11.755

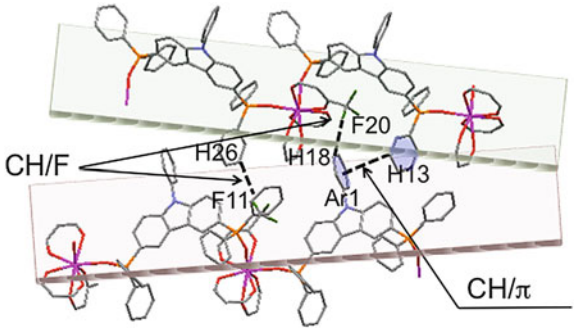

Fig. 2.4 Crystal structures of $[Eu(hfa)_3(dppcz)]_n$ focused on the intermolecular interactions between one-dimensional polymeric chains. *Dashed lines* denote CH/F and CH/π interactions. Two CH/F interactions ($d_{CH/F} = 2.62$ Å (H18–F20), 2.74 Å (H26–F11)) and one CH/π interaction ($d_{CH/\pi} = 3.07$ Å (H13–Ar1)) are displayed

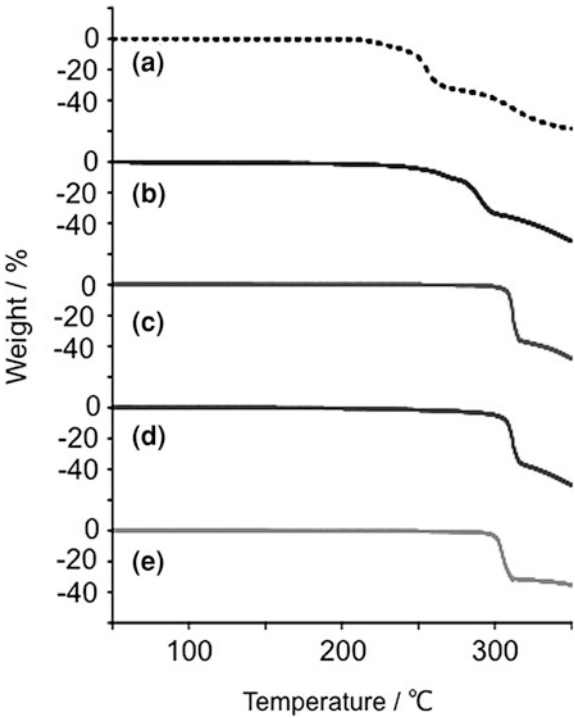

Fig. 2.5 TGA thermograms of **a** $[Eu(hfa)_3(biphepo)]$, **b** $[Eu(hfa)_3(dpb)]_n$, **c** $[Eu(hfa)_3(dpbp)]_n$, **d** $[Eu(hfa)_3(dpbt)]_n$, and **e** $[Eu(hfa)_3(dppcz)]_n$ under an argon atmosphere

2.3.2 Thermal Analyses

To estimate the thermal stability of Eu(III) coordination polymers, TGA and DSC were conducted. Decomposition points from the TGA thermograms are 261, 308, and 300 °C for $[Eu(hfa)_3(dpb)]_n$, $[Eu(hfa)_3(dpbp)]_n$, and $[Eu(hfa)_3(dppcz)]_n$, respectively (Fig. 2.5). In contrast, the decomposition point of the reported Eu(III) complex, $[Eu(hfa)_3(biphepo)]$ (biphepo: 2,2′-bis(diphenylphosphoryl)biphenyl),

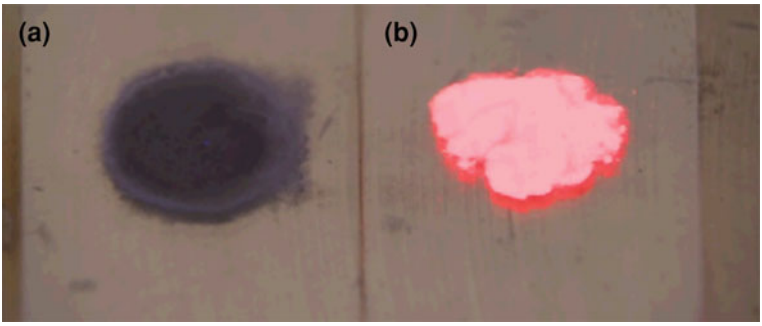

Fig. 2.6 Photographs of **a** [Eu(hfa)$_3$(biphepo)] and **b** [Eu(hfa)$_3$(dpbp)]$_n$ after heating at 300 °C for 10 min under UV irradiation

was found to be 230 °C. The high thermal stability of [Eu(hfa)$_3$(dpbp)]$_n$ and [Eu(hfa)$_3$(dppcz)]$_n$ might be due to their tight-binding structures supported by a combination of CH/F and CH/π interactions (Fig. 2.4). The binding energies of CH/F (hydrogen bond) and CH/π interactions are generally known to be 10–30 and 2–10 kJ mol^{-1}, respectively [21]. The author considers that a combination of both CH/F and CH/π interactions in coordination polymers is effective for the construction of thermostable luminophore compounds. As displayed in Fig. 2.6, [Eu(hfa)$_3$(dpbp)]$_n$ after heating at 300 °C for 10 min exhibits brilliant red luminescence under UV irradiation (excitation at 365 nm), whereas [Eu(hfa)$_3$(biphepo)] does not emit photons owing to thermal decomposition at 230 °C. The enhanced photostability of organic molecules containing hydrogen bonds has been reported [22]. In the author's system, high photostability of [Eu(hfa)$_3$(dpbp)]$_n$ has been also observed under UV irradiation. The DSC thermograms of [Eu(hfa)$_3$(dpb)]$_n$, [Eu(hfa)$_3$ (dpbp)]$_n$, and [Eu(hfa)$_3$(dppcz)]$_n$ show that exothermic peaks based on the decomposition points and endothermic peaks corresponding to melting points were observed (Fig. 2.7). Thus, the Eu(III) coordination polymers exhibit thermal behavior similar to polymer compounds.

2.3.3 Photophysical Properties

Steady-state emission spectra of the Eu(III) coordination polymers in the solid state are shown in Fig. 2.8 (right). Emission bands were observed at around 578, 591, 613, 650, and 698 nm, and are attributed to the f–f transitions of $^5D_0$–^7F_J with $J = 0$, 1, 2, 3, and 4, respectively. The emission band at 613 nm ($^5D_0$–$^7F_2$) is due to electric dipole transitions, which is strongly dependent on the coordination geometry. Their time-resolved emission profiles revealed single-exponential decays with millisecond scale lifetimes. The observed emission lifetimes from $^5D_0$ excited level (τ_{obs}) were determined from the slopes of logarithmic decay profiles. The emission lifetimes of [Eu(hfa)$_3$(dpb)]$_n$, [Eu(hfa)$_3$(dpbp)]$_n$, and [Eu(hfa)$_3$ (dppcz)]$_n$ were determined to be 0.93, 0.85, and 0.93 ms, respectively (Fig. 2.9).

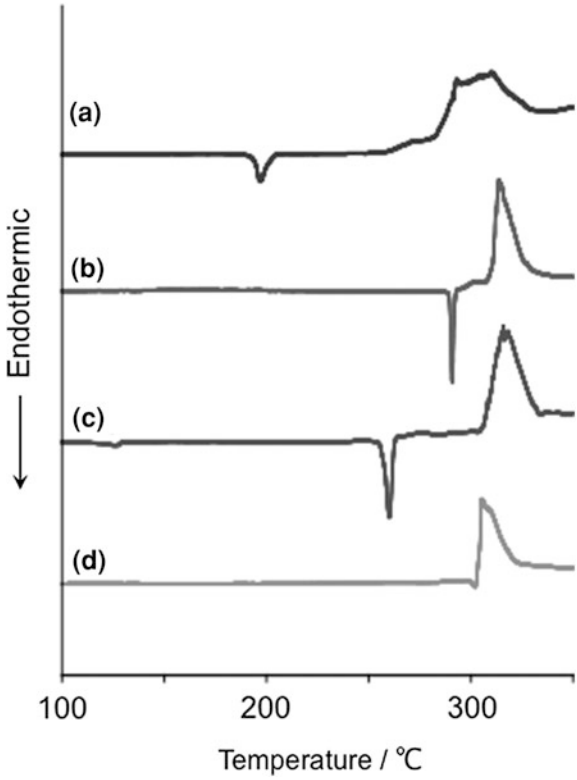

Fig. 2.7 DSC thermograms of **a** $[Eu(hfa)_3(dpb)]_n$, **b** $[Eu(hfa)_3(dpbp)]_n$, **c** $[Eu(hfa)_3(dpbt)]_n$, and **d** $[Eu(hfa)_3(dppcz)]_n$

The photophysical properties of the Eu(III) coordination polymers in the solid state are summarized in Table 2.3. The 4f–4f emission quantum yields (Φ_{Ln}) [18, 23, 24] for $[Eu(hfa)_3(dpb)]_n$, $[Eu(hfa)_3(dpbp)]_n$, and $[Eu(hfa)_3(dppcz)]_n$ were estimated to be 70, 72, and 83 %, respectively. These quantum yields are approximately four times larger than that for $[Eu(hfa)_3(H_2O)_2]$ [25, 26], and similar to that reported for [Eu(hfa)$_3$(biphepo)] (Φ_{Ln} = 73 % in the solid state), which have been reported as high luminescent Eu(III) complexes. According to the photosensitized energy transfer efficiency (η_{sens}) calculated from Φ_{Ln} (excited at 465 nm) and Φ_{tot} (excited at 380 nm), $[Eu(hfa)_3$ (dppcz)$]_n$ are approximately five times larger than that for reported $[Eu(hfa)_3(H_2O)_2]$. Since absorption band at 380 nm is assigned to a π–π^* transition of hfa ligand (Fig. 2.8 left), these results suggest that the photosensitized energy transfer from hfa ligands to Eu(III) ions is enhanced in the coordination polymers, in particular, $[Eu(hfa)_3(dppcz)]_n$.

The nonradiative rate constants (k_{nr}) for the Eu(III) coordination polymers ($1.8–3.3 \times 10^2$ s^{-1}) were approximately ten times smaller than that for $[Eu(hfa)_3(H_2O)_2]$ (3.7×10^3 s^{-1}). The smaller k_{nr} for the Eu(III) coordination polymers is attributed to the structural rigidity and low-vibrational frequencies in the crystal lattice. Our research group has previously reported that the nonradiative

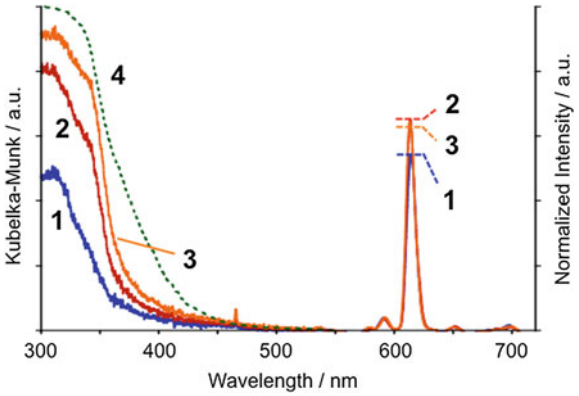

Fig. 2.8 Left: Diffuse-reflectance absorption spectra of $[Eu(hfa)_3(dpb)]_n$ (*line 1*), $[Eu(hfa)_3(dpbp)]_n$ (*line 2*), $[Eu(hfa)_3(dppcz)]_n$ (*line 3*), and $[Eu(hfa)_3(H_2O)_2]$ (*dot line 4*) in the solid state. The absorption bands at 310 nm are attributed to a π-π^* transition of the hfa lilgands. The small bands at 465 nm are assigned to the $^7F_{0-5}D_2$ transition in the Eu(III) ion. Right: Emission spectra of $[Eu(hfa)_3(dpbp)]_n$, $[Eu(hfa)_3(dppcz)]_n$, and $[Eu(hfa)_3(dpb)]_n$ in the solid state. Excitation wavelength is 465 nm. The spectra were normalized with respect to the magnetic dipole transition ($^5D_0$–$^7F_1$)

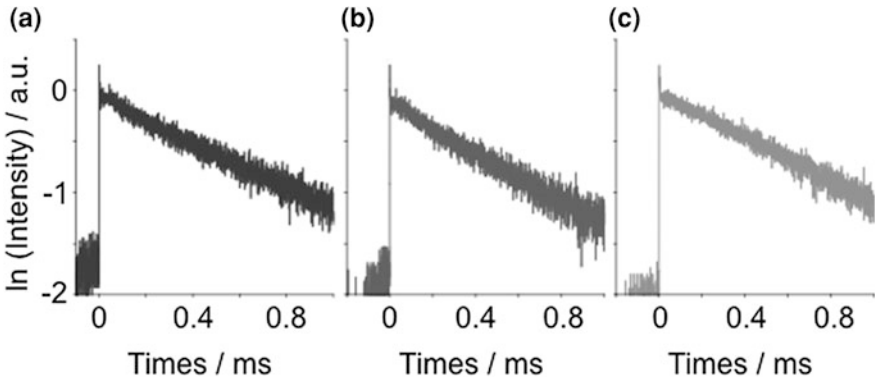

Fig. 2.9 The decay profiles of **a** $[Eu(hfa)_3(dpb)]_n$, **b** $[Eu(hfa)_3(dpbp)]_n$, and **c** $[Eu(hfa)_3(dppcz)]_n$ in the solid state

transitions of lanthanide complexes are caused by the high-vibrational frequency of O–H bonds, such as in water and alcohol. k_{nr} for $[Eu(hfa)_3(biphepo)]$ is similar to those of $[Eu(hfa)_3(dpb)]_n$, $[Eu(hfa)_3(dpbp)]_n$, and $[Eu(hfa)_3(dppcz)]_n$. We consider that introduction of the LVF phosphine oxide ligand as a linker part in the polymer chains is effective for preparation of luminophores with high thermal stabilities and emission quantum yields.

Table 2.3 Photophysical and thermal properties of Eu(III) compounds in the solid state

Compound	interaction[a]	Decomp. point/°C[b]	Photophysical properties						
			τ_{obs} / ms[c]	τ_{rad} / ms[d]	Φ_{Ln} /%[d]	Φ_{tot} /%[e]	η_{sens} / %[f]	k_r /s^{-1} [d]	k_{nr} /s^{-1} [d]
$[Eu(hfa)_3(H_2O)_2]$	–	220[g]	0.22[h]	1.1[h]	19[h]	2.6[h]	13[h]	8.8×10^2	3.7×10^3
$[Eu(hfa)_3(biphepo)]$	–	230	0.94	1.3	73	21	29	7.8×10^2	2.8×10^2
$[Eu(hfa)_3(dpb)]_n$	CH/F	261	0.93	1.3	70	31	44	7.5×10^2	3.3×10^2
$[Eu(hfa)_3(dpbp)]_n$	CH/F, CH/π	308	0.85	1.2	72	29	40	8.5×10^2	3.2×10^2
$[Eu(hfa)_3(dppcz)]_n$	CH/F, CH/π	300	0.93	1.1	83	53	64	8.9×10^2	1.8×10^2

[a] From X-ray single crystal analyses (Fig. 2.4)
[b] From TGA thermograms (Fig. 2.5)
[c] Emission lifetime (τ_{obs}) of the Eu(III) coordination polymer were measured by excitation at 355 nm (Nd:YAG 3ω)
[d] Calculation methods are described in Experimental section
[e] Total emission quantum yield (excitation at 380 nm)
[f] Photosensitized energy transfer efficiency $\eta_{sens} = \Phi_{tot} / \Phi_{Ln}$
[g] From Ref. [18]
[h] From Ref. [25]

Fig. 2.10 The conceptual diagram in Chap. 2

2.3.4 Conclusions

The thermostable luminophores composed of Eu(III) coordination polymers were successfully synthesized (Fig. 2.10). In particular, $[Eu(hfa)_3(dppcz)]_n$ exhibits both high emission quantum yields ($\Phi_{Ln} = 83$ %) and remarkable thermal stability (decomposition point =300 °C) due to a tight-binding structure composed of Eu(III) ions and low-vibrational phosphine oxide, although many types of

luminescent organic dyes are generally decomposed at temperatures under 200 °C. The emission quantum yields of the author's coordination polymers are similar to those of strong-luminescent coordination polymers in former chapters. Reported new luminophores are expected to employ in optics applications such as luminescent plastics, displays, and opto-electronic devices.

References

1. A. Thirumurugan, S.K. Pati, M.A. Greenc, S. Natarajan, J. Mater. Chem. **13**, 2937 (2003)
2. C. Daiguebonne, N. Kerbellec, O. Guillou, J.-C.G. Bünzli, F. Gumy, L. Catala, T. Mallah, N. Audebrand, Y. Geraut, K. Bernot, G. Calvez, Inorg. Chem. **47**, 3700 (2008)
3. K. Binnemans, Chem. Rev. **109**, 4283 (2009)
4. C. Marchal, Y. Filinchuk, X.-Y. Chen, D. Imbert, M. Mazzanti, Chem. Eur. J. **15**, 5273 (2009)
5. T.K. Prasad, M.V. Rajasekharan, Inorg. Chem. **48**, 11543 (2009)
6. J. Rocha, L.D. Carlos, F.A. Almeida Paz, D. Ananias, Chem. Soc. Rev. **40**, 926 (2011)
7. S.V. Eliseeva, D.N. Pleshkov, K.A. Lyssenko, L.S. Lepnev, J.-C.G. Bünzli, N.P. Kuzmina, Inorg. Chem. **49**, 9300 (2010)
8. F. Marchetti, C. Pettinari, A. Pizzabiocca, A.A. Drozdov, S.I. Troyanov, C.O. Zhuravlev, S.N. Semenov, Y.A. Belousov, I.G. Timokhin, Inorg. Chim. Acta **363**, 4038 (2010)
9. C. Wang, Y. Xing, Z. Li, J. Li, X. Zeng, M. Ge, S. Niu, J. Mol. Struct. **931**, 76 (2009)
10. Y. Hasegawa, Y. Kimura, K. Murakoshi, Y. Wada, J. Kim, N. Nakashima, T. Yamanaka, S. Yanagida, J. Phys. Chem. **100**, 10201 (1996)
11. Y. Hasegawa, K. Murakoshi, Y. Wada, J. Kim, N. Nakashima, T. Yamanaka, S. Yanagida, Chem. Phys. Lett. **260**, 173 (1996)
12. P.W. Miller, M. Nieuwenhuyzen, J.P.H. Charmant, S.L. James, Inorg. Chem. **47**, 8367 (2008)
13. J.S. Field, R.J. Haines, E.I. Lakoba, M.H. Sosabowski, J. Chem. Soc. Perkin Trans. **1**, 3352 (2001)
14. R.D. Myrex, C.S. Colbert, G.M. Gray, Organometallics **23**, 409 (2004)
15. I.O. Koshevoy, A.J. Karttunen, S.P. Tunik, M. Haukka, S.I. Selivanov, A.S. Melnikov, P.Y. Serdobintsev, M.A. Khodorkovskiy, T.A. Pakkanen, Inorg. Chem. **47**, 9478 (2008)
16. M.C. Burla, R. Caliandro, M. Camalli, B. Carrozzini, G.L. Cascarano, L.D. Caro, C. Giacovazzo, G. Polidori, R. Spagana, J. Appl. Crystallogr. **38**, 381 (2005)
17. G.M. Sheldrick, Acta Crystallogr. Sect. A: Found. Crystallogr **64**, 112 (2008)
18. R. Pavithran, N.S. Saleesh Kumar, S. Biju, M.L. P. Reddy, S., Jr. Alves, R.O. Freire, Inorg. Chem. **45**, 2184 (2006)
19. Y. Hasegawa, M. Yamamuro, Y. Wada, N. Kanehisa, Y. Kai, S. Yanagida, J. Phys. Chem. A **107**, 1697 (2003)
20. R.B. King, J. Am. Chem. Soc. **91**, 7211 (1969)
21. G.R. Desiraju, T. Steiner, *The Weak Hydrogen Bond in Structural Chemistry and Biology* (Oxford University Press, Oxford 1999)
22. P. Slavíček, M. Fárník, Phys. Chem. Chem. Phys. **13**, 12123 (2011)
23. M.H.V. Werts, R.T.F. Jukes, J.W. Verhoeven, Phys. Chem. Chem. Phys. **4**, 1542 (2002)
24. J.-C.G. Bünzli, S.V. Eliseeva, In Springer *Series on Fluorescence. Lanthanide Luminescence: Photophysical, Analytical and Biological Aspects*, Vol. 8 ed. by P. Hänninen, H. Härmä, (Springer Verlag: Berlin, 2010)
25. S.V. Eliseeva, M. Ryazanov, F. Gumy, S.I. Troyanov, L.S. Lepnev, J.-C.G. Bünzli, N.P. Kuzmina, Eur. J. Inorg. Chem. **23** 4809 (2006)
26. S.V. Eliseeva, D.N. Pleshkov, K.A. Lyssenko, L.S. Lepnev, J.-C.G. Bünzli, N.P. Kuzmina, Inorg. Chem. **50**, 5137 (2011)

Chapter 3
Chameleon Luminophore for a Wide Range Temperature-Sensor Composed of Lanthanide Coordination Polymers

3.1 Introduction

In the fields of fluid dynamics, aeronautical engineering, environment engineering, and energy technology, it is critical to accurately measure the physical parameters of a material surface [1]. Optoelectronic devices have generally been employed as temperature and pressure sensors [2]. However, their sensing area is limited to a single point on a surface. There is a need to measure entire surfaces and obtain multidimensional data for mapping surfaces. There are high expectations that materials for surface measurements, such as temperature and pressure-sensitive dyes, will overcome this intrinsic limitation of optoelectronic devices.

The author proposes a new idea to employ the temperature-dependent energy transfer process in lanthanide complexes for thermosensing in this chapter. First, the author seeks to design temperature-sensitive dyes using luminescent lanthanide complexes. Lanthanide complexes exhibit characteristic luminescence with narrow emission bands and long emission lifetimes as described in Chap. 1 [3–11], which make them suitable for use in sensing devices. In 2003, Amao reported the first temperature-sensitive dye that employed Eu(III) complex in a polymer film [12]. Khalil demonstrated the high performance of Eu(III) complex for temperature-sensitive paint (temperature sensitivity: 4.42 % $°C^{-1}$) [13]. Katagiri has reported Tb(III) complex, $Tb(hfa)_3(H_2O)_2$ (hfa: hexafluoroacetylacetonato), that is suitable as a temperature-sensing probe since it exhibits effective back energy transfer (BEnT) from the emitting level of the Tb(III) ion to the excited triplet state of the hfa ligand [14]. Since BEnT depends on the energy barrier of the process, the emission intensity varies with temperature.

To improve the thermosensing performance, it is necessary to develop a thermostable structure for high temperature sensing and to implement a dual sensing unit for a high sensing ability. First, the author focused on a lanthanide coordination polymer to produce a thermostable structure based on the findings of Chap. 2. Introducing Tb(III) ion and hfa ligands to coordination polymer frameworks will produce a Tb(III) coordination polymer that can be used as a temperature-sensing probe. The triplet state of hfa (22,000 cm^{-1}) is very close to the emitting level of the

K. Miyata, *Highly Luminescent Lanthanide Complexes with Specific Coordination Structures*, Springer Theses,
DOI: 10.1007/978-4-431-54944-4_3, © Springer Japan 2014

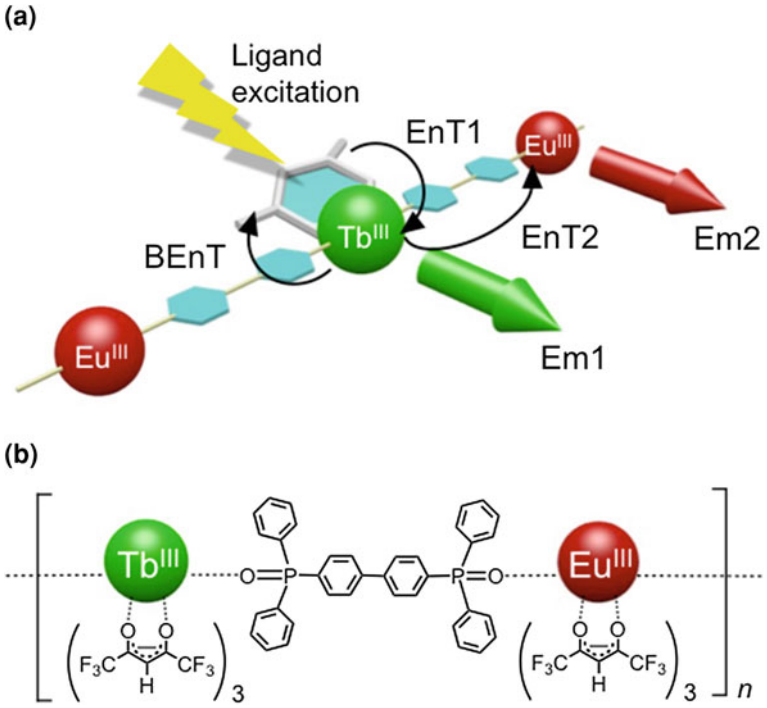

Fig. 3.1 **a** A schematic representation of energy transfer processes of Eu(III) and Tb(III) coordination polymer (*EnT* energy transfer, *BEnT* back energy transfer, *Em* emission). **b** Chemical structure of $[Ln(hfa)_3(dpbp)]_n$ (Ln = Eu, Tb)

Tb(III) ion (20,500 cm^{-1}), resulting in effective EnT1 and BEnT and thus high-performance thermosensing dyes (Fig. 3.1a and 3.2). The author also selected low-vibrational frequency phosphine oxide as the linking part in the Tb(III) coordination polymer because lanthanide complexes with high emission quantum yields composed of hfa and bidentate phosphine oxide ligands were described in former chapters. Second, the author attempted to impart ratiometric temperature sensing by using luminescent Eu(III) and Tb(III) ions in coordination polymer frameworks to realize a high thermosensing ability. Two independent emission bands are expected to enable more accurate thermal measurements than a previous single lanthanide complex [15–18]. Their emission intensities may be also dependent on the temperature based on the energy transfer from Tb(III) to Eu(III), EnT2 (Fig. 3.1a). Temperature-sensitive dyes with a thermostable structure and dual sensing units have not been previously reported.

In this chapter, the author reports a novel thermosensing dye that consists of a lanthanide coordination polymer; $[Ln(hfa)_3(dpbp)]_n$ (dpbp: 4,4′-bis(diphenylphosphoryl)biphenyl, Ln = Eu, Tb), as shown in Fig. 3.1b. Its thermal stability and luminescence properties are characterized by thermogravimetric analysis

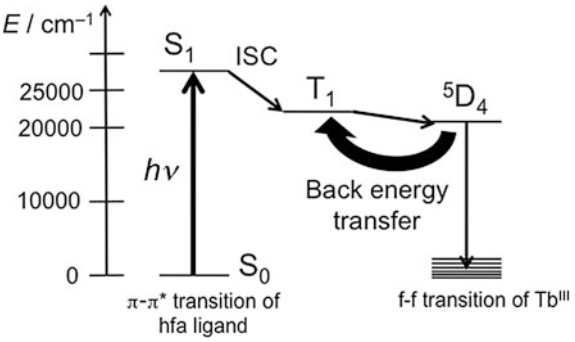

Fig. 3.2 Energy diagram of Tb(III) complexes and back energy transfer processes

(TGA) and by emission quantum yield and emission lifetime measurements. This coordination polymer has a high emission quantum yield ($\Phi_{tot} = 40$ % for $[Tb(hfa)_3(dpbp)]_n$ at room temperature) and a temperature sensitivity over a wide temperature range of 200–500 K. The thermosensing dye composed of Tb(III) and Eu(III) coordination polymers is expected to open up new fields in the molecular chemistry of temperature-sensing materials.

3.2 Experimental Section

3.2.1 General

All chemicals were reagent grade and were used without further purification. Infrared spectra were recorded on a JASCO FT/IR–350 spectrometer. Mass spectra were measured using a JEOL JMS–T100LP. Elemental analyses were performed on a Yanaco CHN corder MT-6. Inductively coupled plasma (ICP) emission spectroscopy was performed on a Shimadzu ICPE-9000. Thermogravimetric analyses were performed on a MAC TG-DTA 2000 in an argon atmosphere at a heating rate of 1 °C min^{-1}.

3.2.2 Syntheses

3.2.2.1 Preparation of $[Tb(hfa)_3(dpbp)]_n$

Phosphine oxide ligand (70 mg, 0.13 mmol) and $Tb(hfa)_3(H_2O)_2$ (120 mg, 0.14 mmol) were dissolved in methanol (15 mL). The solution was refluxed while stirring for 2 h to give a white precipitate. The precipitate was filtered, washed with methanol and chloroform for several times, and dried in vacuo.

Yield: 105 mg (63 %). IR (KBr): 1653 (st, C=O), 1253–1142 (st, C–F), 1125 (st, P=O) cm^{-1}. ESI-Mass (*m/z*) = 1127.05 $[Tb(hfa)_2(dpbp)]^+$. Anal. Calcd. for $[C_{51}H_{31}F_{18}O_8P_2Tb]_n$: C, 45.90; H, 2.34. Found: C, 45.76; H 2.48.

3.2.2.2 Preparation of $[Tb_{0.99}Eu_{0.01}(hfa)_3(dpbp)]_n$

Phosphine oxide ligand (1.0 eq), $Tb(hfa)_3(H_2O)_2$ (0.99 eq), and $Eu(hfa)_3(H_2O)_2$ (0.01 eq) were dissolved in methanol. The solution was refluxed while stirring for 2 h to give a white precipitate. The precipitate was filtered, washed with methanol and chloroform for several times, and dried in vacuo.

To determine a Eu:Tb ratios of $[Tb_xEu_{1-x}(hfa)_3(dpbp)]_n$, ICP-AES was conducted. ICP samples were prepared by thoroughly drying $[Tb_xEu_{1-x}(hfa)_3(dpbp)]_n$, then digesting the samples to concentrated (60 %) HNO_3 and diluting to 1.2 % HNO_3. Calibration standards were made by diluting 1000 ppm standards of both Eu and Tb (purchased from Kanto Chemical) over the range of 0.0–1.0 ppm for each. Calibration curves for high and low concentrations were made for three emission wavelengths because instrument response was not linear over the broad range of concentrations required to accurately determine small *x* values. Three emission wavelengths for each Eu (381.967, 412.970, and 420.505 nm) and Tb (350.917, 367.635, and 384.873 nm) were measured. Concentrations were calculated from the emission intensities for the three Eu and three Tb wavelengths for each sample were converted to concentrations using the appropriate calibration curves and averaged. These analyses revealed a ratio of Eu:Tb = 0.9:99.1 (calcd. 1:99).

3.2.3 Optical Measurements

Emission spectra were recorded on a JASCO F-6300-H spectrometer and corrected for the response of the detector system. Emission lifetimes (τ_{obs}) were measured using the third harmonics (355 nm) of a Q-switched Nd:YAG laser (Spectra Physics, INDI-50, fwhm = 5 ns, λ = 1064 nm) and a photomultiplier (Hamamatsu photonics, R5108, response time $\leq$ 1.1 ns). The Nd:YAG laser response was monitored with a digital oscilloscope (Sony Tektronix, TDS3052, 500 MHz) synchronized to the single-pulse excitation. Emission lifetimes were determined from the slope of logarithmic plots of the decay profiles. The emission quantum yields of $[Tb(hfa)_3(dpbp)]_n$ excited at 380 nm (Φ_{tot}) were estimated using JASCO F-6300-H spectrometer attached with JASCO ILF-533 integrating sphere unit (ϕ = 100 mm). The wavelength dependences of the detector response and the beam intensity of Xe light source for each spectrum were calibrated using a standard light source. Emission spectra at low temperature (77–300 K) were measured with a nitrogen bath cryostat (Oxford Instruments, Optistat DN) and a temperature controller (Oxford, Instruments, ITC 502S). As displayed in Fig. 3.3, emission

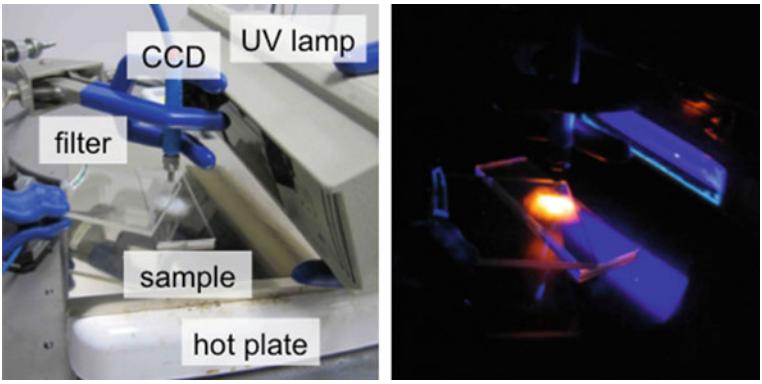

Fig. 3.3 Experimental setup of optical measurements at high temperature

spectra at high temperature (300–500 K) were measured using an electrical hot plate equipped with a digital temperature indicator, and an Ocean Optics multi-channel Analyzer USB4000 corrected for the response of the detector system.

3.3 Results and Discussion

3.3.1 Syntheses and Characterization of Eu/Tb Coordination Polymer

$[Ln(hfa)_3(dpbp)]_n$ and $[Tb_{0.99}Eu_{0.01}(hfa)_3(dpbp)]_n$ (Ln = Eu, Tb) were synthesized by complexing phosphine oxide ligands (dpbp) and $Ln(hfa)_3(H_2O)_2$ in methanol for 2 h. The structure of $[Eu(hfa)_3(dpbp)]_n$ was determined by X-ray single crystal analyses as described in Chap. 2. Phosphine oxide ligands acted as a bidentate bridge between lanthanide ions in one-dimensional polymeric chains. The coordination sites of $[Eu(hfa)_3(dpbp)]_n$ comprised three hfa ligands and two phosphine oxide units. This coordination structure was categorized as an octa-coordinated square antiprism. The powder XRD spectra of $[Eu(hfa)_3(dpbp)]_n$, $[Tb(hfa)_3(dpbp)]_n$, and $[Tb_{0.99}Eu_{0.01}(hfa)_3(dpbp)]_n$ are shown in Fig. 3.4. The XRD patterns of $[Tb(hfa)_3(dpbp)]_n$ and $[Tb_{0.99}Eu_{0.01}(hfa)_3(dpbp)]_n$ are the same as that of $[Eu(hfa)_3(dpbp)]_n$, because of their ionic radii (Eu^{III}: 0.95 Å, Tb^{III}: 0.92 Å). These results indicate that the coordination structures of $[Tb(hfa)_3(dpbp)]_n$ and $[Tb_{0.99}Eu_{0.01}(hfa)_3(dpbp)]_n$ are much similar to that of $[Eu(hfa)_3(dpbp)]_n$.

To evaluate the thermal stability of lanthanide coordination polymers, the author conducted thermogravimetric analyses (TGA) in an argon atmosphere at a heating rate of 1 °C min^{-1} (Fig. 3.5). Their TGA thermograms revealed that $[Eu(hfa)_3(dpbp)]_n$ and $[Tb(hfa)_3(dpbp)]_n$ have decomposition points of 308 and 317 °C, respectively (Table 3.1). In contrast, the decomposition point of Tb(III)

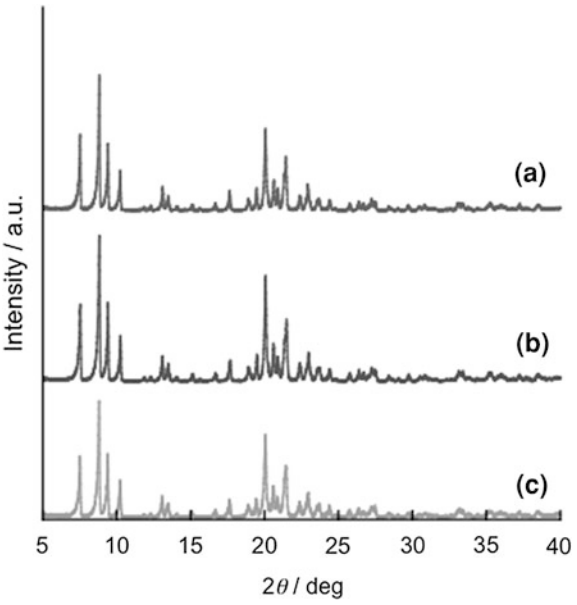

Fig. 3.4 Powder XRD patterns of **a** $[Eu(hfa)_3(dpbp)]_n$, **b** $[Tb(hfa)_3(dpbp)]_n$, and **c** $[Tb_{0.99}Eu_{0.01}(hfa)_3(dpbp)]_n$ coordination polymers

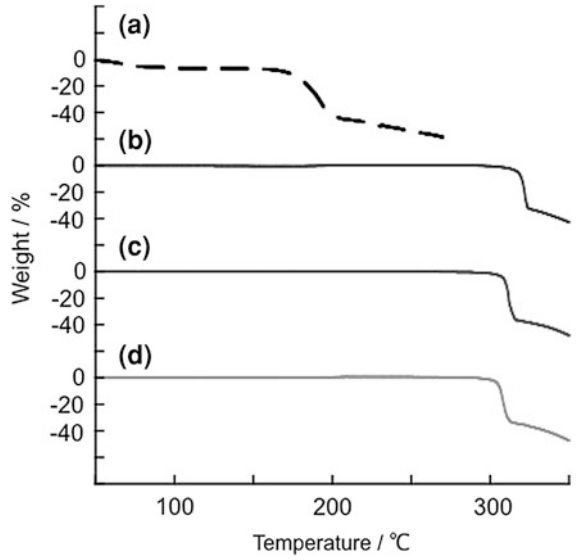

Fig. 3.5 TGA thermograms of **a** $Tb(hfa)_3(H_2O)_2$, **b** $[Tb(hfa)_3(dpbp)]_n$, **c** $[Eu(hfa)_3(dpbp)]_n$, and **d** $[Tb_{0.99}Eu_{0.01}(hfa)_3(dpbp)]_n$ in an argon atmosphere at a heating rate of 1 °C min^{-1}

complex, $Tb(hfa)_3(H_2O)_2$ was found to be 177 °C. The high thermal stability of $[Eu(hfa)_3(dpbp)]_n$ and $[Tb(hfa)_3(dpbp)]_n$ might be due to their tight-binding structures in coordination polymer units as described in Chap. 2 [19].

Table 3.1 The emission and thermal properties of Ln(III) compounds in the solid state

	Decomp. point/ °C	Φ_{tot}/%[a]	τ_{obs}/ms[a,b]	E_a/kJ mol^{-1} [c]	$\Delta G^{\ddagger}$/ kJ mol^{-1}	Temp. sensitivity/ % °C^{-1} [d]
$Tb(NO_3)_3$	–	–	0.86	–	–	<0.03
$Tb(hfa)_3(H_2O)_2$	177	27[e]	0.37	33	57	0.70
$[Tb(hfa)_3(dpbp)]_n$	317	40[e]	0.35	24	58	0.64
$[Eu(hfa)_3(dpbp)]_n$	308[g]	72[f,g]	0.85[g]	–	–	<0.05

[a] At room temperature. [b] Emission lifetimes (τ_{obs}) were measured by excitation at 355 nm (Nd:YAG 3ω). [c] From the slope of the Arrhenius plot (Fig. 3.7). [d] In the temperature range of 200–300 K. [e] Excited at 380 nm. [f] Excited at 465 nm. [g] From Chap. 2

Temperature-dependent emission spectra of $Tb(NO_3)_3$, $[Tb(hfa)_3(dpbp)]_n$, and $[Eu(hfa)_3(dpbp)]_n$ in the solid state are shown in Fig. 3.6. The emission intensities of $[Tb(hfa)_3(dpbp)]_n$ decreased dramatically with increasing temperature. In contrast, changes of the emission intensities of $Tb(NO_3)_3$ and $[Eu(hfa)_3(dpbp)]_n$ were not observed. The energy gaps between the emitting level of the lanthanide ion and the excited triplet state of the hfa ligand in $[Tb(hfa)_3(dpbp)]_n$ and $[Eu(hfa)_3(dpbp)]_n$ are 1700 and 4900 cm^{-1}, respectively [14, 20]. When the energy gap is less than 1850 cm^{-1}, the BEnT from lanthanide ion to the ligands is enhanced [21]. Therefore, the combination of Tb(III) ions with hfa ligands should lead to a condition for enhancement of BEnT, resulting in a high-temperature sensitivity.

The temperature-dependence of the BEnT rate is expected to follow an Arrhenius type equation with an energy barrier E_a. To analyze the BEnT mechanism in detail, the author attempted to estimate the back energy transfer rates (k_{back}) using kinetic analysis. k_{back} is assumed to obey the following Arrhenius type equation:

$$\ln k_{back} = \ln\left(\frac{1}{\tau_{obs}} - \frac{1}{\tau_{77K}}\right) = \ln A - \frac{E_a}{RT} \tag{3.1}$$

where τ_{obs}, τ_{77K}, A, E_a, R, T are emission lifetime, emission lifetime at 77 K, frequency factor, activation energy, gas constant, and temperature, respectively. This assumption is supported by the findings of Blasse and Grabmaier [22]. In order to estimate E_a using Eq. (3.1), the author measured the temperature-dependences of the emission lifetimes of $Tb(hfa)_3(H_2O)_2$ and $[Tb(hfa)_3(dpbp)]_n$. Figure 3.7 shows the temperature-dependences of the emission lifetimes and the Arrhenius plots for k_{back} and Table 3.1 lists the calculated activation energy E_a and the activation Gibbs function $\Delta G^{\ddagger}$ values. The author found that E_a and $\Delta G^{\ddagger}$ of $[Tb(hfa)_3(dpbp)]_n$ are similar to those of $Tb(hfa)_3(H_2O)_2$. These results indicate that phosphine oxide ligands might not affect to the back energy transfer rate.

The emission and thermosensing properties of lanthanide coordination polymers in the solid state are also summarized in Table 3.1. The emission quantum yields (Φ_{tot}) for $Tb(hfa)_3(H_2O)_2$ and $[Tb(hfa)_3(dpbp)]_n$ were estimated to be 27 and

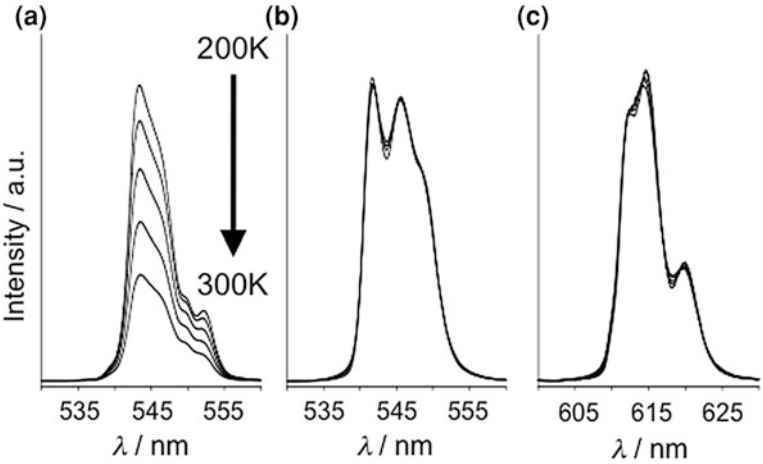

Fig. 3.6 Temperature-dependent emission spectra of **a** $[Tb(hfa)_3(dpbp)]_n$. **b** $Tb(NO_3)_3$, and **c** $[Eu(hfa)_3(dpbp)]_n$ in the solid state in the temperature range of 200–300 K ($\lambda_{ex} = 380$ nm)

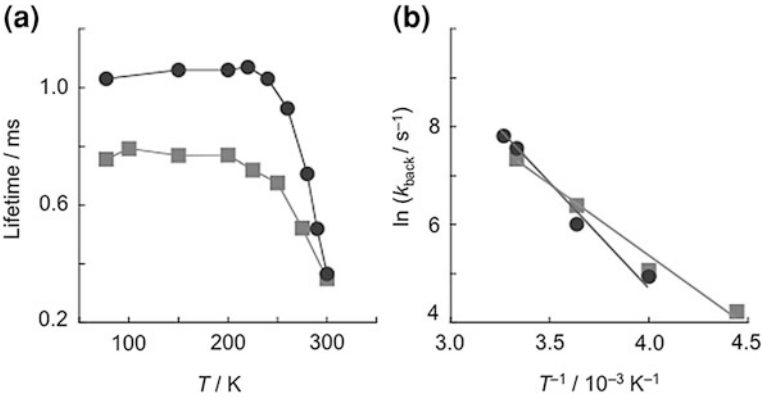

Fig. 3.7 **a** Temperature-dependences of emission lifetimes and **b** Arrhenius plots for back energy transfer rate constants of $Tb(hfa)_3(H_2O)_2$ (●) and $[Tb(hfa)_3(dpbp)]_n$ (■)

40 % at room temperature, respectively. The quantum yields of $[Tb(hfa)_3(dpbp)]_n$ are approximately 1.5 times larger than that of $Tb(hfa)_3(H_2O)_2$. The phosphine oxide ligands should contribute to the enhanced emission of the Tb(III) coordination polymer since they should suppress vibrational relaxation. $[Tb(hfa)_3(dpbp)]_n$ is the best dye in the view point of high-performance of thermosensing dyes.

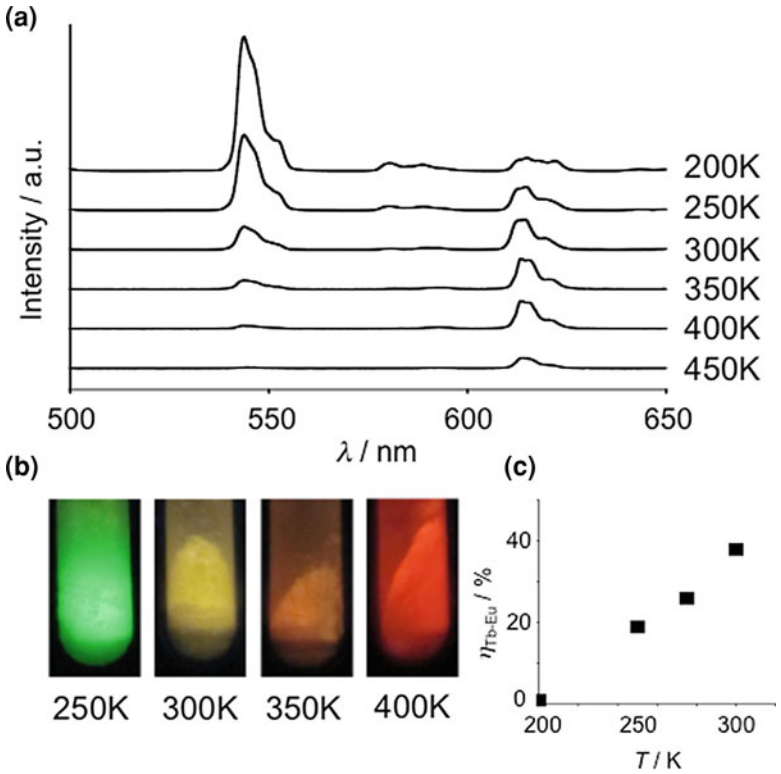

Fig. 3.8 **a** Temperature-dependent emission spectra of $[Tb_{0.99}Eu_{0.01}(hfa)_3(dpbp)]_n$ in the solid state in the temperature range of 200–450 K ($\lambda_{ex} = 380$ nm). **b** Color pictures of the samples under UV (365 nm) irradiation. **c** Temperature-dependence of the energy transfer efficiency (η_{Tb-Eu}) of $[Tb_{0.99}Eu_{0.01}(hfa)_3(dpbp)]_n$

3.3.2 Temperature-Dependent Photosensitized Luminescence of Eu/Tb Coordination Polymer

In order to investigate the ratiometric temperature-sensing properties of coordination polymers, $[Tb_{0.99}Eu_{0.01}(hfa)_3(dpbp)]_n$ containing Tb(III) and Eu(III) ions was prepared. Temperature-dependent emission spectra of $[Tb_{0.99}Eu_{0.01}(hfa)_3(dpbp)]_n$ in the solid state in the temperature range of 200–450 K are shown in Fig. 3.8a, and color pictures of the samples are displayed in Fig. 3.8b. The characteristic emission bands at 543 and 613 nm are attributed to the f–f transitions of Tb(III) ($^5D_4$–$^7F_5$) and Eu(III) ($^5D_0$–$^7F_2$), respectively. The emission intensities at 543 nm dramatically decreased with increasing temperature. In contrast, the emission intensities at 613 nm slightly increased. $[Tb_{0.99}Eu_{0.01}(hfa)_3(dpbp)]_n$ exhibits brilliant green, yellow, orange, and red photoluminescence under UV irradiation (365 nm) at 250, 300, 350, and 400 K, respectively. The

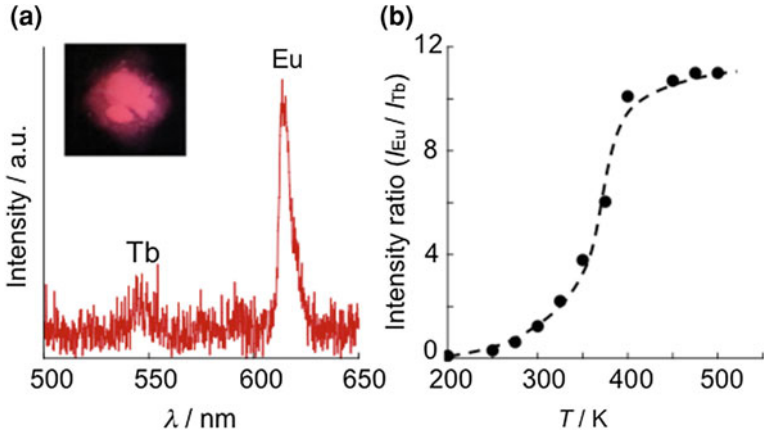

Fig. 3.9 **a** Emission spectra of $[Tb_{0.99}Eu_{0.01}(hfa)_3(dpbp)]_n$ in the solid state at 500 K ($\lambda_{ex} = 365$ nm). *Photograph* emission of $[Tb_{0.99}Eu_{0.01}(hfa)_3(dpbp)]_n$ under UV (365 nm) irradiation at 500 K. **b** The relationship between the ratio of the two emission intensities (I_{Eu}/I_{Tb}) and temperature

author achieved color tuning of the coordination polymers in response to temperature changes.

The temperature sensitivity for $[Tb_{0.99}Eu_{0.01}(hfa)_3(dpbp)]_n$ (0.83 % $°C^{-1}$) is higher than that for $[Tb(hfa)_3(dpbp)]_n$ (0.64 % $°C^{-1}$). This result indicates that the energy is transferred to both the excited triplet state of the hfa ligands (BEnT) and to the Eu(III) ion from the emitting level of the Tb(III) ion. The energy transfer from Tb(III) to Eu(III) strongly depends on the temperature, giving rise to temperature-dependent ratios of the luminescence intensities of the Tb(III) emission bands and the Eu(III) emission bands. The energy transfer can be explained by the Förster mechanism. The energy transfer efficiency from the Tb(III) to Eu(III) ion (η_{Tb-Eu}) is calculated from the following equation [23]:

$$\eta_{Tb-Eu} = 1 - \left(\frac{\tau_{obs}}{\tau_{Tb}}\right) \tag{3.2}$$

where τ_{obs} and τ_{Tb} are the emission lifetimes of $[Tb_{0.99}Eu_{0.01}(hfa)_3(dpbp)]_n$ and $[Tb(hfa)_3(dpbp)]_n$, respectively. The relation between η_{Tb-Eu} and the temperature (200–300 K) are shown in Fig. 3.8c. The values of η_{Tb-Eu} at 200, 250, 275, and 300 K are estimated to be 1, 19, 26, and 38 %, respectively. η_{Tb-Eu} is increased with increasing temperature. The author considered that the energy transfer occurs both to the excited triplet state of hfa ligands and to the Eu(III) ion. $[Tb_{0.99}Eu_{0.01}(hfa)_3(dpbp)]_n$ exhibits dual emission under UV irradiation even at 500 K as shown in Fig. 3.9a. It is also possible to monitor the temperature changes by using the ratios of the luminescence intensities of the Tb(III) emission bands and the Eu(III) emission bands (Fig. 3.9b). The author also demonstrated that the

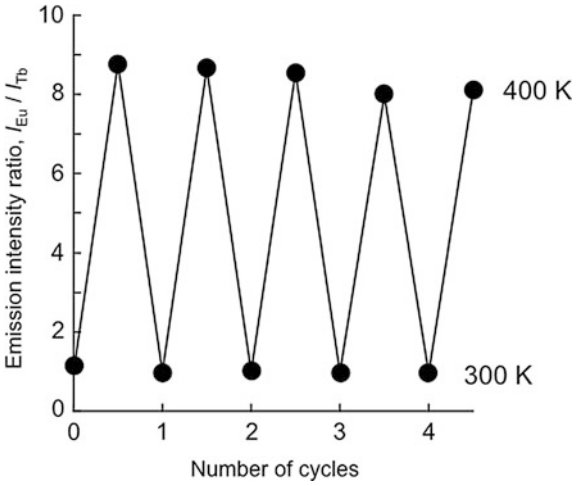

Fig. 3.10 The reversible changes of emission intensity ratio of Eu(III) and Tb(III) (I_{Eu}/I_{Tb}) of $[Tb_{0.99}Eu_{0.01}(hfa)_3(dpbp)]_n$ by the alternative thermo-cycles in the range of 300 and 400 K

luminescent reversibly undergo repeated thermo-cycles. The reversible changes of emission intensity ratio of Eu(III) and Tb(III) (I_{Eu}/I_{Tb}) of $[Tb_{0.99}Eu_{0.01}(hfa)_3(dpbp)]_n$ are observed by the alternative thermo-cycles in the range of 300 and 400 K (Fig. 3.10). The changes in the emission intensity ratio are stably repeated between the I_{Eu}/I_{Tb} values of 1.0 (300 K, yellow emission) and 8.7 (400 K, red emission). Thus, the author successfully synthesized an effective luminophore with a wide temperature sensing range of 200 to 500 K.

3.4 Conclusions

A novel thermosensing dye; "chameleon luminophore" (Fig. 3.11) composed of a lanthanide coordination polymer was successfully synthesized. This coordination polymer is thermally stable and exhibits a high emission quantum yield ($\Phi_{tot} = 40$ % for $[Tb(hfa)_3(dpbp)]_n$ at room temperature) and a temperature sensitivity over a wide temperature range of 200–500 K. The results obtained in this study will provide insights for designing lanthanide coordination polymers for developing temperature-sensing devices based on their luminescence. In future, the chameleon luminophore $[Tb_{0.99}Eu_{0.01}(hfa)_3(dpbp)]_n$ are expected to be promising candidates for temperature-sensitive dyes, which are used for temperature distribution measurements of material surfaces such as an aerospace plane in wind tunnel experiments. Such lanthanide coordination polymers with thermosensing properties have the potential to open up new fields in supramolecular chemistry, polymer science, and molecular engineering.

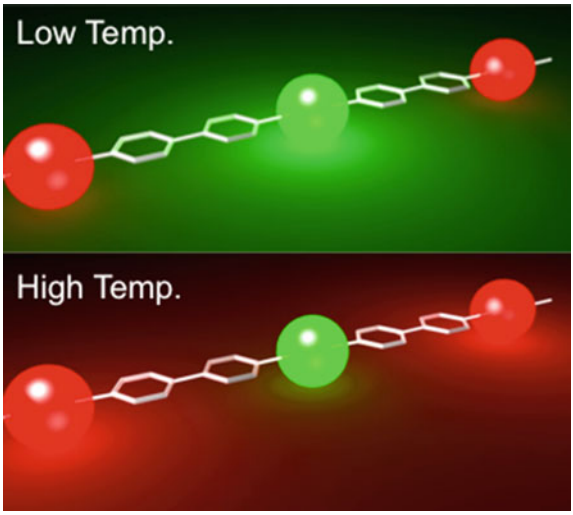

Fig. 3.11 The conceptual diagram

References

1. S. Shindo, *Low-Speed Wind Tunnel Testing Technique,* Chap. 1 (ed. By Corona publishing Co., Ltd., Japan, 1992)
2. *Proceedings of MOSAIC International Workshop*, November 10–11, 2003, Tokyo, Japan
3. N. Weibel, L.J. Charbonniere, M. Guardigli, A. Roda, R. Ziessel, J. Am. Chem. Soc. **126**, 4888 (2004)
4. S. Faulkner, B.P. Burton-Pye, pH dependent self-assembly of dimetallic lanthanide complexes. Chem. Commun. **49**, 259 (2005)
5. J. Yu, D. Parker, R. Pal, R.A. Poole, M.J. Cann, J. Am. Chem. Soc. **128**, 2294 (2006)
6. B. McMahon, P. Mauer, C.P. McCoy, T.C. Lee, T. Gunnlaugsson, J. Am. Chem. Soc. **131**, 17542 (2009)
7. K. Binnemans, Chem. Rev. **109**, 4283 (2009)
8. J.-C.G. Bünzli, Chem. Rev. **110**, 2729 (2010)
9. S.V. Eliseeva, J.-C.G. Bünzli, Chem. Soc. Rev. **39**, 189 (2010)
10. M. Tropiano, N.L. Kilah, M. Morten, H.R.J.J. Davis, P.D. Beer, S. Faulkner, J. Am. Chem. Soc. **133**, 11847 (2011)
11. L.D. Carlos, R.A.S. Ferreira, V. de Zea Bermudez, B. Julian-Lopez, P. Escribano, Chem. Soc. Rev. **40**, 536 (2011)
12. M. Mitsuishi, S. Kikuchi, T. Miyashita, Y. Amao, J. Mater. Chem. **13**, 2875 (2003)
13. G.E. Khalil, K. Lau, G.D. Phelan, B. Carlson, M. Gouterman, J.B. Callis, L.R. Dalton, Rev. Sci. Instrum. **75**, 192 (2004)
14. S. Katagiri, Y. Hasegawa, Y. Wada, S. Yanagida, Chem. Lett. **33**, 1438 (2004)
15. M.S. Tremblay, M. Halim, D. Sames, J. Am. Chem. Soc. **129**, 7570 (2007)
16. N. Kerbellec, D. Kustaryono, V. Haquin, M. Etienne, C. Daiguebonne, O. Guillou, Inorg. Chem. **48**, 2837 (2009)
17. Y. Xiao, Z. Ye, G. Wang, J. Yuan, Inorg. Chem. **51**, 2940 (2012)
18. S. Comby, S.A. Tuck, L.K. Truman, O. Kotova, T. Gunnlaugsson, Inorg. Chem. **51**, 10158 (2012)
19. K. Miyata, T. Ohba, A. Kobayashi, M. Kato, T. Nakanishi, K. Fushimi, Y. Hasegawa, ChemPlusChem **77**, 277 (2012)

20. D.J. Lewis, P.B. Glover, M.C. Solomons, Z. Pikramenou, J. Am. Chem. Soc. **133**, 1033 (2011)
21. S. Sato, M. Wada, Bull. Chem. Soc. Jpn. **43**, 1955 (1970)
22. G. Blasse, B.C. Grabmaier, *Luminescent materials* (Springer-Verlag, New York, 1994), p. 92
23. C. Piguet, J.-C.G. Bünzli, G. Bernardinelli, G. Hopfgartner, A.F. Williams, J. Am. Chem. Soc. **115**, 8197 (1993)

Chapter 4
Characteristic Structures and Photophysical Properties of Nona-Coordinated Eu(III) Complexes with Tridentate Phosphine Oxides

4.1 Introduction

Lanthanide complexes with characteristic narrow emission bands and long emission lifetimes have been regarded as attractive luminescent materials for use in electroluminescent (EL) devices [1–4], lasers [5], and luminescent biosensing applications [6–10]. The coordination number of lanthanide ions in solution varies from eight to twelve, depending on the nature of the ligating molecules [11]. Specific coordination structures result in lanthanide complexes with strong luminescence [12–14]. As described in Chap. 1, the coordination structure of the lanthanide complex dominates the characteristics of the two main parameters that describe the luminescence properties, namely, the radiative (k_r) and nonradiative rate constants (k_{nr}). Firstly, the radiative rate constants observed for lanthanide complexes greatly depend on the geometrical symmetry of the coordination structure. Richardson has estimated the transition intensity parameters of lanthanide complexes on the basis of the ligand field [15]. Binnemans has proposed evaluation of intensity enhancement versus symmetry and polarization by using Judd–Ofelt analysis [16]. Since these studies, it has been widely accepted that the radiative transition probability between the 4f orbitals is enhanced by reducing the geometrical symmetry of the coordination structures [17–19]. Secondly, the emission properties of lanthanide complexes also depend on their vibronic properties, which dominate the kinetics of nonradiative transitions. According to the energy gap theory, nonradiative transitions are promoted by ligands and solvents with high-frequency vibrational structures [20]. For these reasons, lanthanide complexes with large k_r and small k_{nr} constants are the most favorable for strongly luminescent materials. Additionally, efficient energy transfer from the various ligand states [singlet, triplet, and intraligand charge transfer (ILCT)] and the presence of charge transfer (CT) bands are also key factors for strongly luminescent Eu(III) complexes [21–23].

Recently, considerable attentions have been focused on lanthanide complexes with polydentate (tridentate, tetradentate, pentadentate and hexadetate) ligands and their characteristic luminescence properties to suppress the symmetry of the ligand field and vibronic quenching [24–31]. In most of these previous works, however, the

K. Miyata, *Highly Luminescent Lanthanide Complexes with Specific Coordination Structures*, Springer Theses,
DOI: 10.1007/978-4-431-54944-4_4, © Springer Japan 2014

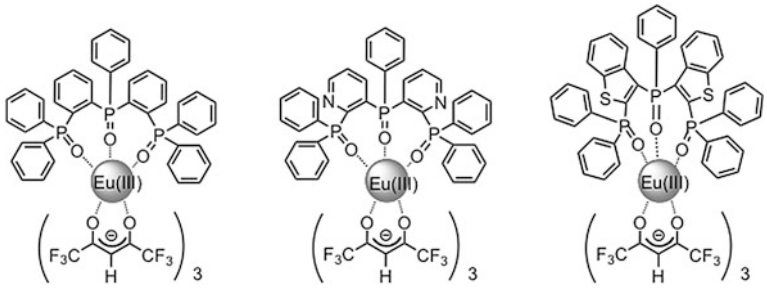

Fig. 4.1 Chemical structures of Eu(hfa)$_3$(dpppo), Eu(hfa)$_3$(dppypo), and Eu(hfa)$_3$(dpbtpo)

lanthanide complexes with polydentate ligands have C–H units close to the metal center. The author here attempted to prepare luminescent Eu(III) complexes with a tridentate phosphine oxide and three hfa as LVF ligands, which are anticipated to construct an asymmetrical nona-coordinated structure (mono-capped square antiprism: 9-SAP). Hasegawa et al. have also reported that the radiative rate constant of Sm(III) complex with 9-SAP structure is larger than those of symmetrical ten-coordinated Sm(III) complexes [32]. Polydentate ligands may also provide stable coordination bindings which show promise toward improved emission properties.

In this chapter, the author reports on luminescent properties of Eu(III) complexes with three kinds of novel tridentate phosphine oxide ligands: Eu(hfa)$_3$(dpppo) (dpppo: bis(*o*-diphenylphosphorylphenyl)phenylphosphine oxide), Eu(hfa)$_3$(dppypo) (dppypo: bis(*o*-diphenylphosphorylpyridyl)phenylphos phine oxide), and Eu(hfa)$_3$(dpbtpo) (dpbtpo: bis(*o*-diphenylphosphorylbenzo thienyl)phenylphosphine oxide) as shown in Fig. 4.1. The geometrical structures of the Eu(III) complexes were characterized using NMR and X-ray single crystal analyses. The author also compared the emission spectral shapes, the emission quantum yields, the emission lifetimes, the radiative and the non-radiative rate constants in nona-coordinated Eu(III) complexes with those of octa-coordinated Eu(III) complexes; Eu(hfa)$_3$(biphepo) and Eu(hfa)$_3$(tppo)$_2$. The photophysical properties of nona-coordinated Eu(III) complexes with tridentate phosphine oxide ligand are elucidated in terms of geometrical, vibrational and chemical structures.

4.2 Experimental Section

4.2.1 Materials

Acetone-d_6 (D, 99.9 %) and chloroform-*d* (D, 99.8 %) were obtained from Cambridge Isotope laboratories, Inc. Dry THF was prepared by distillation over benzophenone and Na metal. All other chemicals and solvents were reagent grade and were used without further purification.

4.2.2 Apparatus

Infrared spectra were recorded on JASCO FT/IR–420 spectrometer. ^{1}H (300 MHz), ^{19}F (500 MHz) and ^{31}P NMR (500 MHz) spectra were recorded on JEOL ECP–500. Chemical shifts are reported in d ppm, referenced to internal tetramethylsilane standard for ^{1}H NMR, external trifluoroacetic acid standard (δ–76.5 ppm) for ^{19}F NMR and internal 85 % H_3PO_4 standard for ^{31}P NMR. ESI–mass spectra were measured on JEOL JMS–700 M Station. Elemental analyses were performed by Perkin Elmer 2400II.

4.2.3 Syntheses

4.2.3.1 Preparation of (2-bromophenyl)diphenylphosphine

In Schlenk tube, 1-bromo-2-iodobenzene (2.5 g, 8.8 mmol), diphenylphosphine (1.4 mL, 8.0 mmol), triethylamine (1.5 mL, 11 mmol), and a catalytic amount of $Pd(PPh_3)_4$ (50 mg, 4.4×10^{-2} mmol) were dissolved in 2 mL of toluene under nitrogen atmosphere. The solution was heated at 80 °C under stirring for 16 h. The reaction mixture was washed with brine and extracted with diethyl ether three times. The organic layer was dried over anhydrous magnesium sulfate, and concentrated to dryness. Column chromatography on silica gel (hexane/dichloromethane = 4:1) afforded the titled compound as a white solid [33].

Yield: 2.1 g (79 %). ^{1}H NMR (500 MHz, $CDCl_3$, 25 °C) δ 7.59–7.61 (m, 1H, Ar), 7.34–7.38 (m, 6H, Ar), 7.26–7.30 (m, 4H, Ar), 7.19–7.21 (m, 2H, Ar), 6.74–6.76 (m, 1H, Ar) ppm.

4.2.3.2 Preparation of bis(o-diphenylphosphorylphenyl)phenylphosphine oxide (dpppo)

Bis(*o*-diphenylphosphorylphenyl)phenylphosphine (dpppo) was synthesized according to the published procedure. (2-bromophenyl)diphenylphosphine (3.0 g, 9.6 mmol) and dry THF (90 mL), were placed in a 200 mL, three necked flask equipped with a dropping funnel and a nitrogen balloon. The solution was cooled to –80 °C and then 1.6 M *n*-butyllithium hexane solution (6.0 mL, 9.64 mmol) was added dropwise via dropping funnel. After the mixture was stirred at −80 °C for 30 min, dichlorophenylphosphine (0.86 g, 4.8 mmol) was added. The reaction mixture was warmed to room temperature and stirred at room temperature for 3 h. The reaction was quenched by addition of water (ca. 30 mL), and then the resulting white solid was collected by filtration. The solid was dissolved in chloroform (ca. 100 mL) and washed with water three times. The organic layer was separated and dried over anhydrous magnesium sulfate, and concentrated to

dryness. The obtained powder and dichloromethane (50 mL) were placed in a 100 mL flask. The solution was cooled to 0 °C and then 30 % H_2O_2 aqueous solution (8 mL) was added to it. The reaction mixture was stirred at −0 °C for 2 h. The organic layer was separated and washed with water three times, then dried over anhydrous magnesium sulfate and concentrated to dryness. Recrystallization from chloroform/hexane gave white solid of the titled compound [34].

Yield: 1.4 g (50 %). MALDI–TOF Mass (*m/z*) = 679.2 $[M+H]^+$. ^1H NMR (500 MHz, $CDCl_3$, 25 °C) δ 7.98 (m, 2H, Ar), 7.25–7.60 (m, 31H, Ar) ppm. ^{31}P NMR (200 MHz, $CDCl_3$, 25 °C) δ 36.78 (1P), 33.65 (2P) ppm. Anal. Calcd for $C_{42}H_{33}O_3P_3 \cdot 0.3CHCl_3$; C, 70.77; H, 4.68. Found: C, 70.88; H, 4.60.

4.2.3.3 Preparation of (*o*-bromopyridyl)diphenylphosphine

2,3-dibromopyridine (8.0 g, 34 mmol), diphenylphosphine (6.3 g, 34 mmol), triethylamine (6.9 g, 68 mmol), and a catalytic amount of $Pd(PPh_3)_4$ (390 mg, 0.34 mmol) were dissolved in 40 mL of toluene under nitrogen atmosphere. The solution was heated at 80 °C under stirring for 16 h. The reaction mixture was washed with brine and extracted with diethyl ether three times. The organic layer was dried over anhydrous magnesium sulfate, and concentrated to dryness. Recrystallization from ethyl acetate/hexane gave colorless block crystals of the titled compound.

Yield: 9.3 g (81 %). IR (ATR) 1559, 1478, 1436, 1382, 1011 cm^{-1}. MALDI–TOF Mass (*m/z*) = 342.0 $[M+H]^+$. ^1H NMR (300 MHz, $CDCl_3$, 25 °C) δ 8.58–8.56 (m, 1H, Ar), 7.78–7.83 (m, 1H, Ar), 7.35–7.40 (m, 10H, Ar), 7.06–7.10 (m, 1H, Ar) ppm. Anal. Calcd for $C_{17}H_{13}BrNP$: C, 59.67; H, 3.83; N 4.09. Found: C, 59.82; H, 3.71; N, 4.10.

4.2.3.4 Preparation of bis(*o*-diphenylphosphorylpyridyl)phenylphosphine oxide (dppypo)

(*o*-bromopyridyl)diphenylphosphine (1.7 g, 5.0 mmol) and dry THF (40 mL) were placed in a 200 mL, three necked flask equipped with a dropping funnel and a nitrogen balloon. The solution was cooled to −80 °C and then 1.6 M *n*-butyllithium hexane solution (3.3 mL, 5.3 mmol) was added dropwise via syringe. After the mixture was stirred at −80 °C for 1 h, dichlorophenylphosphine (0.45 g, 2.5 mmol) was added dropwise via dropping funnel. The reaction mixture was warmed to room temperature and stirred at room temperature for 3 h. The reaction was quenched by addition of water (ca. 5 mL) and extracted with chloroform three times. The organic layer was dried over anhydrous magnesium sulfate, and concentrated to dryness. The obtained powder was dissolved in dichloromethane (15 mL) in a 100 mL flask. The solution was cooled to 0 °C, and then 30 % H_2O_2 aqueous solution (3 mL) was added. The reaction mixture was stirred at 0 °C for 2 h, and then reaction mixture was extracted with dichloromethane three times.

The organic layer was dried over anhydrous magnesium sulfate, and concentrated to dryness. Recrystallization from acetone/hexane gave white powder of the titled compound.

Yield: 0.36 g (21 %). IR (ATR) 1548, 1434, 1390, 1197, 1119, 1107 cm^{-1}. MALDI–TOF Mass (*m/z*) = 681.5 $[M + H]^+$. ^1H NMR (300 MHz, $CDCl_3$, 25°C) δ 8.73 (s, 2H, Ar), 7.92–7.99 (m, 2H, Ar), 7.21–7.64 (m, 27H, Ar) ppm. ^{31}P NMR (200 MHz, $CDCl_3$, 25 °C) δ 29.71 (s,1P), 25.20 (br. 2P) ppm. Anal. Calcd for $C_{40}H_{31}N_2O_3P_3 \cdot H_2O$: C, 68.77; H, 4.76; N, 4.01. Found: C, 69.02; H, 4.66; N, 3.97.

4.2.3.5 Preparation of 2,3-dibromobenzothiophene

2,3-dibromobenzothiophene was synthesized according to the published procedure. Benzothiophene (19 g, 140 mmol) were dissolved in chloroform (200 mL). Then, Br_2 (16 mL, 310 mmol) was added dropwise to the solution. The reaction mixture was stirred at room temperature for 24 h. The resulting solution was washed with $Na_2S_2O_3$ aqueous solution, and extracted with ethyl acetate three times. The organic layer was dried over anhydrous magnesium sulfate, and concentrated to dryness. Column chromatography on silica gel (hexane/dichloromethane = 4:1) afforded the titled compound as a white solid [35].

Yield: 40 g (96 %). IR (ATR) 1419, 1298, 1245, 987, 893, 743, 716 cm^{-1}. MALDI–TOF Mass (*m/z*) = 290.8 $[M+H]^+$. ^1H NMR (300 MHz, $CDCl_3$, 25 °C) δ 7.69–7.76 (m, 2H, Ar), 7.35–7.45 (m, 2H, Ar) ppm.

4.2.3.6 Preparation of (*o*-bromobenzothienyl)diphenylphosphine

2,3-dibromobenzothiophene (20 g, 69 mmol) and dry THF (500 mL) were placed in a 1000 mL, three-necked flask equipped with a dropping funnel and a nitrogen balloon. The solution was cooled to −80 °C and then 1.6 M *n*-butyllithium hexane solution (43 mL, 69 mmol) was added dropwise via dropping funnel. After the mixture was stirred at −80 °C for 1 h, chlorodiphenylphosphine (15 g, 69 mmol) was added dropwise. The reaction mixture was warmed to room temperature and stirred at room temperature for 12 h. The reaction was quenched by addition of water, and extracted with diethyl ether 3 times. The organic layer was dried over anhydrous magnesium sulfate, and concentrated to dryness. Recrystallization from chloroform/hexane for a month gave white yellow crystals of the titled compound.

Yield: 15 g (54 %). IR (ATR) 1431, 1243, 999, 891, 743, 726, 692 cm^{-1}. MALDI–TOF Mass (*m/z*) = 397.3 $[M+H]^+$. ^1H NMR (300 MHz, $CDCl_3$, 25 °C) δ 7.83–7.86 (d, J = 9 Hz, 1H, Ar), 7.68–7.71 (d, J = 9 Hz, 1H, Ar), 7.37–7.47 (m, 12H, Ar) ppm. Anal. Calcd for $C_{20}H_{14}BrPS$: C, 60.47; H, 3.55. Found: C, 60.26; H, 3.36.

4.2.3.7 Preparation of bis(*o*-diphenylphosphorylbenzothienyl) phenylphos phine oxide (dpbtpo)

(*o*-bromobenzothienyl)diphenylphosphine (4.0 g, 10 mmol) and dry THF (100 mL) were placed in a 300 mL, three necked flask equipped with a dropping funnel and a nitrogen balloon. The solution was cooled to −80 °C and then 1.6 M *n*-butyllithium hexane solution (6.6 mL, 11 mmol) was added dropwise via syringe. After the mixture was stirred at −80 °C for 1 h, dichlorophenylphosphine (0.90 g, 5.0 mmol) was added dropwise via dropping funnel. The reaction mixture was warmed to room temperature and stirred at room temperature for 3 h. The reaction was quenched by addition of water (ca. 5 mL), and extracted with chloroform three times. The organic layer was dried over anhydrous magnesium sulfate, and concentrated to dryness. The obtained powder was dissolved in dichloromethane (30 mL) in a 100 mL flask. The solution was cooled to 0 °C, and then 30 % H_2O_2 aqueous solution (6 mL) was added. The reaction mixture was stirred at 0 °C for 2 h, and then reaction mixture was extracted with dichloromethane three times. The organic layer was dried over anhydrous magnesium sulfate, and concentrated to dryness. Recrystallization from acetone/hexane gave white powder of the titled compound.

Yield: 1.0 g (26 %). IR (ATR) 1457, 1437, 1388, 1203, 1116, 1102, 1010, 898, 801 cm^{-1}. MALDI–TOF Mass (*m/z*) = 791.5 $[M+H]^+$. ^1H NMR (300 MHz, $CDCl_3$, 25 °C) δ 8.34–8.42 (d, $J = 24$ Hz, 2H, Ar), 7.64–7.71 (m, 6H, Ar), 7.45–7.47 (m, 9H, Ar), 7.24–7.30 (m, 14H, Ar), 6.86 (br, 2H, Ar) ppm. ^{31}P NMR (200 MHz, $CDCl_3$, 25 °C) δ 21.80–21.83 (d, $J = 6$ Hz, 2P), 14.81–14.87 (t, $J = 6$ Hz, 1P) ppm. Anal. Calcd for $C_{46}H_{33}S_2O_3P_3{\cdot}0.5CH_2Cl_2$: C, 67.02; H, 4.11. Found: C, 67.33; H, 4.11.

4.2.3.8 General Procedure for the Preparation of Eu(III) Complexes

Phosphine oxide ligand (1 equiv) and $Eu(hfa)_3(H_2O)_2$ (1.2 equiv) were dissolved in methanol (20 mL). The solution was refluxed while stirring for 8 h, and the reaction mixture was concentrated to dryness. The residue was washed with chloroform several times. The insoluble material was removed by filtration, and the filtrate was concentrated. Recrystallization from acetone gave colorless crystals of the Eu(III) complexes.

[$Eu(hfa)_3$(dpppo)]: Yield: 90 mg (26 %). IR (ATR) 1657, 1537, 1439, 1252, 1176, 1136, 789, 746, 727, 692, 660 cm^{-1}. ^{19}F NMR (470 MHz, acetone–d_6, 25 °C) δ–79.36 ppm. ^{31}P NMR (200 MHz, acetone–d_6, 25 °C) δ 0.55 (1P), –29.03 (1P), –68.37 (1P) ppm. ESI–Mass (*m/z*) = 1245.052 $[M–(hfa)]^+$. Anal. Calcd for $C_{57}H_{36}EuF_{18}O_9P_3$: C, 47.16; H, 2.50. Found: C, 47.10; H 2.50.

[$Eu(hfa)_3$(dppypo)]: Yield: 380 mg (59 %). IR (ATR) 1653, 1550, 1525, 1507, 1440, 1252, 1191, 1138, 1124, 1097 cm^{-1}. ^{19}F NMR (470 MHz, acetone–d_6, 25 °C) δ –78.71 (s) ppm. ^{31}P NMR (200 MHz acetone–d_6, 25 °C) δ–12.08 (s, 1P), –15.81 (s, 1P), –64.75 (s, 1P) ppm. ESI–Mass (*m/z*) = 1247.052 $[M–(hfa)]^+$. Anal.

Calcd for $C_{55}H_{34}Eu\ F_{18}N_2O_9P_3{\cdot}1.5CHCl_3$: C, 41.59; H, 2.13; N, 1.72. Found: C, 41.71; H, 2.13; N, 1.70.

[Eu(hfa)$_3$(dpbtpo)]: Yield: 170 mg (28 %). IR (ATR) 1657, 1534, 1440, 1251, 1185, 1138, 1125, 1104 cm^{-1}. ^{19}F NMR (470 MHz, acetone–d_6, 25 °C) δ–78.55 (s) ppm. ^{31}P NMR (200 MHz, acetone–d_6, 25 °C) δ–47.78 (s, 1P), –53.29 (s, 1P), –78.18 (s, 1P) ppm. ESI–Mass (m/z) = 1357.001 [M–(hfa)]$^+$. Anal. Calcd for $C_{61}H_{36}EuF_{18}S_2O_9P_3$: C, 46.85; H, 2.32. Found: C, 46.68; H, 2.24.

4.2.4 Crystallography

Colorless single crystals of Eu(hfa)$_3$(dpppo) and Eu(hfa)$_3$(dpbtpo) obtained from acetone solution were mounted on a glass fiber using epoxy resin glue. All measurements were made on a Rigaku RAXIS RAPID imaging plate area detector with graphite monochromated MoKα radiation. The data were collected at a temperature range of -120 ± 1 °C to a maximum 2θ value of 48.8°. Corrections for decay and Lorentz-polarization effects were made with empirical absorption correction, solved by direct methods and expanded using Fourier techniques. The non-hydrogen atoms were refined anisotropically. Hydrogen atoms were refined using the riding model. The final cycle of full-matrix least-squares refinement was based on observed reflections and variable parameters. All calculations were performed using the crystal structure crystallographic software package. CCDC-737332 (for Eu(hfa)$_3$(dpppo)) and -737333 (for Eu(hfa)$_3$(dpbtpo)) contain the supplementary crystallographic data for this paper. CIF data confirmed by using checkCIF/PLATON service.

4.2.5 Optical Measurements

UV–Vis absorption spectra were recorded on a JASCO V–550 spectrometer. Emission spectra of the Eu(III) complexes were measured with a Hitachi F–4500 spectrometer and corrected for the response of the detector system. The emission quantum yields of Eu(hfa)$_3$(dpppo), Eu(hfa)$_3$(dppypo) and Eu(hfa)$_3$(dpbtpo) (5.0 mM in acetone-d_6) were obtained by comparison with the emission signal integration (570–640 nm) of Eu(hfa)$_3$(biphepo) as a reference ($\Phi_{Ln} = 0.60$: 50 mM in acetone-d_6) with excitation wavelength of 465 nm [36]. Emission lifetimes of Eu(hfa)$_3$(dpppo), Eu(hfa)$_3$(dppypo) and Eu(hfa)$_3$(dpbtpo) (1.0 mM in acetone-d_6) were measured with the third harmonics (355 nm) of a Q-swiched Nd:YAG laser (Spectra Physics, INDI-50, fwhm = 5 ns, $\lambda = 1064$ nm) and a photomultiplier (Hamamatsu photonics, R5108, response time $\leq$1.1 ns). The Nd:YAG laser response was monitored with a digital oscilloscope (Sony Tektronix, TDS3052, 500 MHz) synchronized to the single-pulse excitation. Emission

lifetimes were determined from the slope of logarithmic plots of decay profiles. High-resolution emission spectra were measured with a SPEX-Fluorolog τ-3 (JOBIN YVON).

4.3 Results and Discussion

4.3.1 Syntheses and Coordination Structures

Eu(III) complexes with tridentate phosphine oxides, $Eu(hfa)_3$(dpppo), $Eu(hfa)_3$(dppypo) and $Eu(hfa)_3$(dpbtpo) were synthesized by complexation of phosphine oxide ligands with $Eu(hfa)_3(H_2O)_2$ in methanol for 8 h as illustrated in Scheme 4.1. The IR spectra and elemental analyses indicate that no water molecule existed in the coordination sites of Eu(III) complexes. The author also observed the signals of corresponding $[Eu(hfa)_2(dpppo)]^+$, $[Eu(hfa)_2(dppypo)]^+$ and $[Eu(hfa)_2(dpbtpo)]^+$ in ESI-mass spectra. The ^{31}P NMR spectra of the Eu(III) complexes in acetone-d_6 exhibited three specific signals. These results indicate that the magnetic environments of phosphine oxides were different from each other in the solution phase.

The single crystals of $Eu(hfa)_3$(dpppo) and $Eu(hfa)_3$(dpbtpo) were successfully prepared for X-ray single-crystal analyses by way of recrystallization from acetone solutions. The ORTEP views and crystal data from the X-ray single-crystal analyses are summarized in Fig. 4.2 and Table 4.1. The ORTEP views of both $Eu(hfa)_3$(dpppo) and $Eu(hfa)_3$(dpbtpo) show the nona-coordinated structures with one tridentate phosphine oxide (dpppo or dpbtpo) and three hfa ligands. The coordination geometries of $Eu(hfa)_3$(dpppo) and $Eu(hfa)_3$(dpbtpo) are categorized as Mono-capped square antiprisms (9-SAP) [37]. In $Eu(hfa)_3$(dpppo) and $Eu(hfa)_3$(dpbtpo), the Eu–O bond lengths that are attached with two terminal phosphine oxides in Table 4.2 are similar to those of the reported $Eu(hfa)_3$(biphepo), 2.32 and 2.34 Å [38]. The Eu–O bond length for the central phosphine oxide in $Eu(hfa)_3$(dpppo) (Eu–O2: 2.51 Å) and $Eu(hfa)_3$(dpbtpo) (Eu–O1: 2.48 Å) are considerably longer than those of the terminal phosphine oxides. Specific interactions between ligands, such as CH–F hydrogen bonds, CH–π, π–π interactions, have not been observed. The coordination structures of $Eu(hfa)_3$(dpppo) and $Eu(hfa)_3$(dpbtpo) are thus considerably distorted compared with the usual 9-SAP shapes and would be categorized according to their quasi-C_1 symmetry, consistent with octa-coordinated $Eu(hfa)_3$(biphepo) (Fig. 4.3).

Two terminal phosphine oxides of $Eu(hfa)_3$(dpppo) are located on the upper square of 9-SAP, while those of $Eu(hfa)_3$(dpbtpo) are attached to the upper and lower squares of 9-SAP. The author thus considers that the coordination structures of Eu(III) complexes with tridentate phosphine oxide ligands are markedly influenced by the moiety between the phosphine oxides.

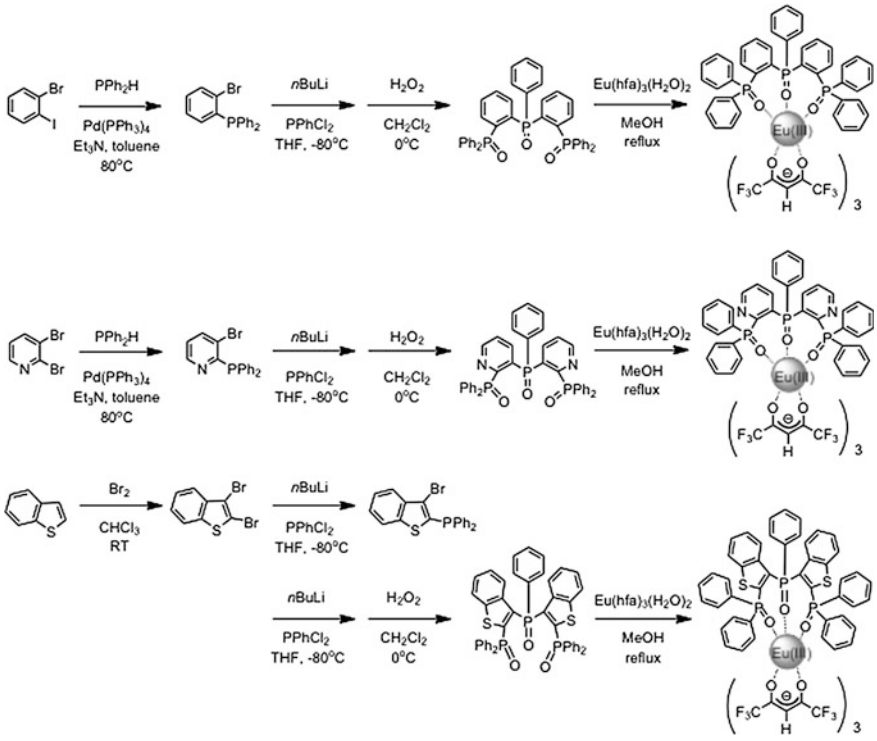

Scheme 4.1 Synthetic routes of nona-coordinated Eu(III) complexes

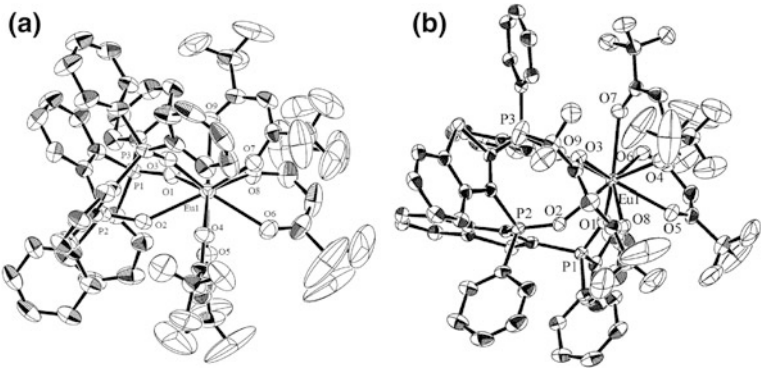

Fig. 4.2 ORTEP drawings of single crystals of **a** $Eu(hfa)_3(dpppo)$ from acetone/water solution and **b** $Eu(hfa)_3(dpbtpo)$ from acetone solution. Hydrogen atoms have been omitted for clarity and thermal ellipsoids are shown at the 50 % probability level

Based on the X-ray single crystal analyses, the author carried out calculations of charge densities of phosphorus atoms by using DFT calculation (6-31G(d)/B3LYP). According to the calculation, charge densities of phosphorus atoms were

Table 4.1 Crystal data of Eu(III) complexes with tridentate phosphine oxides

	Eu(hfa)$_3$(dpppo)	2Eu(hfa)$_3$(dpbtpo) + 0.5 acetone
Chemical formula	$C_{57}H_{36}EuF_{18}O_9P_3$	$C_{125}H_{78}Eu_2F_{36}O_{19}P_6S_4$
Formula weight	1451.76	3185.93
Crystal color, habit	Colorless, block	Colorless, block
Crystal system	Trigonal	Monoclinic
Space group	R3c	C2/c
a/Å	40.3572(7)	24.6695(14)
b/Å		12.3999(6)
c/Å	24.5364(5)	42.565(2)
β/°		99.3595(14)
V/Å^3	34608.5(10)	12847.4(11)
Z	18	4
d_{calc}/g cm^{-3}	1.254	1.645
T/ °C	−80 ± 1	−120 ± 1
μ (Mo Kα)/cm^{-1}	9.617	12.226
max 2θ/deg	50.6	48.8
No. of measured reflections	91569	44801
No. of unique reflections	13372	10505
R ($I > 2\sigma$(I))[a]	0.0344	0.0351
R_w ($I > 2\sigma$(I))[b]	0.1106	0.0870

[a] $R = \Sigma\ ||F_o| - |F_c||/\Sigma\ |F_o|$
[b] $R_w = [(\Sigma\ w\ (|F_o| - |F_c|)^2\ /\Sigma\ w\ F_o^2)]^{1/2}$

Table 4.2 Selected bond lengths [Å] of Eu(III) complexes

Bond	Eu(hfa)$_3$(dpppo)	Eu(hfa)$_3$(dpbtpo)
Eu−O1 (P=O)	2.360 (terminal)	2.482 (central)
Eu−O2 (P=O)	2.511 (central)	2.403 (terminal)
Eu−O3 (P=O)	2.322 (terminal)	2.355 (terminal)

found to be P1: 0.22, P2: 0.14, P3 0.29 (dpppo), P1: 0.04, P2: 0.35, P3: 0.11 (dpbtpo), respectively (Fig. 4.4). The author thus considers that three peaks in ^{31}P NMR spectra of Eu(III) complexes might be caused by different electron densities of phosphorus atoms.

4.3.2 Photophysical Properties

The steady-state emission spectra of Eu(hfa)$_3$(dpppo), Eu(hfa)$_3$(dppypo) and Eu(hfa)$_3$(dpbtpo) in acetone-d_6 are shown in Fig. 4.5a. Emission bands were observed at around 578, 592, 614, 650, and 700 nm, and are attributed to the f–f transitions of $^5D_0$–^7F_J with $J = 0$, 1, 2, 3 and 4, respectively. The spectra were normalized with respect to the magnetic dipole transition intensity ($^5D_0$–$^7F_1$) at

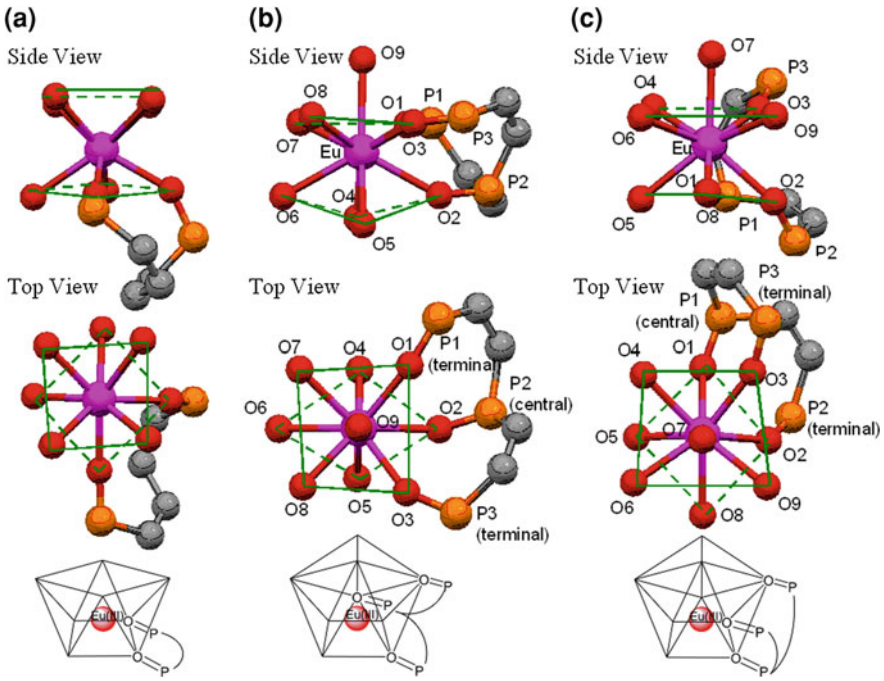

Fig. 4.3 Coordination polyhedrons of **a** $Eu(hfa)_3(biphepo)$, **b** $Eu(hfa)_3(dpppo)$ and **c** $Eu(hfa)_3(dpbtpo)$

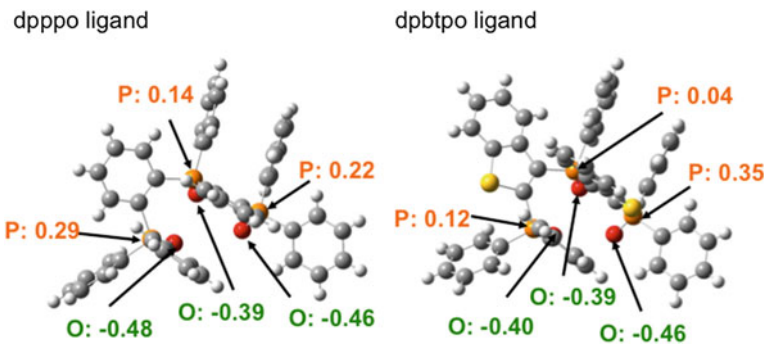

Fig. 4.4 Charge densities of phosphorus atoms in **a** dpppo and **b** dpbtpo ligand

592 nm which is known to be insensitive to the surrounding environment of the Eu(III) ion. The emission band at 614 nm ($^5D_0$–$^7F_2$) is due to the electric dipole transition for which intensity is greatly dependent on the chemical structures. In order to analyze the transition intensity, the author here estimated the relative emission intensity of $^5D_0$–$^7F_2$ transition with respect to that of $^5D_0$–$^7F_1$ as $I_{rel} = I_{614}/I_{592}$ in the

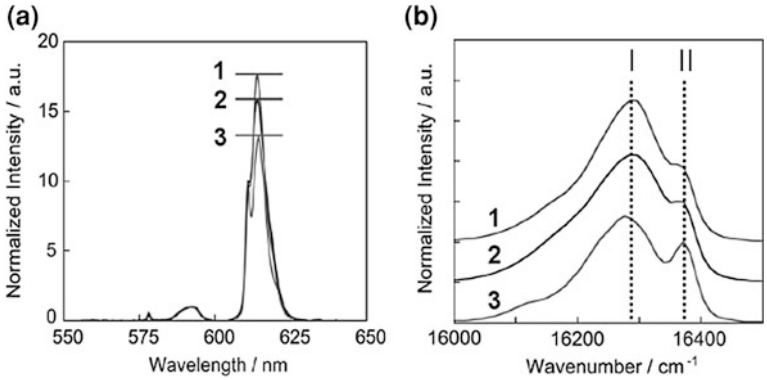

Fig. 4.5 **a** Emission spectra of $Eu(hfa)_3(dpbtpo)$ (*line* 1), $Eu(hfa)_3(dppypo)$ (*line* 2) and $Eu(hfa)_3(dpppo)$ (*line* 3) in acetone-d_6 at room temperature. Excited at 465 nm. The spectra were normalized with respect to the magnetic dipole transition ($^5D_0$–$^7F_1$). **b** Stark splitting at the electric dipole transition ($^5D_0$–$^7F_2$) of the Eu(III) complexes

Table 4.3 Photophysical properties of Eu(III) complexes at room temperature[a]

Complex	Φ_{Ln}/%[b]	τ_{obs}/ms[c]	k_r/s^{-1}	k_{nr}/s^{-1}	I_{rel}[d]
$Eu(hfa)_3(dpbtpo)$	62	1.3	5.0×10^2	3.0×10^2	18
$Eu(hfa)_3(dppypo)$	61	1.2	5.1×10^2	3.2×10^2	16
$Eu(hfa)_3(dpppo)$	60	1.2	5.0×10^2	3.3×10^2	13
$Eu(hfa)_3(biphepo)$[e]	60	1.3	4.6×10^2	3.4×10^2	-
$Eu(hfa)_3(tppo)_2$[e]	65	1.2	5.4×10^2	3.0×10^2	-

[a] The emission spectra, quantum yield (Φ_{Ln}) and lifetime (τ_{obs}) were measured by excitation at 465 nm. Radiative rate constant $k_r = \Phi_{Ln}/\tau_{obs}$. Nonradiative rate constant $k_{nr} = 1/\tau_{obs} - k_r$

[b] Emission quantum yields were determined by comparing with the emission signal integration (570–640 nm) of $Eu(hfa)_3(biphepo)$ as $\Phi_{Ln} = 0.60$

[c] Emission lifetimes (τ_{obs}) of the Eu(III) complexes were measured by excitation at 355 nm (Nd:YAG 3ω)

[d] Relative emission intensity of the electric dipole transition ($^5D_0$–$^7F_2$) to the magnetic dipole transition ($^5D_0$–$^7F_1$)

[e] [13]

normalized emission spectra. The I_{rel} values of $Eu(hfa)_3(dpbtpo)$, $Eu(hfa)_3(dppypo)$ and $Eu(hfa)_3(dpppo)$ were found to be 18, 16 and 13, respectively, as summarized in Table 4.3. The emission spectra with Stark splittings at the electric dipole transition ($^5D_0$–$^7F_2$) of Eu(III) complexes in acetone-d_6 are also shown in Fig. 4.5b. Five-fold degenerated $^7F_2$ states of Eu(III) complexes are known to split into some Stark levels between one and five depending on symmetry of the coordination structure. The author found that the emission spectral profiles and the wavenumbers of transition bands I and II of $Eu(hfa)_3(dpppo)$ and $Eu(hfa)_3(dpbtpo)$ well agreed with those of $Eu(hfa)_3(dppypo)$ (16280 cm^{-1}, 16370 cm^{-1}). The energy gaps between the transition bands I and II of these Eu(III) complexes were approximately 85 cm^{-1}.

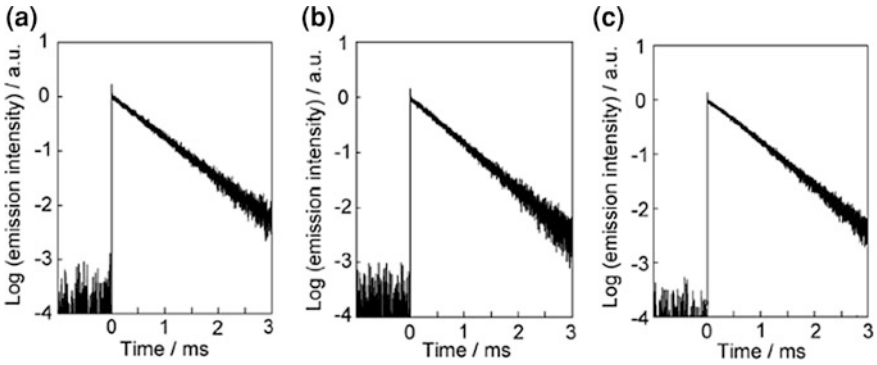

Fig. 4.6 The decay profiles of **a** $Eu(hfa)_3(dpppo)$, **b** $Eu(hfa)_3(dppypo)$, and **c** $Eu(hfa)_3$ (dpbtpo) in acetone-d_6

Since the energy gap between the Stark splitting levels reflects its geometrical symmetry [32], $Eu(hfa)_3(dppypo)$ might be similar to $Eu(hfa)_3(dpppo)$ and $Eu(hfa)_3(dpbtpo)$ in its structure in acetone-d_6. The emission quantum yields of $Eu(hfa)_3(dpppo)$, $Eu(hfa)_3(dppypo)$ and $Eu(hfa)_3(dpbtpo)$ in acetone-d_6 were found to be 0.60, 0.61 and 0.62, respectively (Table 4.3). These emission quantum yields are similar to those reported for $Eu(hfa)_3(biphepo)$ ($\Phi_{Ln} = 0.60$ in acetone-d_6) and $Eu(hfa)_3(tppo)_2$ ($\Phi_{Ln} = 0.65$ in acetone-d_6), both of which have been reported as highly luminescent Eu(III) complexes [38].

The time-resolved emission profiles of all Eu(III) complexes revealed single-exponential decays with lifetimes in the millisecond time scale as shown in Fig. 4.6. The emission lifetimes were determined from the slopes of logarithmic plots of the decay profiles. The radiative (k_r) and nonradiative (k_{nr}) rate constants estimated using the emission lifetimes and the emission quantum yields are summarized in Table 4.3. The author observed that the radiative rate constants of nona-coordinated $Eu(hfa)_3(dpppo)$ (5.0×10^2 s^{-1}), $Eu(hfa)_3(dppypo)$ (5.1×10^2 s^{-1}) and $Eu(hfa)_3(dpbtpo)$ (5.0×10^2 s^{-1}) were similar to those of the octa-coordinated $Eu(hfa)_3(biphepo)$ (4.6×10^2 s^{-1}) and $Eu(hfa)_3(tppo)_2$ (5.4×10^2 s^{-1}). Generally, reduction of the geometrical symmetry of coordination structure leads to a larger radiative rate constant. The radiative rate constant of Eu(III) complex with phosphine oxides seems to depend on the symmetry of the coordination sites, but not on the coordination number. The nonradiative rate constants of $Eu(hfa)_3(dpppo)$ (3.3×10^2 s^{-1}), $Eu(hfa)_3(dppypo)$ (3.2×10^2 s^{-1}) and $Eu(hfa)_3(dpbtpo)$ (3.0×10^2 s^{-1}) were also quite similar to that of $Eu(hfa)_3(biphepo)$ (3.4×10^2 s^{-1}) and $Eu(hfa)_3(tppo)_2$ (3.0×10^2 s^{-1}). The nonradiative rate constant of Eu(III) might not be affected by vibrational, electric and steric structures of the chemical species attached with LVF phosphine oxides.

In this chapter, the author found that the emission intensities at the electric dipole transition of Eu(III) complexes depended on the organic linker species in phosphine oxide ligands, although the energy gap between Stark splitting levels, radiative and non-radiative rate constants were not affected by them. It seems that

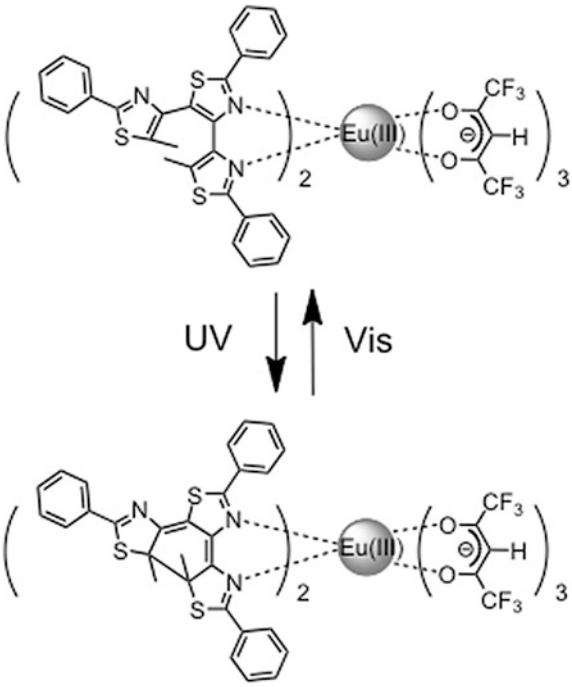

Fig. 4.7 Eu(III) complexes with photochromic terarylene ligands

the transition intensity at the electric dipole transition is affected by chemical structures of attached tridentate phosphine oxide ligands. Recently, Nakagawa has observed that the transition intensity of Eu(III) complex with photochromic terarylene ligands is influenced by the polarizability of attached photochromic units (Fig. 4.7) [39–41]. The effect of polarizability on lanthanide complexes has also been suggested [42, 43]. The author reasons that the emission spectral shapes of Eu(III) complexes with tridentate phosphine oxide ligands might be related not only to geometrical and vibrational structures of Eu(III) complexes, but also to the chemical structures of their ligands.

4.4 Conclusions

The author successfully synthesized novel Eu(III) complexes containing characteristic tridentate phosphine oxide ligands, dpppo, dppypo and dpbtpo with high emission quantum yields ($\Phi_{Ln} > 60$ %). These Eu(III) complexes showed characteristic emission properties depending on their moiety between phosphine oxides. In this chapter, the author has reported on nona-coordinated lanthanide complexes with characteristic photophysical properties. The photophysical properties of Eu(III) complexes with tridentate phosphine oxide ligands would be discussed on the basis of geometrical, vibrational and chemical structures of the ligands.

References

1. T. Justel, H. Nikol, C. Ronda, Angew. Chem. Int. Ed. **37**, 3084 (1998)
2. J. Kido, Y. Okamoto, Chem. Rev. **102**, 2357 (2002)
3. J. Yu, L. Zhou, H. Zhang, Y. Zheng, H. Li, R. Deng, Z. Peng, Z. Li, Inorg. Chem. **44**, 1611 (2005)
4. H. Xu, K. Yin, W. Huang, J. Phys. Chem. C **114**, 1674 (2010)
5. K. Kuriki, Y. Koike, Y. Okamoto, Chem. Rev. **102**, 2347 (2002)
6. N. Weibel, L.J. Charbonniere, M. Guardigli, A. Roda, R. Ziessel, J. Am. Chem. Soc. **126**, 4888 (2004)
7. J.-C.G. Bunzli, C. Piguet, Chem. Soc. Rev. **34**, 1048 (2005)
8. S. Faulkner, B.P. Burton-Pye, Chem. Commun. 259 (2005)
9. J. Yu, D. Parker, R. Pal, R.A. Poole, M.J. Cann, J. Am. Chem. Soc. **128**, 2294 (2006)
10. B. McMahon, P. Mauer, C.P. McCoy, T.C. Lee, T. Gunnlaugsson, J. Am. Chem. Soc. **131**, 17542 (2009)
11. V.S. Sastri, J.-C.G. Bünzli, V. Ramachandra Rao, G.V.S. Rayudu, J.R. Perumareddi, *Modern Aspects of Rare Earths and Their Complexes*, (Elsevier, Amsterdam, 2003)
12. K. Lunstroot, P. Nockemann, K.V. Hecke, L.V. Meervelt, C. Görller-Walrand, K. Binnemans, K. Driesen, Inorg. Chem. **48**, 3018 (2009)
13. S. Petoud, S.M. Cohen, J.-C.G. Bunzli, K.N. Raymond, J. Am. Chem. Soc. **125**, 13324 (2003)
14. Y. Hasegawa, Y. Wada, S. Yanagida, J. Photochem. Photobiol. C: Photochem. Rev. **5**, 183–202 (2004)
15. A.F. Kirby, F.S. Richardson, J. Phys. Chem. **87**, 2544 (1983)
16. K. Binnemans, R.V. Deun, C. Görller-Walrand, S.R. Collinson, F. Martin, D.W. Bruce, C. Wickleder, Phys. Chem. Chem. Phys. **2**, 3753 (2000)
17. S.F. Mason, J. Indian Chem. Soc. **63**, 73 (1986)
18. F. Gan, *Laser Materials* (World Scientific, Singapore, 1995)
19. A. Wada, M. Watanabe, Y. Yamanoi, T. Nankawa, K. Namiki, M. Yamasaki, M. Murata, H. Nishihara, Bull. Chem. Soc. Jpn **80**, 335 (2007)
20. G. Stein, E. Würzberg, J. Chem. Phys. **62**, 208 (1975)
21. S.V. Eliseeva, J.-C.G. Bünzli, Chem. Soc. Rev. **39**, 189 (2010)
22. S.V. Eliseeva, O.V. Kotova, F. Gumy, S.N. Semenov, V.G. Kessler, L.S. Lepnev, J.-C.G. Bünzli, N.P. Kuzmina, J. Phys. Chem. A **112**, 3614 (2008)
23. Q.-B. Bo, H.-Y. Wang, D.-Q. Wang, Z.-W. Zhang, J.-L. Miao, G.-X. Sun, Inorg. Chem. **50**, 10163 (2011)
24. L.J. Charbonnire, R. Ziessel, M. Montalti, L. Prodi, C. Boehme, G. Wipff, J. Am. Chem. Soc. **124**, 7779 (2002)
25. S. Faulkner, J.A. Pope, J. Am. Chem. Soc. **125**, 10526 (2003)
26. G.S. Kottas, M. Mehlstäubl, R. Fröhlich, L. De Cola, Eur. J. Inrog. Chem. **22**, 3465 (2007)
27. M. Seitz, E.G. Moore, A.J. Ingram, G. Muller, K.N. Raymond, J. Am. Chem. Soc. **129**, 15468 (2007)
28. S. Petoud, G. Muller, E.G. Moore, J. Xu, J. Sokolnicki, J.P. Riehl, U.N. Le, S.M. Cohen, K.N. Raymond, J. Am. Chem. Soc. **129**, 77 (2007)
29. E. Deiters, B. Song, A. Chauvin, C.D.B. Vandevyver, F. Gumy, J.-C.G. Bünzli, Chem. Eur. J. **15**, 885 (2009)
30. D. Imperio, G.B. Giovenzana, G.-L. Law, D. Parker, J.W. Walton, Dalton Trans. **39**, 9897 (2010)
31. J. Xu, T.M. Corneillie, E.G. Moore, G.-L. Law, N.G. Butlin, K.N. Raymond, J. Am. Chem. Soc. **133**, 19900 (2011)
32. Y. Hasegawa, S. Tsuruoka, T. Yoshida, H. Kawai, T. Kawai, J. Phys. Chem. A **112**, 803 (2008)
33. M.T. Whited, E. Rivard, J.C. Peters, Chem. Commun. 1613 (2006)
34. J.G. Hartley, L.M. Venanzi, D.C. Goodall, J. Chem. Soc. 3930 (1963)

35. A. Heynderickx, A. Samat, R. Guglielmetti, Synthesis **2**, 213 (2002)
36. K. Nakamura, Y. Hasegawa, H. Kawai, N. Yasuda, Y. Tsukahara, Y. Wada, Thin Solid Films **516**, 2376 (2008)
37. R.B. King, J. Am. Chem. Soc. **91**, 7211 (1969)
38. K. Nakamura, Y. Hasegawa, H. Kawai, N. Yasuda, N. Kanehisa, Y. Kai, T. Nagamura, S. Yanagida, Y. Wada, J. Phys. Chem. A **111**, 3029 (2007)
39. T. Nakagawa, Y. Hasegawa, T. Kawai, J. Phys. Chem. A **112**, 5096 (2008)
40. T. Nakagawa, K. Atsumi, T. Nakashima, Y. Hasegawa, T. Kawai, Chem. Lett. **36**, 372 (2007)
41. T. Nakagawa, Y. Hasegawa, T. Kawai, Chem. Commun. 5630 (2009)
42. S.F. Mason, J. Indian Chem. Soc. **63**, 73 (1986)
43. J.J. Dallara, M.F. Reid, F.S. Richardson, J. Phys. Chem. **88**, 3587 (1984)

Chapter 5
Photophysical Properties of Lanthanide Complexes with Asymmetric Dodecahedron Structures

5.1 Introduction

As described in Chap. 4, the geometrical symmetry of lanthanide complex is regarded as a significant factor influencing the transition probability. It has been widely accepted that the radiative transition probability between 4f orbitals is enhanced by reducing the coordination structure's geometrical symmetry [1–9]. In 2000, Raymond has proposed a symmetric factor, the shape measure *S*, to estimate the geometrical distortion of lanthanide complexes [10]. Harada has also found that distortion of the coordination structures of Eu(III) complexes leads to enhancement of the electric dipole transition probability [11, 12]. Here, the author focused on oxo-linked bidentate phosphine framework as a novel ligand of lanthanide complex for enhancement of geometrical distortion. The oxo-linked bidentate phosphine ligands have been known to provide a large bite angle between a metal ion and phosphorus atoms in metal complex [13]. The author considered that the introduction of oxo-linked bidentate phosphine framework into coordination sites of lanthanide complexes might lead to expansion of their bite angles related to geometrical distortion (Fig. 5.1a). Based on these structural and photophysical findings, a lanthanide complex with distorted coordination structure composed of oxo-linked bidentate phosphine oxide ligands is expected to give rise to an increase in the electric dipole transition probability.

In this chapter, the author reports on the characteristic photophysical properties of lanthanide complexes with novel asymmetric structures (trigonal dodecahedron structures) composed of three kinds of oxo-linked bidentate phosphine oxide ligands (4,5-bis(diphenylphosphoryl)-9,9-dimethylxanthene: xantpo, 4,5-bis(di-*tert*-butylphosphoryl)-9,9-dimethylxanthene: *t*Bu-xantpo, and bis[(2-diphenylphosphoryl)phenyl] ether: dpepo) as shown in Fig. 5.1b. Robertson has recently reported that Eu(III) complexes with hfa and dpepo ligands exhibited strong luminescence properties in polymer thin films, [14] however, the geometrical structure and radiative rate constants of lanthanide complexes with dpepo ligands have not been reported. The author characterized the geometrical structures of the Eu(III) and Sm(III) complexes using X-ray single crystal analyses and shape

K. Miyata, *Highly Luminescent Lanthanide Complexes with Specific Coordination Structures*, Springer Theses,
DOI: 10.1007/978-4-431-54944-4_5, © Springer Japan 2014

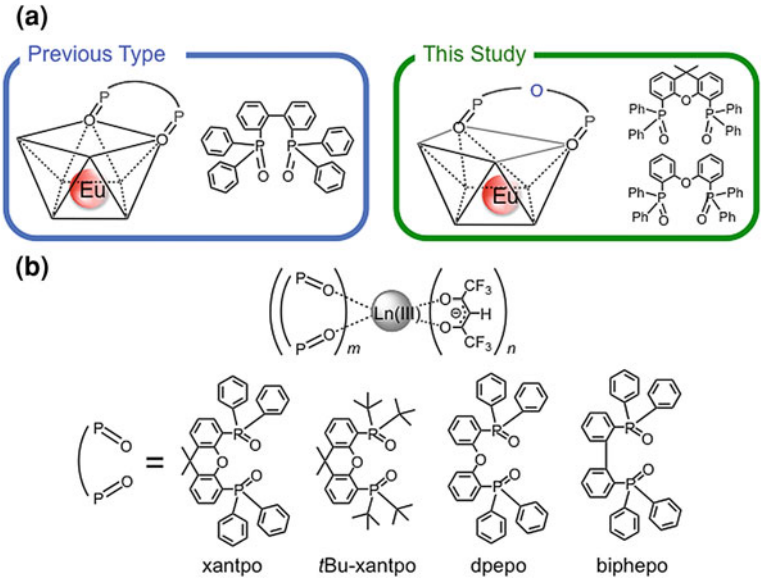

Fig. 5.1 **a** The research concept in this study and **b** chemical structures of lanthanide(III) complexes (Ln = Eu, Sm)

measure criteria. The luminescence properties were characterized by their emission quantum yields, emission lifetimes, and their radiative and nonradiative rate constants. Based on the structural and photophysical results, remarkable luminescence properties of lanthanide complexes with dodecahedron structures were demonstrated for the first time. The author also reports that the emission quantum yield of $Sm(hfa)_3(dpepo)$ with a trigonal dodecahedron structure is the highest in previous reported Sm(III) complexes. These remarkable luminescence properties will be elucidated in terms of their distorted coordination structures.

5.2 Experimental Section

5.2.1 Materials

Europium acetate monohydrate (99.9 %), samarium acetate tetrahydrate (99.9 %), acetone-d_6 (D, 99.9 %) and $CDCl_3$ (D, 99.8 %) were purchased from Wako Pure Chemical Industries Ltd. 1,1,1,5,5,5-hexafluoro-2,4-pentanedione, 4,5-bis(diphenylpho-sphino)-9,9-dimethylxanthene, 4,5-bis(di-*tert*-butylphosphino)-9,9-dimethylxanthene and bis[(2-diphenylphosphino)phenyl]ether were obtained from Tokyo Kasei

Organic Chemicals and Aldrich Chemical Company Inc. All other chemicals and solvents were reagent grade and were used without further purification.

5.2.2 Apparatus

Infrared spectra were recorded on a JASCO FT/IR–420 spectrometer. ^{1}H (300 and 500 MHz) and ^{31}P NMR (200 MHz) spectra were recorded on a JEOL ECP–500. Chemical shifts are reported in δ ppm, referenced to an internal tetramethylsilane standard for ^{1}H NMR and an external 85 % H_3PO_4 standard for ^{31}P NMR. Mass spectra were measured using a JEOL JMS–700 M Station. Elemental analyses were performed using a Perkin Elmer 2400II.

5.2.3 Syntheses

5.2.3.1 Preparation of Tris(hexafluoroacetylacetonato)europium Dihydrates [$Eu(hfa)_3(H_2O)_2$]

Europium acetate monohydrate (8.0 g, 23 mmol) was dissolved in distilled water (100 mL) in a 300 mL flask. A solution of 1,1,1,5,5,5-hexafluoro-2,4-pentanedione (16 g, 77 mmol) was added dropwise to the solution. The reaction mixture produced a precipitation of white yellow powder after stirring for 2 h at room temperature. The reaction mixture was filtered, and the resulting powder was recrystallized from methanol/water to afford colorless needle crystals of the titled compound.

Yield: 15 g (79 %). IR (KBr): 1650 (st, C=O), 1145–1258 (st, C–F) cm^{-1}. Anal. Calcd for $C_{15}H_7EuF_{18}O_8$: C, 22.48; H, 0.88. Found: C, 22.12; H, 1.01.

5.2.3.2 Preparation of Tris(hexafluoroacetylacetonato)samarium Dihydrates [$Sm(hfa)_3(H_2O)_2$]

Samarium acetate tetrahydrate (5.0 g, 13 mmol) was dissolved in distilled water (60 mL) in a 100 mL flask. A solution of 1,1,1,5,5,5-hexafluoro-2,4-pentanedione (10 g, 48 mmol) was added dropwise to the solution. The reaction mixture produced a precipitation of white yellow powder after stirring for 2 h at room temperature. The reaction mixture was filtered, and the resulting powder was recrystallized from methanol to afford colorless needle crystals of the titled compound.

Yield: 8.3 g (82 %). IR (KBr): 1646 (st, C=O), 1094–1251 (st, C–F) cm^{-1}. Anal. Calcd for $C_{15}H_7SmF_{18}O_8$: C, 22.31; H, 0.87. Found: C, 21.92; H, 1.10.

5.2.3.3 Preparation of 4,5-bis(diphenylphosphoryl)-9, 9-dimethylxanthene (xantpo)

4,5-bis(diphenylphosphino)-9,9-dimethylxanthene (1.0 g, 1.7 mmol) was dissolved in dichloromethane (20 mL) in a 100 mL flask. The solution was cooled to 0 °C, and then a 30 % H_2O_2 aqueous solution (4.0 mL) was added. The reaction mixture was stirred at 0 °C for 2 h, and was then washed with water and extracted three times with dichloromethane. The organic layer was dried over anhydrous magnesium sulfate, and concentrated to dryness. Reprecipitation from hexane gave a white powder of the titled compound.

Yield: 1.1 g (99 %). IR (ATR) 1190 (st, P=O), 1100–1229 (st, C–O–C) cm^{-1}. ^1H NMR (300 MHz, $CDCl_3$, 25 °C) δ 7.58–7.60 (d, $J = 6$ Hz, 2H, Ar), 7.30–7.47 (m, 20H, Ar), 6.94–7.00 (t, $J = 6$ Hz, 2H, Ar), 6.78–6.85 (m, 2H, Ar), 1.69 (s, 6H, 2Me) ppm. ^{31}P NMR (200 MHz, $CDCl_3$, 25 °C) δ 33.55 (1P), 30.32 (1P) ppm. FAB–Mass (m/z) = 611 $[M+H]^+$.

5.2.3.4 Preparation of 4,5-bis(di-*tert*-butylphosphoryl)-9, 9-dimethylxanthene (*t*Bu-xantpo)

4,5-bis(di-*tert*-butylphosphino)-9,9-dimethylxanthene (1.0 g, 2.0 mmol) was dissolved in dichloromethane (20 mL) in a 100 mL flask. The solution was cooled to 0 °C, and then a 30 % H_2O_2 aqueous solution (4.5 mL, 40 mmol) was added. The reaction mixture was stirred at 0 °C for 2 h, and was then washed with water and extracted three times with dichloromethane. The organic layer was dried over anhydrous magnesium sulfate, and concentrated to dryness. Reprecipitation from hexane gave a white powder of the titled compound.

Yield: 0.97 g (91 %). IR (ATR) 1180 (st, P=O), 1103–1200 (st, C–O–C) cm^{-1}. ^1H NMR (300 MHz, $CDCl_3$, 25 °C) δ 7.82–7.84 (d, $J = 6$ Hz, 2H, Ar), 7.53–7.60 (m, 2H, Ar), 7.40–7.46 (m, 2H, Ar), 1.67 (s, 6H, 2Me), 1.35–1.46 (m, 36H, 4*t*Bu) ppm. ^{31}P NMR (200 MHz, $CDCl_3$, 25 °C) δ 69.53 (1P), 58.36 (1P) ppm. FAB–Mass (m/z) = 531 $[M+H]^+$.

5.2.3.5 Preparation of Bis[(2-diphenylphosphoryl)phenyl]ether (dpepo)

Bis[(2-diphenylphosphino)phenyl]ether (5.0 g, 9.3 mmol) was dissolved in dichloromethane (100 mL) in a 300 mL flask. The solution was cooled to 0 °C, and then a 30 % H_2O_2 aqueous solution (20 mL) was added. The reaction mixture was stirred at 0 °C for 2 h, and was then washed with water and extracted three times with dichloromethane. The organic layer was dried over anhydrous magnesium sulfate, and concentrated to dryness. Reprecipitation from hexane gave a white powder of the titled compound.

Yield: 5.0 g (94 %). IR (ATR) 1183 (st, P=O), 1070–1226 (st, C–O–C) cm^{-1}. ^1H NMR (300 MHz, $CDCl_3$, 25 °C) δ 7.06–7.71 (m, 26H, Ar), 6.02–6.07 (m, 2H, Ar) ppm. ^{31}P NMR (200 MHz, $CDCl_3$, 25 °C) δ 26.41 (2P) ppm. FAB–Mass (m/z) = 571 $[M+H]^+$.

5.2.3.6 General Procedure for the Preparation of Eu(III) and Sm(III) Complexes

Phosphine oxide ligand (1 equiv) and $Ln(hfa)_3(H_2O)_2$ (1.2 equiv) were dissolved in methanol (30 mL). The solution was refluxed while stirring for 8 h, and the reaction mixture was concentrated to dryness. The residue was washed with chloroform several times. The insoluble material was removed by filtration, and the filtrate was concentrated. The obtained powder was dissolved in hot methanol solution, and was then permitted to stand at room temperature. Recrystallization from methanol gave colorless block crystals of the lanthanide complexes.

[Eu(hfa)$_2$(xantpo)$_2$]: Yield: 0.32 g (49 %). IR (ATR) 1653 (st, C=O), 1137 (st, P=O), 1095–1251 (st, C–O–C and st, C–F) cm^{-1}. ^1H NMR (300 MHz, $CDCl_3$, 25 °C) δ 6.74–7.65 (m), 1.88 (s, Me) ppm. ^{31}P NMR (200 MHz, acetone-d_6, 25 °C) δ –92.12 (2P), –98.86 (2P) ppm. ESI–Mass (m/z) Calcd for $C_{88}H_{66}EuF_{12}O_{10}P_4$ $[M–(hfa)]^+$: 1787.264; Found: 1787.264. Anal. Calcd for $C_{93}H_{67}EuF_{18}O_{12}P_4$ 1.5$CHCl_3$: C, 52.22; H, 3.18. Found: C, 52.11; H, 3.25.

[Sm(hfa)$_2$(xantpo)$_2$]: Yield: 0.79 g (46 %). IR (ATR) 1653 (st, C=O), 1138 (st, P=O), 1100–1252 (st, C–O–C and st, C–F) cm^{-1}. ^1H NMR (500 MHz, acetone-d_6, 25 °C) δ 5.81–8.09 (m), 1.67 (s, Me), 1.52 (s, Me) ppm. ^{31}P NMR (200 MHz, acetone-d_6, 25 °C) δ 33.03 (2P), 32.80 (2P) ppm. ESI–Mass (m/z) Calcd for $C_{88}H_{66}SmF_{12}O_{10}P_4$ $[M–(hfa)]^+$: 1786.257; Found: 1786.261. Anal. Calcd for $C_{93}H_{78}SmF_{15}O_{15}P_4$: C, 55.99; H, 3.94. Found: C, 55.54; H, 3.53.

[Eu(hfa)$_3$(*t*Bu-xantpo)]: Yield: 0.35 g (66 %). IR (ATR) 1653 (st, C=O), 1138 (st, P=O), 1098–1249 (st, C–O–C and st, C–F) cm^{-1}. ^1H NMR (300 MHz, $CDCl_3$, 25 °C) δ 7.41 (m, 2H, Ar), 7.07 (m, 2H, Ar), 6.83 (m, 2H, Ar), 5.92 (s, 3H, hfa-H), 2.97–3.02 (m, 6H, 2Me), 1.41–1.68 (m, 36H, 4*t*Bu) ppm. ^{31}P NMR (200 MHz, acetone-d_6, 25 °C) δ 68.41 (2P) ppm. ESI–Mass (m/z) Calcd for $C_{41}H_{50}EuF_{12}O_7P_2$ $[M–(hfa)]^+$: 1097.206; Found: 1097.206. Anal. Calcd for $C_{46}H_{51}EuF_{18}O_9P_2$: C, 42.38; H, 3.94. Found: C, 42.93; H, 4.00.

[Sm(hfa)$_3$(*t*Bu-xantpo)]: Yield: 0.39 g (53 %). IR (ATR) 1653 (st, C=O), 1137 (st, P=O), 1100–1252 (st, C–O–C and st, C–F) cm^{-1}. ^1H NMR (500 MHz, acetone-d_6, 25 °C) δ 8.06–8.08 (d, J = 7.5 Hz, 2H, Ar), 7.73–7.77 (m, 2H, Ar), 7.50–7.53 (t, J = 7.5 Hz, 2H, Ar), 6.73 (s, 3H, hfa-H), 1.83 (s, 6H, 2Me), 0.52–0.55 (d, J = 15 Hz, 36H, 4*t*Bu) ppm. ^{31}P NMR (200 MHz, acetone, 25 °C) δ 62.37 (2P) ppm. ESI–Mass (m/z) Calcd for $C_{41}H_{50}SmF_{12}O_7P_2$ $[M–(hfa)]^+$: 1096.204. Found: 1096.200. Anal. Calcd for $C_{46}H_{51}SmF_{18}O_9P_2$: C, 42.43; H, 3.95. Found: C, 42.68; H, 3.71.

[Eu(hfa)$_3$(dpepo)]: Yield: 0.62 g (74 %). IR (ATR) 1653 (st, C=O), 1135 (st, P=O), 1098–1251 (st, C–O–C and st, C–F) cm^{-1}. ^1H NMR (500 MHz, acetone,

25 °C) δ 7.32–7.64 (m, 22H, Ar), 7.10–7.13 (t, $J = 7.5$ Hz, 2H, Ar), 6.90–6.95 (dd, $J = 7.5$ Hz, 2H, Ar), 6.73 (s, 3H, hfa-H), 6.29–6.30 (m, 2H, Ar) ppm. ^{31}P NMR (200 MHz, acetone-d_6, 25 °C) δ −113.42 (2P) ppm. ESI–Mass (*m/z*) Calcd for $C_{46}H_{30}EuF_{12}O_7P_2$ $[M–(hfa)]^+$: 1137.049; Found: 1137.049. Anal. Calcd for $C_{51}H_{31}EuF_{18}O_9P_2$: C, 45.59; H, 2.33. Found: C, 45.76; H, 2.11.

[Sm(hfa)$_3$(dpepo)]: Yield: 0.66 g (79 %). IR (ATR) 1653 (st, C=O), 1134 (st, P=O), 1098–1250 (st, C–O–C and st, C–F) cm^{-1}. ^{1}H NMR (500 MHz, acetone-d_6, 25 °C) δ 7.32–7.64 (m, 22H, Ar), 7.10–7.13 (t, $J = 7.5$ Hz, 2H, Ar), 6.90–6.95 (dd, $J = 7.5$ Hz, 2H, Ar), 6.73 (s, 3H, hfa-H), 6.29–6.30 (m, 2H, Ar) ppm. ^{31}P NMR (200 MHz, acetone-d_6, 25 °C) δ 29.17 (2P) ppm. ESI–Mass (*m/z*) Calcd for $C_{46}H_{30}SmF_{12}O_7P_2$ $[M–(hfa)]^+$: 1136.048; Found: 1136.044. Anal. Calcd for $C_{51}H_{31}SmF_{18}O_9P_2$: C, 45.64; H, 2.33. Found: C, 45.54; H, 2.18.

5.2.4 Crystallography

Colorless single crystals of lanthanide complexes obtained from the methanol solution were mounted on a glass fiber using epoxy resin glue. All measurements were made on a Rigaku RAXIS RAPID imaging plate area detector with graphite monochromated MoKα radiation. Corrections for decay and Lorentz-polarization effects were made using empirical absorption correction, solved by direct methods and expanded using Fourier techniques. Non-hydrogen atoms were refined anisotropically. Hydrogen atoms were refined using the riding model. The final cycle of full-matrix least-squares refinement was based on observed reflections and variable parameters. All calculations were performed using the crystal structure crystallographic software package. The author confirmed the CIF data using the check CIF/PLATON service.

5.2.5 Optical Measurements

UV–Vis absorption spectra were recorded on a JASCO V–660 spectrometer. Emission spectra of the lanthanide complexes were measured with a Hitachi F–4500 spectrometer and corrected for the response of the detector system. The emission quantum yields of lanthanide complex solutions degassed with an argon (10 mM in acetone-d_6) were obtained by comparison with the integrated emission signal (550–750 nm) of Eu(hfa)$_3$(biphepo) as a reference ($\Phi_{Ln} = 0.60$: 50 mM in acetone-d_6) with an excitation wavelength of 465 nm (direct excitation of Eu(III) ions) for Eu(III) complexes [15] or Sm(hfa)$_3$(H$_2$O)$_2$ as a reference ($\Phi_{Ln} = 0.031$: 100 mM in DMSO-d_6) with an excitation wavelength of 481 nm (direct excitation of Sm(III) ions) for Sm(III) complexes. Emission lifetimes of lanthanide complexes (10 mM in acetone-d_6) were measured using the third harmonics (355 nm) of a Q-switched Nd:YAG laser (Spectra Physics, INDI-50, fwhm = 5 ns, $\lambda = 1064$ nm) and a photomultiplier (Hamamatsu photonics, R5108, response

Table 5.1 Crystal data of Eu(III) complexes

	$Eu(hfa)_2(xantpo)_2$	$Eu(hfa)_3$ (*t*Bu-xantpo)	$Eu(hfa)_3(dpepo)$	$Eu(hfa)_3(biphepo)$
Chemical formula	$C_{93}H_{67}F_{18}O_{12}P_4Eu$	$C_{46}H_{51}F_{18}O_9P_2Eu$	$C_{51}H_{31}F_{18}O_9P_2Eu$	$C_{51}H_{31}F_{18}O_8P_2Eu$
Formula weight	1994.37	1303.78	1343.68	1327.68
Crystal color, habit	Colorless, block	Colorless, block	Colorless, block	Colorless, block
Crystal system	Triclinic	Monoclinic	Triclinic	Monoclinic
Space group	*P*-1(#2)	$P2_1/c$(#14)	*P*-1(#2)	$P2_1/n$(#14)
a/Å	12.8434(2)	21.9134(5)	12.3802(5)	13.1819(2)
b/Å	17.9406(3)	20.1740(5)	13.3535(5)	31.5572(6)
c/Å	19.2651(4)	24.1073(6)	18.6388(9)	13.5087(3)
α/deg	84.3311(7)		82.4190(13)	
β/deg	82.6768(7)	149.9133(7)	77.2612(15)	111.4181(7)
γ/deg	80.9203(7)		62.3602(9)	
V/Å^3	4333.60(14)	5342.7(2)	2660.94(19)	5231.31(17)
Z	2	4	2	4
d_{calc}/g cm^{-3}	1.528	1.621	1.677	1.686
T/°C	−170 ± 1	−90 ± 1	−90 ± 1	−170 ± 1
μ (Mo K*α*)/cm^{-1}	8.967	13.449	13.535	13.745
Max 2*θ*/deg	55.0	50.6	50.7	55.0
No. of measured reflections	43429	42405	21981	51911
No. of unique reflections	19805	9700	9698	11985
R ($I > 2\sigma(I)$)[a]	0.0453	0.0287	0.0385	0.0340
R_w ($I > 2\sigma(I)$)[b]	0.1366	0.0720	0.1062	0.0910

[a] $R = \Sigma \, ||F_o| - |F_c|| / \Sigma \, |F_o|$

[b] $R_w = [(\Sigma \, w \, (|F_o| - |F_c|)^2 / \Sigma \, w \, F_o^2)]^{1/2}$

time ≤1.1 ns). The Nd:YAG laser response was monitored with a digital oscilloscope (Sony Tektronix, TDS3052, 500 MHz) synchronized to the single-pulse excitation. Emission lifetimes were determined from the slope of logarithmic plots of the decay profiles. High-resolution spectra of the emission were measured with a HORIBA SPEX fluorolog.

5.3 Results and Discussion

5.3.1 Coordination Structures

Single crystals of the lanthanide complexes with oxo-linked bidentate phosphine oxides were successfully prepared for X-ray single-crystal analyses by recrystallization from methanol solutions. The resulting crystal data are summarized in Tables 5.1 and 5.2. The ORTEP views of all the lanthanide complexes showed octa-coordinated structures (Figs. 5.2 and 5.3). The coordination sites of $Eu(hfa)_3$(*t*Bu-xantpo), $Eu(hfa)_3(dpepo)$, $Eu(hfa)_3(biphepo)$, $Sm(hfa)_3$(*t*Bu-xantpo)

Table 5.2 Crystal data of Sm(III) complexes

	$Sm(hfa)_2(xantpo)_2$	$Sm(hfa)_3(t$Bu-xantpo)	$Sm(hfa)_3$(dpepo)
Chemical formula	$C_{93}H_{78}F_{15}O_{15}P_4Sm$	$C_{46}H_{51}F_{18}O_9P_2Sm$	$C_{51}H_{31}F_{18}O_9P_2Sm$
Formula weight	1994.9	1302.22	1342.12
Crystal color, habit	colorless, block	colorless, block	colorless, block
Crystal system	Triclinic	Monoclinic	Triclinic
Space group	*P*-1(#2)	$P2_1/n$(#14)	*P*-1(#2)
a/Å	12.9433(4)	12.1153(5)	12.3661(5)
b/Å	17.7795(7)	20.1706(7)	13.4079(6)
c/Å	19.4357(7)	21.8687(8)	18.5261(7)
α/deg	85.0606(10)		82.2082(12)
β/deg	82.9841(10)	95.0228(12)	77.0833(10)
γ/deg	82.0480(11)		61.9059(11)
V/Å^3	4385.6(3)	5323.6(3)	2639.56(19)
Z	2	4	2
d_{calc}/g cm^{-3}	1.511	1.625	1.689
T/°C	−140 ± 1	−100 ± 1	−150 ± 1
μ (Mo Kα)/cm^{-1}	8.143	12.797	12.939
Max 2θ/deg	50.6	50.6	50.6
No. of measured reflections	35841	42569	21444
No. of unique reflections	15874	9688	9574
R ($I > 2\sigma$(I))[a]	0.0309	0.0287	0.0378
R_w ($I > 2\sigma$(I))[b]	0.0705	0.0984	0.1055

[a] $R = \Sigma \, ||F_o| - |F_c|| / \Sigma \, |F_o|$

[b] $R_w = [(\Sigma \, w \, (|F_o| - |F_c|)^2 / \Sigma \, w \, F_o^2)]^{1/2}$

and $Sm(hfa)_3$(dpepo) comprised three hexafluoroacetylacetonato (hfa) ligands and one bidentate phosphine oxide ligand. In contrast, the coordination sites of $Eu(hfa)_2(xantpo)_2$ and $Sm(hfa)_2(xantpo)_2$ comprised two hfa ligands and two bidentate phosphine oxide ligands with hexafluoroacetylacetonato anion (hfa^-: $CF_3COC^-HCOCF_3$) and trifluoroacetate anion (CF_3COO^-) counter ions, respectively. The author considers that the trifluoroacetate anion in Fig. 5.3 might be formed by the oxidation reaction of the hexafluoroacetylacetonato ligand [16].

Based on the crystal data, the author carried out the calculations of the shape factor *S* in order to estimate the degree of distortion of the coordination structure in first coordination sphere [10]. The *S* value is given by:

$$S = \min \sqrt{\left(\frac{1}{m}\right) \sum_{i=1}^{m} (\delta_i - \theta_i)^2} \tag{5.1}$$

where m, δ_i and θ_i are the number of possible edges ($m = 18$ in this study), the observed dihedral angle between planes along the ith edge and the dihedral angle for the ideal structure, respectively. The estimated *S* values of lanthanide complexes are summarized in Tables 5.3, 5.4, 5.5, 5.6, 5.7, 5.8, 5.9, 5.10, 5.11 and Figs. 5.4, 5.5, 5.6. For $Eu(hfa)_2(xantpo)_2$, the *S* value for the octa-coordinated

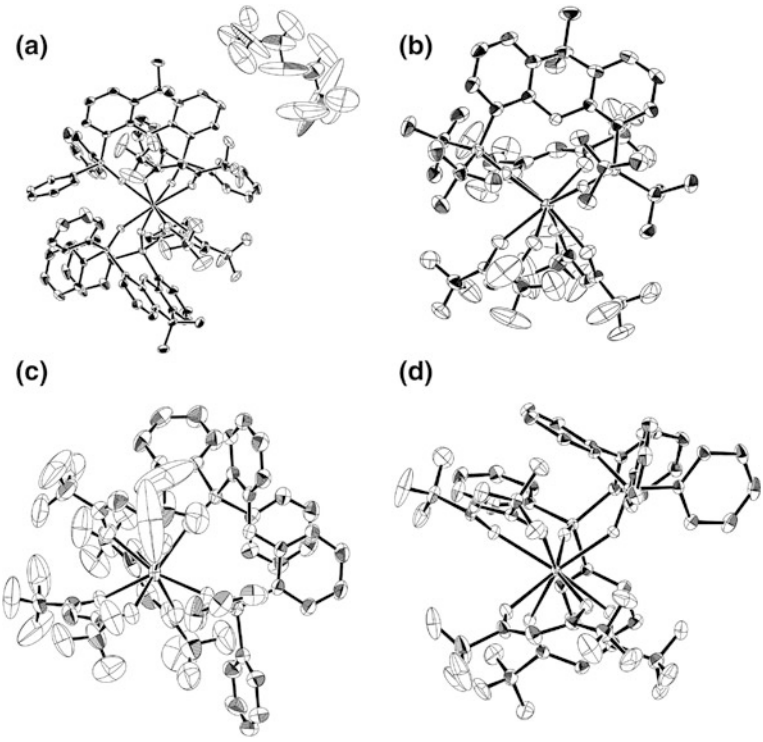

Fig. 5.2 ORTEP drawings of **a** $Eu(hfa)_2(xantpo)_2$, **b** $Eu(hfa)_3(t$Bu-xantpo), **c** $Eu(hfa)_3$(dpepo), and **d** $Eu(hfa)_3$(biphepo). Hydrogen atoms have been omitted for clarity and thermal ellipsoids are shown at the 50 % probability level

square antiprism structure (8-SAP, point group: D_{4d}, $S = 3.0°$) is smaller than that for the octa-coordinated trigonal dodecahedron structure (8-TDH, point group: D_{2d}, $S = 13°$), suggesting that the 8-SAP structure is less distorted than the 8-TDH structure. The author thus determined that the coordination geometry of $Eu(hfa)_2(xantpo)_2$ is 8-SAP. Based on the minimum value of S, the coordination geometries of lanthanide complexes with *t*Bu-xantpo and dpepo ligands are classified as 8-TDH, while those with xantpo and biphepo ligands are classified as 8-SAP. These estimations also suggest that the geometrical symmetry in first coordination sphere of lanthanide complexes with *t*Bu-xantpo and dpepo ligands (point group: D_{2d}) is lower than those of lanthanide complexes with xantpo and biphepo ligands (point group: D_{4d}).

The author also determined the symmetrical point groups of the lanthanide complexes concerned with the locations of phosphine oxide and β-diketonato linker species (Fig. 5.7). The symmetrical point groups of $Eu(hfa)_3(t$Bu-xantpo), $Eu(hfa)_3$(dpepo), $Sm(hfa)_3(t$Bu-xantpo) and $Sm(hfa)_3$(dpepo) were found to be quasi-C_1. On the other hand, those of $Eu(hfa)_2(xantpo)_2$ and $Sm(hfa)_2(xantpo)_2$ were categorized as quasi-C_2 because of their two coordinated xantpo ligands.

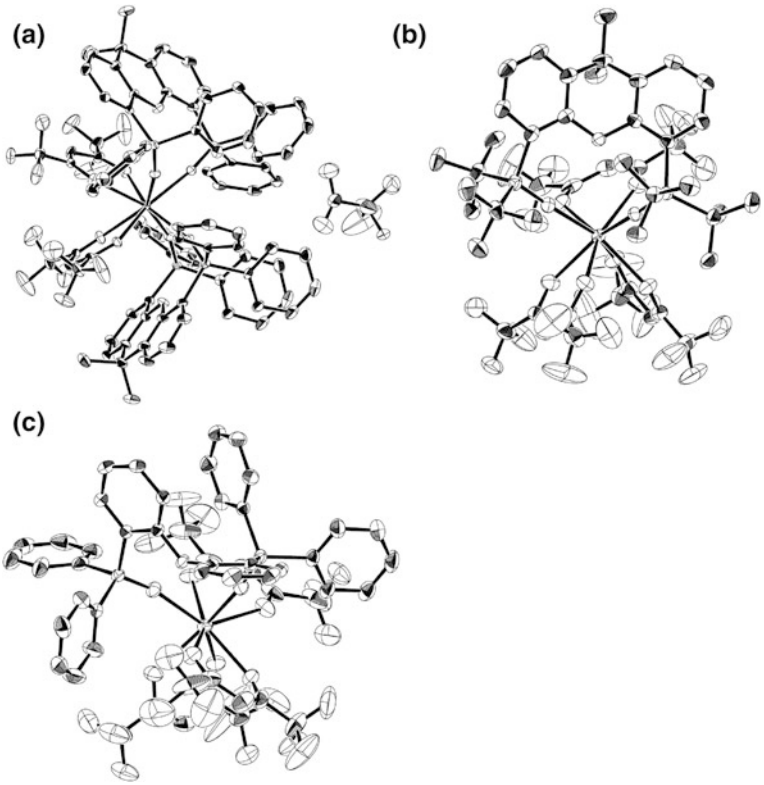

Fig. 5.3 ORTEP drawings of **a** $Sm(hfa)_2(xantpo)_2$, **b** $Sm(hfa)_3$(*t*Bu-xantpo), and **c** $Sm(hfa)_3$(dpepo). Hydrogen atoms have been omitted for clarity and thermal ellipsoids are shown at the 50 % probability level

Hasegawa has reported that the coordination structure of $Eu(hfa)_3$(biphepo) was classified as 8-SAP with quasi-C_1 symmetry [17]. These results indicate that lanthanide complexes with 8-TDH geometry (D_{2d}) and quasi-C_1 symmetry are expected to enhance the electric transition probability in the 4f orbitals related to change of odd parity. The characteristic structures of these lanthanide complexes are likely to significantly affect their photophysical properties.

5.3.2 Photophysical Properties

The steady-state emission spectra of lanthanide complexes in acetone-d_6 are shown in Fig. 5.8. Emission bands of Eu(III) complexes are observed at around 578, 592, 613, 650, and 698 nm, and are attributed to the f–f transitions of $^5D_0$–^7F_J with $J = 0$, 1, 2, 3 and 4 respectively. Emission bands of Sm(III) complexes are

Table 5.3 Observed dihedral angles (δ_i), dihedral angles of idealized square antiprism (θ_i) and measure shape criteria, $S(D_{4d})$ for $Eu(hfa)_2(xantpo)_2$ and $Eu(hfa)_3$(*t*Bu-xantpo)

	$Eu(hfa)_2(xantpo)_2$			$Eu(hfa)_3$(*t*Bu-xantpo)		
θ_i	Edge	δ_i	$\delta_i - \theta_i$	Edge	δ_i	$\delta_i - \theta_i$
0	O6–O7	4.35	4.35	O2–O4	24.70	24.70
0	O1–O10	5.68	5.68	O6–O9	24.48	24.48
77.1	O4–O6	76.58	−0.52	O2–O5	72.71	−4.39
77.1	O4–O7	78.74	1.64	O1–O2	61.45	−15.65
77.1	O7–O8	73.66	−3.44	O1–O4	81.23	4.13
77.1	O6–O8	75.02	−2.08	O4–O5	68.02	−9.08
77.1	O3–O10	77.25	0.15	O7–O9	57.50	−19.6
77.1	O1–O3	76.56	−0.54	O8–O9	69.73	−7.37
77.1	O1–O9	74.25	−2.85	O6–O8	67.37	−9.73
77.1	O9–O10	72.41	−4.69	O6–O7	75.26	−1.84
51.6	O3–O6	52.52	0.92	O5–O9	51.81	0.21
51.6	O3–O4	52.89	1.29	O2–O9	40.08	−11.52
51.6	O1–O4	52.66	1.06	O2–O8	58.73	7.13
51.6	O1–O7	47.36	−4.24	O1–O8	60.64	9.04
51.6	O7–O9	54.47	2.87	O1–O6	54.28	2.68
51.6	O8–O9	48.13	−3.47	O4–O6	32.52	−19.08
51.6	O8–O10	54.43	2.83	O4–O7	57.73	6.13
51.6	O6–O10	47.79	−3.81	O5–O7	57.23	5.63
	$S(D_{4d})$	**3.03**		**$S(D_{4d})$**	**12.51**	

Table 5.4 Observed dihedral angles (δ_i), dihedral angles of idealized square antiprism (θ_i) and measure shape criteria, $S(D_{4d})$ for $Eu(hfa)_3$(dpepo) and $Eu(hfa)_3$(biphepo)

	$Eu(hfa)_3$(dpepo)			$Eu(hfa)_3$(biphepo)		
θ_i	Edge	δ_i	$\delta_i - \theta_i$	Edge	δ_i	$\delta_i - \theta_i$
0	O2–O5	33.82	33.82	O1–O3	1.64	1.64
0	O1–O7	33.02	33.02	O6–O8	1.97	1.97
77.1	O4–O5	70.62	−6.48	O1–O4	81.95	4.85
77.1	O2–O4	61.01	−16.09	O4–O3	75.87	−1.23
77.1	O2–O9	69.51	−7.59	O3–O2	73.75	−3.35
77.1	O5–O9	54.52	−22.58	O2–O1	80.23	3.13
77.1	O6–O7	81.43	4.33	O5–O6	80.41	3.31
77.1	O1–O6	82.45	5.35	O6–O7	76.13	−0.97
77.1	O1–O8	79.32	2.22	O7–O8	73.96	−3.14
77.1	O7–O8	80.43	3.33	O8–O5	78.55	1.45
51.6	O5–O6	29.60	−22.00	O1–O5	45.97	−5.63
51.6	O4–O6	64.21	12.61	O5–O4	56.55	4.95
51.6	O1–O4	60.29	8.69	O4–O6	47.12	−4.48
51.6	O1–O2	55.42	3.82	O6–O3	55.47	3.87
51.6	O2–O8	32.51	−19.09	O3–O7	47.45	−4.15
51.6	O8–O9	65.07	13.47	O7–O2	55.08	3.48
51.6	O7–O9	57.46	5.86	O2–O8	46.22	−5.38
51.6	O5–O7	56.22	4.62	O8–O1	55.53	3.93
	$S(D_{4d})$	**15.81**		**$S(D_{4d})$**	**3.66**	

Table 5.5 Observed dihedral angles (δ_i), dihedral angles of idealized square antiprism (θ_i) and measure shape criteria, $S(D_{2d})$ for $Eu(hfa)_2(xantpo)_2$ and $Eu(hfa)_3(t$Bu-xantpo)

$Eu(hfa)_2(xantpo)_2$				$Eu(hfa)_3(t$Bu-xantpo)			
θ_i	Edge	δ_i	$\delta_i - \theta_i$	θ_i	Edge	δ_i	$\delta_i - \theta_i$
61.48	O1–O3	76.62	15.14	61.48	O1–O2	61.45	−0.030
61.48	O1–O4	52.63	−8.85	74.29	O1–O4	81.23	6.94
29.86	O1–O7	47.34	17.48	61.48	O1–O6	54.28	−7.20
74.29	O1–O9	74.84	0.55	53.12	O1–O8	60.64	7.52
29.86	O1–O10	5.56	−24.30	29.86	O2–O4	24.7	−5.16
53.12	O3–O4	52.85	−0.27	74.29	O2–O5	72.71	−1.58
61.48	O3–O6	52.57	−8.91	61.48	O2–O8	58.73	−2.75
74.29	O3–O10	77.24	2.95	29.86	O2–O9	40.08	10.22
61.48	O4–O6	76.53	15.05	61.48	O4–O5	68.02	6.54
74.29	O4–O7	78.72	4.43	29.86	O4–O6	32.52	2.66
29.86	O6–O7	4.42	−25.44	61.48	O4–O7	57.73	−3.75
74.29	O6–O8	75.00	0.71	53.12	O5–O7	57.23	4.11
29.86	O6–O10	47.76	17.90	61.48	O5–O9	51.81	−9.67
61.48	O7–O8	73.67	12.19	74.29	O6–O7	75.26	0.97
61.48	O7–O9	54.51	−6.97	61.48	O6–O8	67.37	5.89
53.12	O8–O9	48.09	−5.03	29.86	O6–O9	24.48	−5.38
61.48	O8–O10	54.48	−7.00	61.48	O7–O9	57.5	−3.98
61.48	O9–O10	72.47	10.99	74.29	O8–O9	69.73	−4.56
		$S(D_{2d})$	**12.69**			**$S(D_{2d})$**	**5.64**

Table 5.6 Observed dihedral angles (δ_i), dihedral angles of idealized square antiprism (θ_i) and measure shape criteria, $S(D_{2d})$ for $Eu(hfa)_3$(dpepo) and $Eu(hfa)_3$(biphepo)

$Eu(hfa)_3$(dpepo)				$Eu(hfa)_3$(biphepo)			
θ_i	Edge	δ_i	$\delta_i - \theta_i$	θ_i	Edge	δ_i	$\delta_i - \theta_i$
61.48	O1–O2	55.42	−6.06	74.29	O1–O2	76.53	2.24
53.12	O1–O3	60.29	7.17	61.48	O1–O3	56.15	−5.33
61.48	O1–O6	59.53	−1.95	53.12	O1–O5	47.74	−5.38
74.29	O1–O7	80.46	6.17	61.48	O1–O7	74.88	13.40
61.48	O1–O8	61.01	−0.47	29.86	O2–O3	48.01	18.15
29.86	O2–O3	33.82	3.96	61.48	O2–O4	55.83	−5.65
29.86	O2–O4	32.51	2.65	29.86	O2–O7	1.98	−27.88
74.29	O2–O6	69.51	−4.78	61.48	O2–O8	83.23	21.75
61.48	O3–O4	70.62	9.14	74.29	O3–O4	80.77	6.48
61.48	O3–O8	64.21	2.73	61.48	O3–O5	76.31	14.83
29.86	O4–O5	29.60	−0.26	29.86	O3–O6	2.99	−26.87
61.48	O4–O6	56.22	−5.26	61.48	O4–O6	79.24	17.76
61.48	O4–O8	54.52	−6.96	53.12	O4–O8	45.31	−7.81
74.29	O5–O6	77.45	3.16	74.29	O5–O6	74.56	0.27
29.86	O5–O7	28.77	−1.09	61.48	O5–O7	56.10	−5.38
61.48	O5–O8	57.73	−3.75	29.86	O6–O7	45.26	15.4
53.12	O6–O7	57.46	4.34	61.48	O6–O8	55.70	−5.78
61.48	O7–O8	65.07	3.59	74.29	O7–O8	81.29	7.00
		$S(D_{2d})$	**4.71**			**$S(D_{2d})$**	**13.49**

Table 5.7 Observed dihedral angles (δ_i), dihedral angles of idealized square antiprism (θ_i) and measure shape criteria, $S(D_{4d})$ for $Sm(hfa)_2(xantpo)_2$ and $Sm(hfa)_3(t$Bu-xantpo)

	$Sm(hfa)_2(xantpo)_2$			$Sm(hfa)_3(t$Bu-xantpo)		
θ_i	Edge	δ_i	$\delta_i - \theta_i$	Edge	δ_i	$\delta_i - \theta_i$
0	O1–O10	2.67	2.67	O3–O8	24.98	24.98
0	O4–O8	4.97	4.97	O5–O6	19.81	19.81
77.1	O1–O2	76.85	−0.25	O3–O9	72.55	−4.55
77.1	O2–O10	79.81	2.71	O1–O3	61.61	−15.49
77.1	O1–O9	75.63	−1.47	O1–O8	80.96	3.86
77.1	O9–O10	74.98	−2.12	O8–O9	68.13	−8.97
77.1	O4–O7	80.85	3.75	O5–O7	57.44	−19.66
77.1	O7–O8	76.66	−0.44	O6–O7	75.37	−1.73
77.1	O5–O8	77.12	0.02	O4–O6	67.13	−9.97
77.1	O4–O5	80.06	2.96	O4–O5	69.79	−7.31
51.6	O1–O4	53.63	2.03	O5–O9	51.97	0.37
51.6	O2–O4	52.65	1.05	O3–O5	40.10	−11.50
51.6	O2–O5	52.19	0.59	O3–O4	58.41	6.81
51.6	O5–O10	47.54	−4.06	O1–O4	60.55	8.95
51.6	O8–O10	54.94	3.34	O1–O6	54.54	2.94
51.6	O8–O9	47.47	−4.13	O6–O8	32.69	−18.91
51.6	O7–O9	53.71	2.11	O7–O8	57.46	5.86
51.6	O1–O7	48.41	−3.19	O7–O9	57.07	5.47
	$S(D_{4d})$	**2.73**		**$S(D_{4d})$**	**12.03**	

Table 5.8 Observed dihedral angles (δ_i), dihedral angles of idealized square antiprism (θ_i) and measure shape criteria, $S(D_{4d})$ for $Sm(hfa)_3$(dpepo)

$Sm(hfa)_3$(dpepo)			
θ_i	Edge	δ_i	$\delta_i - \theta_i$
0	O3–O4	31.67	31.67
0	O7–O8	22.72	22.72
77.1	O1–O4	80.42	3.32
77.1	O1–O3	56.18	−20.92
77.1	O4–O5	66.06	−11.04
77.1	O3–O5	68.98	−8.12
77.1	O6–O7	80.19	3.09
77.1	O6–O8	87.36	10.26
77.1	O8–O9	86.53	9.43
77.1	O7–O9	80.91	3.81
51.6	O4–O6	30.02	−21.58
51.6	O1–O6	59.33	7.73
51.6	O1–O8	59.94	8.34
51.6	O3–O8	59.83	8.23
51.6	O3–O9	35.21	−16.39
51.6	O5–O9	54.08	2.48
51.6	O5–O7	57.36	5.76
51.6	O4–O7	56.60	5.00
	$S(D_{4d})$	**13.68**	

Table 5.9 Observed dihedral angles (δ_i), dihedral angles of idealized square antiprism (θ_i) and measure shape criteria, $S(D_{2d})$ for $Sm(hfa)_2(xantpo)_2$ and $Sm(hfa)_3$(*t*Bu-xantpo)

$Sm(hfa)_2(xantpo)_2$				$Sm(hfa)_3$(*t*Bu-xantpo)			
θ_i	Edge	δ_i	$\delta_i - \theta_i$	θ_i	Edge	δ_i	$\delta_i - \theta_i$
61.48	O1–O2	76.85	15.37	61.48	O1–O3	61.61	0.13
61.48	O1–O4	53.63	−7.85	53.12	O1–O4	60.55	7.43
29.86	O1–O7	48.41	18.55	61.48	O1–O6	54.54	−6.94
74.29	O1–O9	75.63	1.34	74.29	O1–O8	80.96	6.67
29.86	O1–O10	2.67	−27.19	61.48	O3–O4	58.41	−3.07
53.12	O2–O4	52.65	−0.47	29.86	O3–O5	40.10	10.24
61.48	O2–O5	52.19	−9.29	29.86	O3–O8	24.98	−4.88
74.29	O2–O10	79.81	5.52	74.29	O3–O9	72.55	−1.74
61.48	O4–O5	76.60	15.12	74.29	O4–O5	69.79	−4.50
74.29	O4–O7	77.46	3.17	61.48	O4–O6	67.13	5.65
29.86	O5–O7	4.82	−25.04	29.86	O5–O6	24.57	−5.29
74.29	O5–O8	73.59	−0.70	61.48	O5–O7	57.44	−4.04
29.86	O5–O10	47.54	17.68	61.48	O5–O9	51.97	−9.51
61.48	O7–O8	73.19	11.71	74.29	O6–O7	75.37	1.08
61.48	O7–O9	53.71	−7.77	29.86	O6–O8	32.69	2.83
53.12	O8–O9	47.47	−5.65	61.48	O7–O8	57.46	−4.02
61.48	O8–O10	54.94	−6.54	53.12	O7–O9	57.07	3.95
61.48	O9–O10	74.98	13.50	61.48	O8–O9	68.13	6.65
		$S(D_{2d})$	**13.19**			**$S(D_{2d})$**	**5.58**

Table 5.10 Observed dihedral angles (δ_i), dihedral angles of idealized square antiprism (θ_i) and measure shape criteria, $S(D_{2d})$ for $Sm(hfa)_3$(dpepo)

$Sm(hfa)_3$(dpepo)			
θ_i	Edge	δ_i	$\delta_i - \theta_i$
61.48	O1–O3	56.18	−5.30
74.29	O1–O4	80.42	6.13
61.48	O1–O6	59.33	−2.15
53.12	O1–O8	59.94	6.82
29.86	O3–O4	31.67	1.81
74.29	O3–O5	68.98	−5.31
61.48	O3–O8	59.83	−1.65
29.86	O3–O9	35.21	5.35
61.48	O4–O5	66.06	4.58
29.86	O4–O6	30.02	0.16
61.48	O4–O7	56.60	−4.88
53.12	O5–O7	57.36	4.24
61.48	O5–O9	54.08	−7.40
74.29	O6–O7	77.53	3.24
61.48	O6–O8	64.43	2.95
29.86	O6–O9	28.77	−1.09
61.48	O7–O9	56.92	−4.56
74.29	O8–O9	70.74	−3.55
		$S(D_{2d})$	**4.42**

Table 5.11 Summary of shape-measure calculations of the Eu(III) and Sm(III) complexes

Complex	*S* value for 8-TDH[a]: $S(D_{2d})$	*S* value for 8-SAP[b]: $S(D_{4d})$	Determined coordination geometry
$Eu(hfa)_2(xantpo)_2$	13°	3.0°	8-SAP
$Eu(hfa)_3$(*t*Bu-xantpo)	5.6°	13°	8-TDH
$Eu(hfa)_3$(dpepo)	4.7°	16°	8-TDH
$Eu(hfa)_3$(biphepo)	13°	3.7°	8-SAP
$Sm(hfa)_2(xantpo)_2$	13°	2.7°	8-SAP
$Sm(hfa)_3$(*t*Bu-xantpo)	5.6°	12°	8-TDH
$Sm(hfa)_3$(dpepo)	4.4°	14°	8-TDH

[a] 8-TDH: octa-coordinated trigonal dodecahedron
[b] 8-SAP: octa-coordinated square antiprism

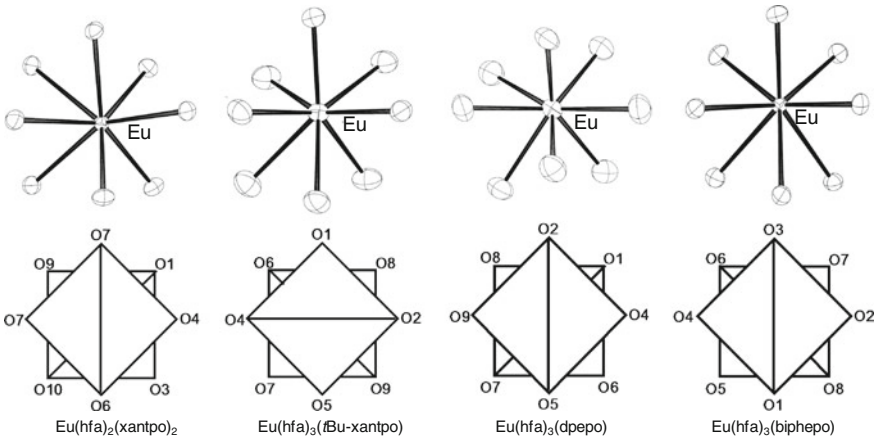

Fig. 5.4 Coordination environments around Eu(III) ion for the calculation of $S(D_{4d})$ values

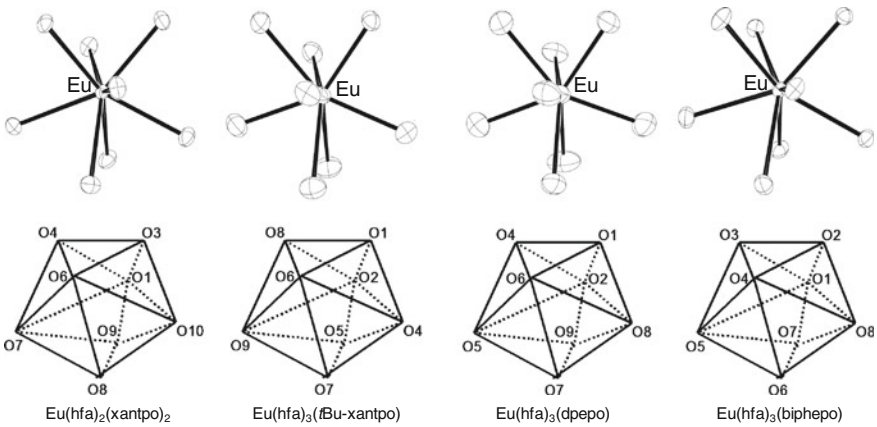

Fig. 5.5 Coordination environments around Eu(III) ion for the calculation of $S(D_{2d})$ values

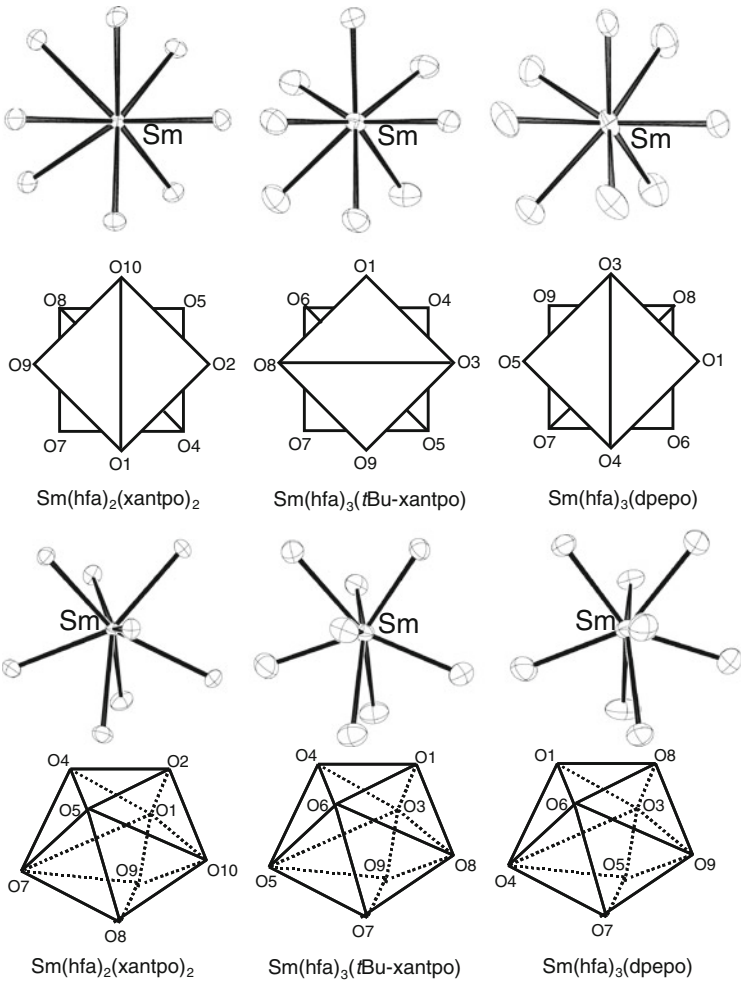

Fig. 5.6 Coordination environments around Sm(III) ion for the calculation of $S(D_{4d})$ and $S(D_{2d})$ values

also observed at around 562, 598, 642 and 704 nm, and are attributed to the f–f transitions of $^4G_{5/2}$–^6H_J with $J = 5/2$, 7/2, 9/2 and 11/2, respectively. The spectra are normalized with respect to the magnetic dipole transition intensities at 592 nm (Eu: $^5D_0$–$^7F_1$) and at 598 nm (Sm: $^4G_{5/2}$–$^6H_{7/2}$) which are known to be insensitive to the surrounding environment of the lanthanide ions [18, 19]. The emission bands at 613 nm (Eu: $^5D_0$–$^7F_2$) and 642 nm (Sm: $^4G_{5/2}$–$^6H_{9/2}$) are due to electric dipole transitions, which are strongly dependent on their coordination geometry. The emission quantum yields for Eu(III) and Sm(III) complexes in acetone-d_6 excited at their 4f orbitals (direct excitation) were found to be 55–72 % and 2.4–5.0 %, respectively (Table 5.12). These values are similar to those reported

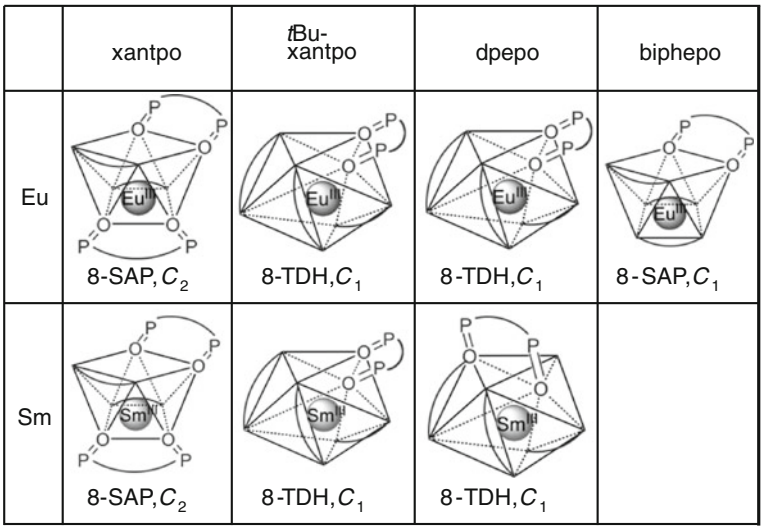

Fig. 5.7 Geometrical coordination structure images of Eu(III) and Sm(III) complexes. Coordinated oxygen atoms are shown as corner polyhedra. *Curved lines* between oxygen atoms represent phosphine oxide and hfa ligands

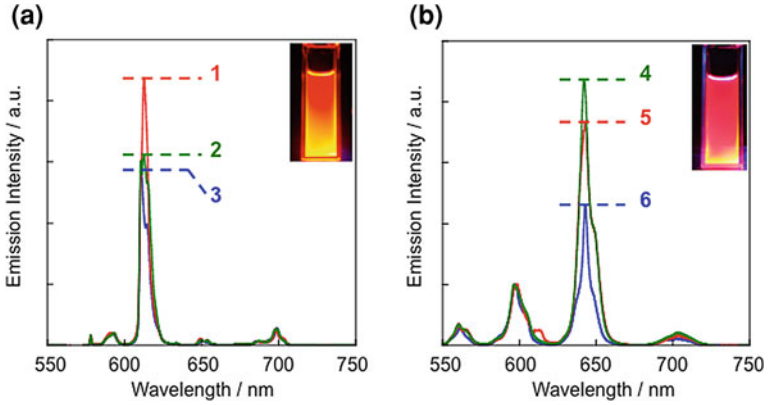

Fig. 5.8 **a** Emission spectra of Eu(hfa)$_3$(*t*Bu-xantpo) (*red line* 1), Eu(hfa)$_3$(dpepo) (*green line* 2) and Eu(hfa)$_2$(xantpo)$_2$ (*blue line* 3) in acetone-d_6 at room temperature. Excited at 465 nm. The spectra were normalized with respect to the magnetic dipole transition ($^5D_0$–$^7F_1$). **b** Emission spectra of Sm(hfa)$_3$(dpepo) (*green line* 4), Sm(hfa)$_3$(*t*Bu-xantpo) (*red line* 5) and Sm(hfa)$_2$(xantpo)$_2$ (*blue line* 6) in acetone-d_6 at room temperature. Excited at 402 nm. The spectra were normalized with respect to the magnetic dipole transition ($^4G_{5/2}$–$^6H_{7/2}$)

for Eu(hfa)$_3$(tppo)$_2$ (Φ_{Ln} = 65 %) and Sm(hfa)$_3$(tppo)$_2$ (Φ_{Ln} = 4.1 %) in acetone-d_6, which have been reported as highly luminescent lanthanide complexes [20]. To the best of our knowledge, the emission quantum yield for Sm(hfa)$_3$(dpepo) (Φ_{Ln} = 5.0 %) is the highest in previous reported Sm(III) complexes.

Table 5.12 Photophysical properties of Eu(III) and Sm(III) complexes in acetone-d_6

Complex	Φ_{Ln}^{a}/%	τ_{obs}^{b}/ms	k_r^{c}/s^{-1}	k_{nr}^{d}/s^{-1}
$Eu(hfa)_2(xantpo)_2$	55	1.3	4.4×10^2	3.6×10^2
$Eu(hfa)_3$(*t*Bu-xantpo)	67	1.2	5.5×10^2	2.7×10^2
$Eu(hfa)_3$(dpepo)	72	1.5	4.7×10^2	1.8×10^2
$Eu(hfa)_3$(biphepo[e]	60	1.3	4.6×10^2	3.4×10^2
$Sm(hfa)_2(xantpo)_2$	3.8	0.35	1.1×10^2	2.8×10^3
$Sm(hfa)_3$(*t*Bu-xantpo)	2.4	0.15	1.6×10^2	6.5×10^3
$Sm(hfa)_3$(dpepo)	5.0	0.28	1.8×10^2	3.3×10^3

[a] Emission quantum yields for Eu(III) complexes were determined by comparing with the integrated emission signal (550–750 nm) of $Eu(hfa)_3$(biphepo) as $\Phi_{Ln} = 0.60$. Excitation at 465 nm. Emission quantum yields for Sm(III) complexes were determined by comparing with the integrated emission signal (550–750 nm) of $Sm(hfa)_3(H_2O)_2$ as $\Phi_{Ln} = 0.031$. Excitation at 481 nm

[b] Emission lifetime (τ_{obs}) of the lanthanide complexes were measured by excitation at 355 nm (Nd:YAG 3ω)

[c] Radiative rate constants $k_r = \Phi_{Ln}/\tau_{obs}$

[d] Nonradiative rate constants $k_{nr} = 1/\tau_{obs} - k_r$

[e] see ref. 20

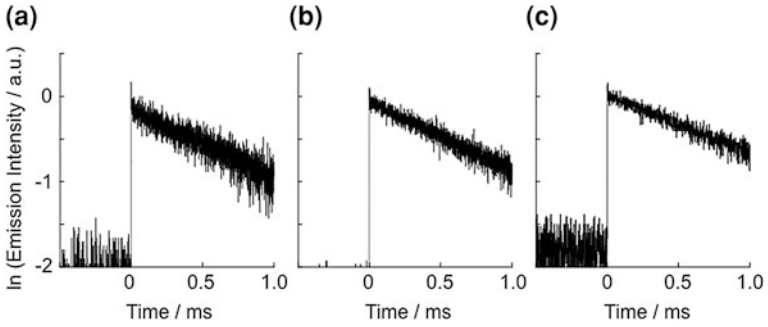

Fig. 5.9 The decay profiles of **a** $Eu(hfa)_2(xantpo)_2$, **b** $Eu(hfa)_3$(*t*Bu-xantpo), and **c** $Eu(hfa)_3$(dpepo) in acetone-d_6

The time-resolved emission profiles of lanthanide complexes revealed single-exponential decays with lifetimes in the millisecond timescale as shown in Fig. 5.9. The emission lifetimes were determined from the slopes of logarithmic plots of the decay profiles. The radiative (k_r) and nonradiative (k_{nr}) rate constants estimated using the emission lifetimes and the emission quantum yields are summarized in Table 5.12. The k_r values for $Eu(hfa)_3$(*t*Bu-xantpo) and $Eu(hfa)_3$(dpepo) were found to be 5.5×10^2 s^{-1} and 4.7×10^2 s^{-1}, respectively. These k_r values are larger than that for $Eu(hfa)_2(xantpo)_2$ (4.4×10^2 s^{-1}). The author also observed that the k_r values for $Sm(hfa)_3$(*t*Bu-xantpo) and $Sm(hfa)_3$(dpepo) are larger than that for $Sm(hfa)_2(xantpo)_2$. In general, reduction of the geometrical symmetry of the coordination structure leads to a larger k_r value. The author suggests that k_r for lanthanide

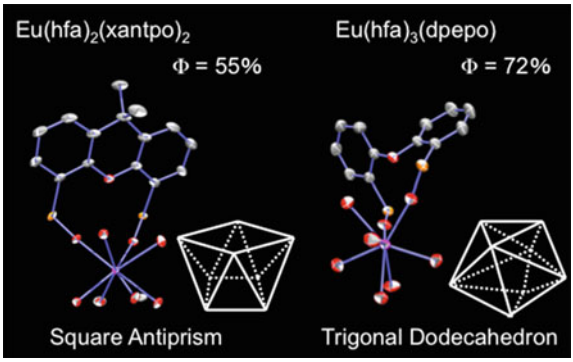

Fig. 5.10 The conceptual diagram in Chapter 5

complexes with phosphine oxides depend on the symmetry of the coordination sites. The characteristic 8-TDH structure of Eu(III) and Sm(III) complexes might be maintained even in acetone-d_6, because the emission spectrum in acetone-d_6 is similar to those of in the solid state. It can also be seen that k_{nr} for Sm(hfa)$_3$(*t*Bu-xantpo) is much larger than the values for the other lanthanide complexes as listed in Table 5.12. Note that the energy gap of the Sm(III) ion is smaller than that of the Eu(III) ion (Sm(III): 7500 cm^{-1}, Eu(III): 12500 cm^{-1}). The excited state of the Sm(III) ion with a smaller energy gap is effectively quenched by vibrational relaxation of the high-vibrational frequency C–H bonds. The author considered that the larger k_{nr} values for Sm(hfa)$_3$(*t*Bu-xantpo) might be attributed to effective vibrational relaxation caused by the 36 C–H bonds in the 4 *tert*-butyl groups attached to the phosphorus atoms.

From these results, the author considers that Eu(III) and Sm(III) complexes with 8-TDH structures lead to high emission quantum yields and large radiative rate constants, which result in strong luminescence.

5.4 Conclusions

The author successfully synthesized novel lanthanide complexes containing the oxo-linked bidentate phosphine oxide ligands xantpo, *t*Bu-xantpo and dpepo with high emission quantum yields (Fig. 5.10). They exhibit characteristic luminescence properties that depend on their coordination structures. The symmetry of coordination structures of lanthanide complexes is correlated with their photophysical properties. In order to produce strong luminescence in luminescent lanthanide complexes, the following intrinsic requirements should be fulfilled:

(1) low-vibrational structure
(2) asymmetrical point group
(3) asymmetrical coordination structure (quasi-C_1).

In this chapter, characteristic photophysical properties for octa-coordinated lanthanide complexes with 8-TDH structures have been demonstrated. Research on the driving force for the formation of the 8-TDH structure is expected to provide molecular strategies for obtaining strongly luminescent Eu(III) complexes directly. Ohkubo et al. have reported that the driving force for the construction of an asymmetric coordination geometry can be estimated from the dipole moments of the ligands [21]. Strongly luminescent Eu(III) complexes with 8-TDH structures may lead to the development of new fields in photophysical, coordination, and material chemistry.

References

1. S.F. Mason, R.D. Peacock, B. Stewart, Chem. Phys. Lett. **29**, 149 (1974)
2. S.F. Mason, J. Indian Chem. Soc. **63**, 73 (1986)
3. A.F. Kirby, F.S. Richardson, J. Phys. Chem. **87**, 2544 (1983)
4. M. Montalti, L. Prodi, N. Zaccheroni, L. Charbonnière, L. Douce, R. Ziessel, J. Am. Chem. Soc. **123**, 12694 (2001)
5. K. Driesen, P. Lenaerts, K. Binnemans, C. Görller-Walrand, Phys. Chem. Chem. Phys. **4**, 552 (2002)
6. W. Liu, T. Jiao, Y. Li, Q. Liu, M. Tan, H. Wang, L. Wang, J. Am. Chem. Soc. **126**, 2280 (2004)
7. J.P. Cross, M. Lauz, P.D. Badger, S. Petoud, J. Am. Chem. Soc. **126**, 16278 (2004)
8. P. Nockemann, B. Thijs, N. Postelmans, K.V. Hecke, L.V. Meervelt, K. Binnemans, J. Am. Chem. Soc. **128**, 13658 (2006)
9. A. Wada, M. Watanabe, Y. Yamanoi, T. Nankawa, K. Namiki, M. Yamasaki, M. Murata, H. Nishihara, Bull. Chem. Soc. Jpn **80**, 335 (2007)
10. J. Xu, E. Radkov, M. Ziegler, K.N. Raymond, Inorg. Chem. **39**, 4156 (2000)
11. T. Harada, Y. Nakano, M. Fujiki, M. Naito, T. Kawai, Y. Hasegawa, Inorg. Chem. **48**, 11242 (2009)
12. T. Harada, H. Tsumatori, K. Nishiyama, J. Yuasa, Y. Hasegawa, T. Kawai, Inorg. Chem. **51**, 6476 (2012)
13. P.W.N.M. van Leeuwen, P.C.J. Kamer, J.N.H. Reek, P. Dierkes, Chem. Rev. **100**, 2741 (2000)
14. O. Moudam, B.C. Rowan, M. Alamiry, P. Richardson, B.S. Richards, A.C. Jones, N. Robertson, *Chem. Commun.* 6649 (2009)
15. K. Nakamura, Y. Hasegawa, H. Kawai, N. Yasuda, Y. Tsukahara, Y. Wada, Thin Solid Films **516**, 2376 (2008)
16. D.A. Johnson, A.B. Waugh, T.W. Hambley, J.C. Taylor, J. Fluorine Chem. **27**, 371 (1985)
17. K. Nakamura, Y. Hasegawa, H. Kawai, N. Yasuda, N. Kanehisa, Y. Kai, T. Nagamura, S. Yanagida, Y. Wada, J. Phys. Chem. A **111**, 3029 (2007)
18. C. Görller-Walrand, L. Fluyt, A. Ceulemans, W.T. Carnall, J. Chem. Phys. **95**, 3099 (1991)
19. M.H.V. Werts, R.T.F. Jukes, J.W. Verhoeven, Phys. Chem. Chem. Phys. **4**, 1542 (2002)
20. H. Kawai, C. Zhao, S. Tsuruoka, T. Yoshida, Y. Hasegawa, T. Kawai, J. Alloys Compd. **488**, 612 (2009)
21. Y. Hasegawa, T. Ohkubo, T. Nakanishi, A. Kobayashi, M. Kato, T. Seki, H. Ito, K. Fushimi, Eur. J. Inorg. Chem. **2013**, 5911 (2013)

Chapter 6
Solvent-Dependent Luminescence of Octa-Coordinated Eu(III) Complexes

6.1 Introduction

As described in Chap. 5, in order to prepare an intensely luminescent lanthanide complex, a large radiative rate constant based on reducing the geometrical symmetry and a small nonradiative rate constant by introducing low-vibrational frequency organic ligands should be required [1, 2]. The author has reported on two asymmetric Eu(III) complexes with hfa and bidentate phosphine oxide ligands, $Eu(hfa)_2(xantpo)_2$ and $Eu(hfa)_3$(*t*Bu-xantpo) as shown in Fig. 6.1. Their coordination geometries were categorized as 8-SAP and 8-TDH structures, respectively. Their coordination structures composed of the low-vibrational frequency phosphine oxide and hfa provide Eu(III) complexes with high emission quantum yields and relatively large radiative rate constants in acetone-d_6. In the photophysical analyses, the author also found that the nonradiative rate constant of $Eu(hfa)_3$(*t*Bu-xantpo) ($k_{nr} = 2.7 \times 10^2\ s^{-1}$) is smaller than that for $Eu(hfa)_2(xantpo)_2$ ($k_{nr} = 3.6 \times 10^2\ s^{-1}$). The author here consider that smaller k_{nr} of $Eu(hfa)_3$(*t*Bu-xantpo) might be achieved by specific coordination structure, 8-TDH.

In general, the nonradiative process of Eu(III) complex is also affected by their coordination structures in liquid media [3]. The coordination structure in organic solvent could be directly linked to performance of coordination ability of the solvent molecule, which is related to dielectric constant of solvent [4]. In this chapter, the author focus on solvent-dependent luminescence of two types of octa-coordinatd Eu(III) complexes, $Eu(hfa)_2(xantpo)_2$ and $Eu(hfa)_3$(*t*Bu-xantpo). Their photophysical properties are estimated using the emission quantum yield, emission lifetime, and radiative and nonradiative rate constant in acetone, acetone-d_6, toluene, chloroform, and DMF. The relationship between photophysical properties and coordination structures of octa-coordinated Eu(III) complexes will be discussed.

K. Miyata, *Highly Luminescent Lanthanide Complexes with Specific Coordination Structures*, Springer Theses,
DOI: 10.1007/978-4-431-54944-4_6,

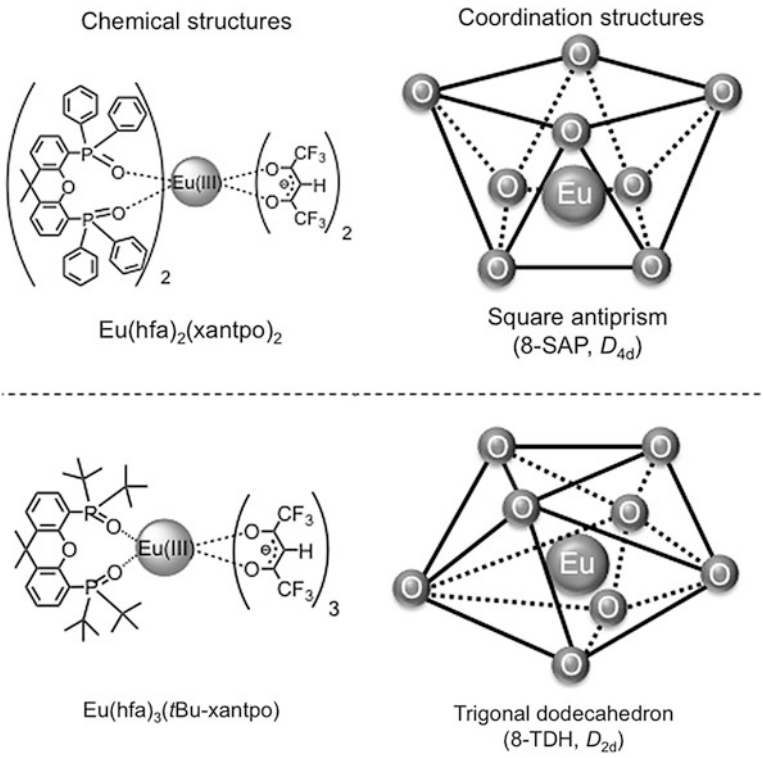

Fig. 6.1 Chemical and coordination structures of $Eu(hfa)_2(xantpo)_2$ and $Eu(hfa)_3(t$Bu-xantpo)

6.2 Experimental Section

6.2.1 Sample Preparation

$Eu(hfa)_2(xantpo)_2$ and $Eu(hfa)_3(t$Bu-xantpo) were prepared according to the procedure described in Chap. 5.

6.2.2 Optical Measurements

UV–Vis absorption spectra were recorded on a JASCO V–550 spectrometer. Emission spectra of the lanthanide complexes were measured with a JASCO F-6300-H spectrometer and corrected for the response of the detector system. The intrinsic emission quantum yields (Φ_{Ln}) of lanthanide complex solutions degassed with an argon (10 mM in toluene, chloroform, acetone, *N*,*N*-dimethylformamide; DMF) were obtained by comparison with the integrated emission signal

(550–750 nm) of Eu(hfa)$_3$(biphepo) as a reference ($\Phi_{Ln} = 0.60$: 50 mM in acetone-d_6) with an excitation wavelength of 465 nm. The emission quantum yields excited at 380 nm (ligand excitation: (Φ_{tot}) were estimated using JASCO F-6300-H spectrometer attached with JASCO ILF-533 integrating sphere unit ($\phi = 100$ mm). The wavelength dependences of the detector response and the beam intensity of Xe light source for each spectrum were calibrated using a standard light source. Emission lifetimes of lanthanide complexes (1.0 mM in toluene, chloroform, acetone, DMF) were measured using the third harmonics (355 nm) of a Q-switched Nd:YAG laser (Spectra Physics, INDI-50, fwhm = 5 ns, $\lambda = 1064$ nm) and a photomultiplier (Hamamatsu photonics, R5108, response time $\leq$ 1.1 ns).

6.3 Results and Discussion

6.3.1 Effects of Deuterated Solvent

The steady-state emission spectra of Eu(hfa)$_2$(xantpo)$_2$ and Eu(hfa)$_3$(*t*Bu-xantpo) in organic solvent are shown in Fig. 6.2. Emission bands are observed at around 578, 591, 613, 650, and 698 nm, and are attributed to the f–f transitions of $^5D_0$–^7F_J with $J = 0$, 1, 2, 3, and 4, respectively. The spectra are normalized with respect to the magnetic dipole transition intensity ($^5D_0$–$^7F_1$) at 591 nm which is known to be insensitive to the surrounding environment of the Eu(III) ion [5, 6]. The emission band at 613 nm ($^5D_0$–$^7F_2$) is due to electric dipole transition, which is strongly dependent on their coordination geometry. We also estimated the relative emission intensity of $^5D_0$–$^7F_2$ transition with respect to that of $^5D_0$–$^7F_1$ as $I_{rel} = I_{613}/I_{591}$ in the normalized emission spectra. The I_{rel} values of Eu(hfa)$_2$(xantpo)$_2$ and Eu(hfa)$_3$(*t*Bu-xantpo) are summarized in Table 6.2. The intrinsic emission quantum yield (Φ_{Ln}) for Eu(hfa)$_3$(*t*Bu-xantpo) in acetone excited at 4f orbitals (excited at 465 nm) was found to be 64 % (Table 6.1). This value is slightly smaller than that for reported Eu(hfa)$_3$(*t*Bu-xantpo) in acetone-d_6 ($\Phi_{Ln} = 67$ %).

The radiative (k_r) and nonradiative (k_{nr}) rate constants estimated using the emission lifetimes (τ_{obs}) and the intrinsic emission quantum yields (Φ_{Ln}) are summarized in Table 6.1. The radiative rate constant for Eu(hfa)$_3$(*t*Bu-xantpo) in acetone was estimated to be 5.4×10^2 s^{-1}. This k_r value is much similar to that for Eu(hfa)$_3$(*t*Bu-xantpo) in acetone-d_6 (5.5×10^2 s^{-1}). The nonradiative rate constant for Eu(hfa)$_3$(*t*Bu-xantpo) in acetone-d_6 (2.7×10^2 s^{-1}) is smaller than that for Eu(hfa)$_3$(*t*Bu-xantpo) in acetone (3.0×10^2 s^{-1}). The relatively smaller k_{nr} for Eu(hfa)$_3$(*t*Bu-xantpo) in acetone-d_6 is attributed to the suppression of vibrational relaxation surroundings of the Eu(III) complex. The nonradiative transitions of lanthanide complexes are affected by the high-vibrational frequency of C–H and O–H bonds of solvent. The author consider that introduction of deuterated solvent is effective for enhancement of emission quantum yield of octa-coordinated Eu(III) complexes.

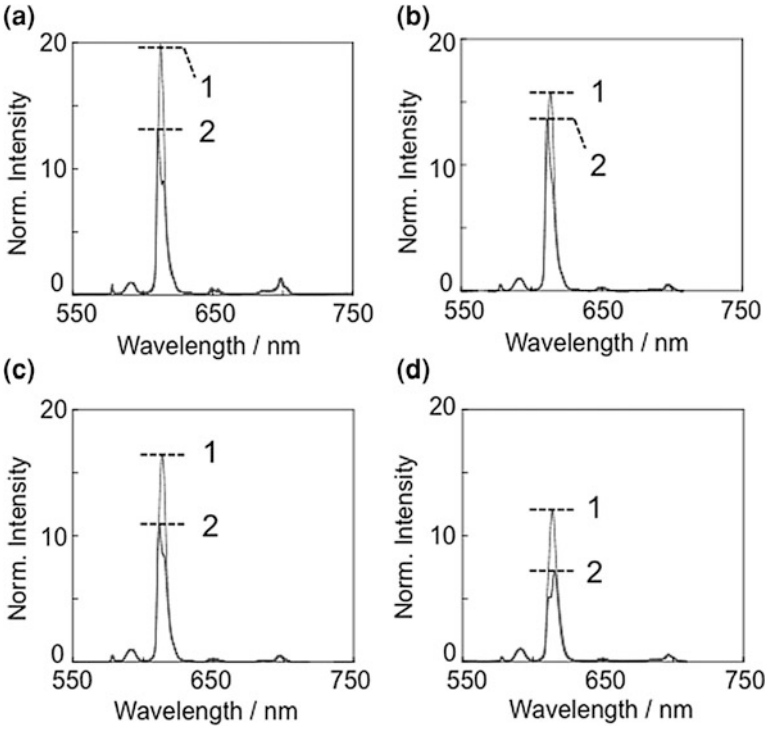

Fig. 6.2 Emission spectra of $Eu(hfa)_3$(*t*Bu-xantpo) (line 1) and $Eu(hfa)_2(xantpo)_2$ (line 2) in **a** acetone, **b** toluene, **c** chloroform, and **d** DMF at room temperature. Excitation wavelength is 465 nm. The spectra are normalized with respect to the magnetic dipole transition ($^5D_0$–$^7F_1$)

Table 6.1 Photophysical properties of $Eu(hfa)_3$(*t*Bu-xantpo) at room temperature

Solvent	τ_{obs} (ms)[a]	Φ_{Ln} (%)	k_r (s^{-1})	k_{nr} (s^{-1})
Acetone	1.2	64	5.4×10^2	3.0×10^2
Acetone-d_6	1.2	67	5.5×10^2	2.7×10^2

6.3.2 Photophysical Properties in Various Organic Solvent

The radiative (k_r) and nonradiative (k_{nr}) rate constants, the emission lifetimes (τ_{obs}), and the intrinsic emission quantum yields (Φ_{Ln}) of $Eu(hfa)_2(xantpo)_2$ and $Eu(hfa)_3$(*t*Bu-xantpo) are summarized in Table 6.2. The radiative rate constants of $Eu(hfa)_3$(*t*Bu-xantpo) ($k_r = 3.6$–$5.6 \times 10^2\ s^{-1}$) were larger than that for $Eu(hfa)_2(xantpo)_2$ ($k_r = 3.0$–$4.9 \times 10^2\ s^{-1}$). Generally, the radiative rate constants of lanthanide complexes are directly linked to their geometrical structures. The symmetrical point groups of $Eu(hfa)_2(xantpo)_2$ and $Eu(hfa)_3$(*t*Bu-xantpo) are D_{4d} and D_{2d}, respectively [7]. The larger radiative rate constants for

Table 6.2 Photophysical properties of Eu(III) complexes in various solvent at room temperature

Complex	Solvent	τ_{obs} (ms)	Φ_{Ln} (%)	Φ_{tot} (%)[a]	η_{sens} (%)[b]	I_{rel}[c]	k_r (10^2 s^{-1})	k_{nr} (10^2 s^{-1})
$Eu(hfa)_3(xantpo)_2$	Toluene	1.3	64	24	38	14	4.9	2.8
	Chloroform	1.3	58	22	38	11	4.3	3.1
	Acetone	1.3	50	20	40	13	3.9	3.8
	DMF	1.7	51	12	23	7.1	3.0	2.9
$Eu(hfa)_3$(*t*Bu-xantpo)	Toluene	1.3	67	29	43	16	5.3	2.6
	Chloroform	1.2	67	24	36	16	5.6	2.7
	Acetone	1.2	64	22	34	20	5.4	3.0
	DMF	1.6	58	12	21	12	3.6	2.6

[a] Total emission quantum yield (excitation at 380 nm)
[b] Photosensitized energy transfer efficiency $\eta_{sens} = \Phi_{tot}/\Phi_{Ln}$. Estimated relative errors: τ_{obs}, ±4 %; Φ_{Ln}, ±3 %; Φ_{tot}, ±9 %; η_{sens}, ±12 %
[c] Relative emission intensity of the electric dipole transition ($^5D_0$–$^7F_2$) to the magnetic dipole transition ($^5D_0$–$^7F_1$)

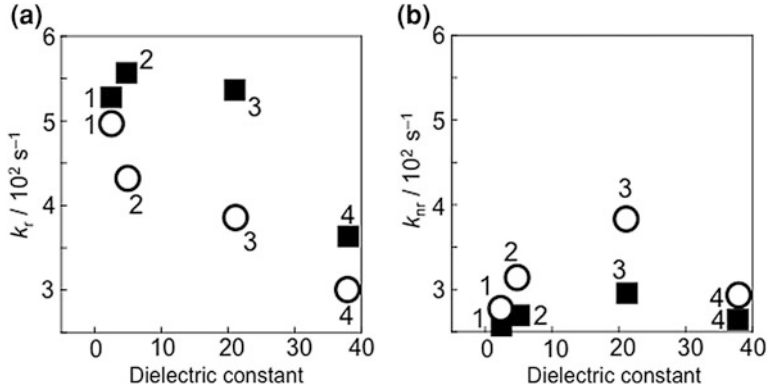

Fig. 6.3 The relationship between rate constants of Eu(III) complexes and dielectric constants of organic solvent. **a** The radiative (k_r) and **b** nonradiative constant (k_{nr}). (■: $Eu(hfa)_3$(*t*Bu-xantpo); 8-TDH, ○: $Eu(hfa)_2(xantpo)_2$; 8-SAP, *1* toluene, *2* chloroform, *3* acetone, *4* DMF)

$Eu(hfa)_3$(*t*Bu-xantpo) should come from asymmetrical D_{2d} structure related to change of odd parity in organic solvent.

The ability of solvent molecules for the coordination to metal centers can be estimated from the dielectric constant or the donor number. The relationship between rate constants of Eu(III) complexes and dielectric constants of organic solvent are shown in Fig. 6.3. In $Eu(hfa)_2(xantpo)_2$, k_r and k_{nr} are much dependent of the dielectric constant of organic solvent. These results indicate that coordination geometry and vibrational structure of $Eu(hfa)_2(xantpo)_2$(8-SAP) is affected by organic solvent with large dielectric constant, solvation to Eu(III) ion

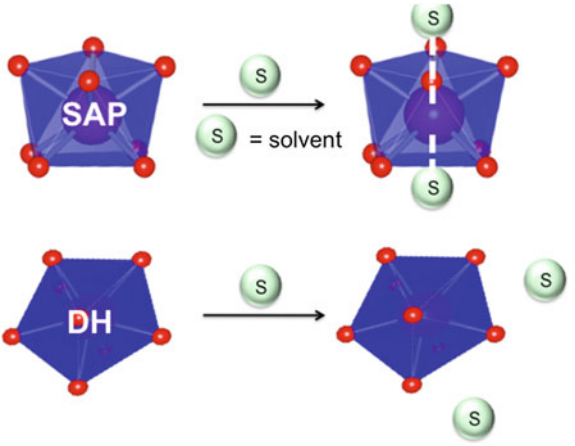

Fig. 6.4 Schematic illustrations of the difference between coordination ability of solvent molecules to metal center in **a** 8-SAP and **b** 8-TDH structures. The author considers that the solvent molecules might be difficult to coordinate to metal center in 8-TDH structures owing to their structural stability

(Fig. 6.4a). In contrast, we found that k_r and k_{nr} of Eu(hfa)$_3$(*t*Bu-xantpo) are maintained constant in acetone, toluene, and chloroform. The structure of 8-TDH in Eu(hfa)$_3$(*t*Bu-xantpo) might not be affected by solvent (Fig. 6.4b), although k_r and k_{nr} of 8-SAP are dependent of solvent. The author here considers that small nonradiative rate of Eu(hfa)$_3$(*t*Bu-xantpo) is caused by structural stability of 8-TDH in organic media.

The author also carried out charge density calculations of xantpo and *t*Bu-xantpo ligand by DFT calculation (6-31G(d)/B3LYP) based on the X-ray single crystal analyses. According to the calculation, charge densities oxygen atoms in phosphine oxides were found to be –0.51 and –0.48 (xantpo), –0.51 and –0.47 (*t*Bu-xantpo), respectively (Fig. 6.5). However, we found that charge densities of phosphorus atoms in *t*Bu-xantpo (–0.11 and 0.12) were higher than those in xantpo (0.22 and 0.23), because phosphorus atoms in *t*Bu-xantpo were affected by electron donating ability of *t*-butyl groups. The effective electron donating ability would be also lead to enhancement of coordination and structural stabilities of Eu(hfa)$_3$(*t*Bu-xantpo).

According to the emission process in DMF, k_r of Eu(hfa)$_3$(*t*Bu-xantpo) is similar to that for Eu(hfa)$_2$(xantpo)$_2$. Eu(hfa)$_2$(xantpo)$_2$ and Eu(hfa)$_3$(*t*Bu-xantpo) might be decomposed in DMF due to coordination to Eu(III) ion of DMF molecules with large dielectric constant. Decomposition of coordination structure by addition of solvent molecule with large dielectric constant has been previously reported [3]. The photosensitized energy transfer efficiency (η_{sens}) based on Φ_{Ln} and the total emission quantum yield (Φ_{tot}: excitation at 380 nm) of Eu(hfa)$_2$(xantpo)$_2$ and Eu(hfa)$_3$(*t*Bu- xantpo) are summarized in Table 6.2. The photosensitized energy transfer efficiencies in DMF (η_{sens} = 21–23 %) are smaller than those in toluene, chloroform, and acetone (34–43 %). The author considers that hfa ligands of the complexes might move away from Eu(III) ion in DMF.

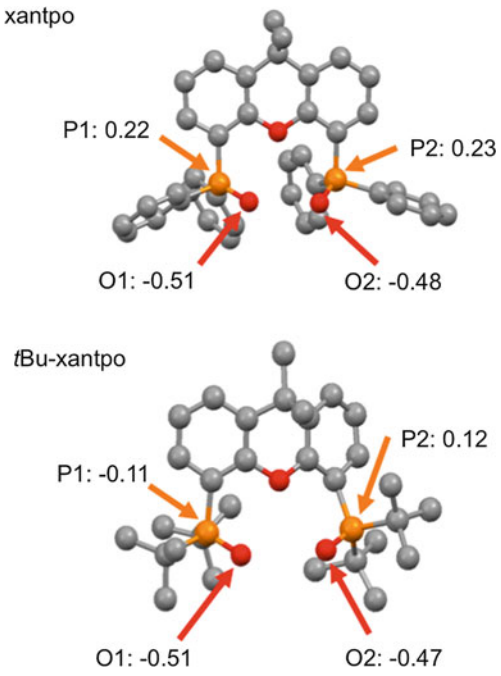

Fig. 6.5 Charge densities of phosphorus and oxygen atoms in xantpo and *t*Bu-xantpo ligand

6.4 Conclusion

Solvent-dependent luminescence of $Eu(hfa)_2(xantpo)_2$ and $Eu(hfa)_3$(*t*Bu-xantpo) are demonstrated. The author found that nonradiative rate process of Eu(III) complex is directly linked to characteristics of surrounding environment, organic solvent. Smaller k_{nr} of $Eu(hfa)_3$(*t*Bu-xantpo) is achieved by characteristic coordination structure, 8-TDH because of their structural stability in organic media. Solvent-dependent luminescence of lanthanide complex with characteristic octacoordination structure is expected to provide a novel aspect in the field of lanthanide photochemistry.

References

1. Y. Hasegawa, M. Yamamuro, Y. Wada, N. Kanehisa, Y. Kai, S. Yanagida, J. Phys. Chem. A **107**, 1697 (2003)
2. K. Miyata, Y. Hasegawa, Y. Kuramochi, T. Nakagawa, T. Yokoo, T. Kawai, Eur. J. Inorg. Chem. **32**, 4777 (2009)
3. Y. Hasegawa, Y. Kimura, K. Murakoshi, Y. Wada, J. Kim, N. Nakashima, T. Yamanaka, S. Yanagida, J. Phys. Chem. **100**, 10201 (1996)
4. B.M. Kurdziel, K. Solymosi, J. Kruk, B. Böddi, K. Strzałka, Eur. Biophys. J. **37**, 1185 (2007)

5. C. Görller-Walrand, L. Fluyt, A. Ceulemans, W.T. Carnall, J. Chem. Phys. **95**, 3099 (1991)
6. M.H.V. Werts, R.T.F. Jukes, J.W. Verhoeven, Phys. Chem. Chem. Phys. **4**, 1542 (2002)
7. K. Miyata, T. Nakagawa, R. Kawakami, Y. Kita, K. Sugimoto, T. Nakashima, T. Harada, T. Kawai, Y. Hasegawa, Chem. Eur. J. **17**, 521 (2011)

Chapter 7
Summary

The luminescence and thermal properties of lanthanide(III) complexes can be manipulated and enhanced by designing organic ligands which coordinate to lanthanide(III) ions. In this thesis, molecular designs for the enhancement of the luminescence properties and functionalization (thermostability and temperature-sensing ability) of lanthanide complexes with LVF phosphine oxide ligands have been described. The results obtained in this study were briefly summarized as follows.

In Chap. 1, the scientific backgrounds about lanthanide(III) luminescence were introduced. Then, issues of former researchers were pointed out in terms of structures of lanthanide complexes. The strategies of molecular designs of lanthanide complexes with the strong-luminescence properties and high thermal stability were also mentioned.

In Chap. 2, novel thermostable luminophores comprised of Eu(III) coordination polymers; $[Eu(hfa)_3(dpb)]_n$, $[Eu(hfa)_3(dpbp)]_n$, and $[Eu(hfa)_3(dppcz)]_n$ were successfully synthesized. In particular, $[Eu(hfa)_3(dppcz)]_n$ exhibited both high emission quantum yields ($\Phi_{Ln} = 83$ %) and remarkable thermal stability (decomposition point = 300 °C) due to a tight-binding structure composed of Eu(III) ions and low-vibrational phosphine oxide, although many types of luminescent organic dyes are generally decomposed at temperatures under 200 °C. The emission quantum yields of these coordination polymers are similar to those of strong-luminescent coordination polymers in former chapters. These coordination polymers are expected to employ in optics applications such as luminescent plastics, displays, and opto-electronic devices.

In Chap. 3, a novel thermosensing dye composed of color-changing luminescent coordination polymers containing Eu(III) and Tb(III) ions was successfully synthesized. This coordination polymer exhibited a high emission quantum yield Φ_{tot} of 40 % at room temperature and an effective temperature-sensing ability over a wide range of 200–500 K. Temperature-sensitive dyes with thermostable structures and dual sensing units were reported for the first time. The results obtained in this chapter will provide insights for designing lanthanide coordination polymers for development of temperature-sensing devices based on their luminescence.

K. Miyata, *Highly Luminescent Lanthanide Complexes with Specific Coordination Structures*, Springer Theses,
DOI: 10.1007/978-4-431-54944-4_7, © Springer Japan 2014

In Chap. 4, novel nona-coordinated Eu(III) complexes containing characteristic tridentate phosphine oxide ligands, dpppo, dppypo, and dpbtpo were successfully synthesized. These Eu(III) complexes exhibited strong-luminescence with high emission quantum yields ($\Phi_{Ln} > 60$ %). The author found that the emission intensities at the electric dipole transition of Eu(III) complexes depended on the organic linker species in phosphine oxide ligands, although the energy gap between Stark splitting levels, radiative and non-radiative rate constants were not affected by them. This result revealed that the transition intensity at the electric dipole transition is affected by chemical structures of attached tridentate phosphine oxide ligands.

In Chap. 5, Eu(III) and Sm(III) complexes with novel asymmetric structures composed of oxo-linked bidentate phosphine oxide ligands (xantpo, *t*Bu-xantpo, and dpepo) have been reported. The author carried out the calculations of the shape factor *S* in order to estimate the degree of distortion of the coordination structure in first coordination sphere. Based on the structural and photophysical findings, remarkably strong luminescence properties of Eu(III) and Sm(III) complexes with characteristic trigonal dodecahedron structures (8-TDH) were demonstrated for the first time. The author also showed that the emission quantum yield of $Sm(hfa)_3$(dpepo) with a trigonal dodecahedron structure is the highest value ($\Phi_{Ln} = 5.0$ %) in previous reported Sm(III) complexes.

In Chap. 6, solvent-dependent luminescence of $Eu(hfa)_2$(xantpo)$_2$ (8-SAP) and $Eu(hfa)_3$(*t*Bu-xantpo) (8-TDH) has been investigated. Their emission quantum yields, emission lifetimes, and radiative and nonradiative rate constants were characterized in acetone, acetone-d_6, toluene, chloroform, and DMF. The author found that nonradiative rate process of Eu(III) complex is directly linked to characteristics of surrounding environment, organic solvent. In particular, smaller nonradiative rate constant of $Eu(hfa)_3$(*t*Bu-xantpo) was achieved by characteristic coordination structure, 8-TDH because of their structural stability in organic media.

The luminescence properties of lanthanide complexes can be enhanced by design of chemical structures. However, the correlation between coordination structures and luminescence properties of lanthanide complexes has been scarcely investigated. In this thesis, the correlation between coordination structures and photophysical properties of lanthanide complexes with phosphine oxide ligands were demonstrated. Additionally, functionalization of lanthanide compounds was also described in terms of lanthanide coordination polymers. This thesis gives the first systematic studies on molecular photo-science between lanthanide(III) coordination chemistry and photo-functional materials science.

The author wishes the strategies for molecular design of luminescent lanthanide complexes described in this thesis would have contribution to development of applications in novel organic lanthanide devices, such as organic liquid lasers, luminescent plastics, optical fibers, EL devices, and temperature-sensing devices. The photochemistry of luminescent lanthanide complexes is expected to open up frontier fields between lanthanide coordination chemistry and photo-functional materials science.

Curriculum Vitae

Kohei Miyata, Ph.D.
Former affiliation address:
Graduate School of Chemical Sciences and Engineering, Hokkaido University
Sapporo, Hokkaido, Japan
Web: http://www.eng.hokudai.ac.jp/labo/amc

Career

- ADEKA Corporation (April 2013–)
- The Japan Society for the Promotion of Science (JSPS) Research Fellow (DC2, 2011–2013)

Education

- Doctor of Engineering, Hokkaido University, 2010–2013 (Supervisor: Prof. Yasuchika Hasegawa)
- Master of Engineering, Nara Institute of Science and Technology, 2008–2010 (Supervisor: Prof. Tsuyoshi Kawai)
- Bachelor of Engineering, The University of Shiga Prefecture, 2004–2008 (Supervisor: Prof. Tsutomu Kumagai)

Award

- The Japan Photochemistry Association, Student Presentation Award

K. Miyata, *Highly Luminescent Lanthanide Complexes with Specific Coordination Structures*, Springer Theses,
DOI: 10.1007/978-4-431-54944-4, © Springer Japan 2014